Accepted Manuscript

A new framework for large strain electromechanics based on convex multi-variable strain energies: Finite Element discretisation and computational implementation

Rogelio Ortigosa, Antonio J. Gil

PII: S0045-7825(15)00409-0
DOI: http://dx.doi.org/10.1016/j.cma.2015.12.007
Reference: CMA 10786

To appear in: *Comput. Methods Appl. Mech. Engrg.*

Please cite this article as: R. Ortigosa, A.J. Gil, A new framework for large strain electromechanics based on convex multi-variable strain energies: Finite Element discretisation and computational implementation, *Comput. Methods Appl. Mech. Engrg.* (2015), http://dx.doi.org/10.1016/j.cma.2015.12.007

A new framework for large strain electromechanics based on convex multi-variable strain energies: Finite Element discretisation and computational implementation.

Rogelio Ortigosa, Antonio J. Gil[1]

Zienkiewicz Centre for Computational Engineering, College of Engineering
Swansea University, Bay Campus, SA1 8EN, United Kingdom

Abstract

In Reference [1], Gil and Ortigosa introduced a new convex multi-variable framework for the numerical simulation of Electro Active Polymers (EAP) in the presence of extreme deformations and electric fields. This extends the concept of polyconvexity to strain energies which depend on non-strain based variables. The consideration of the new concept of multi-variable convexity guarantees the well posedness of generalised Gibbs' energy density functionals and, hence, opens up the possibility of a new family of mixed variational principles. The aim of this paper is to present, as an example, the Finite Element implementation of two of these mixed variational principles. These types of enhanced methodologies are known to be necessary in scenarios in which the simpler displacement-potential based formulation yields non-physical results, such as volumetric locking, bending and shear locking, pressure oscillations and electro-mechanical locking, to name but a few. Crucially, the use of interpolation spaces in which some of the unknown fields are described as piecewise discontinuous across elements can be used in order to efficiently condense these fields out. This results in mixed formulations with a computational cost comparable to that of the displacement-potential based approach, yet far more accurate. Finally, a series of very challenging numerical examples are presented in order to demonstrate the accuracy, robustness and efficiency of the proposed methodology.

[1]Corresponding author: a.j.gil@swansea.ac.uk

Keywords: Electro active polymers, Nonlinear electro-elasticity, Polyconvexity, Mixed variational principles, Material stability, Finite Elements

1. Introduction

The present manuscript presents a Finite Element computational framework tailor–made for the simulation of Electro Active Polymers (EAPs) [2–7] in applications where very large deformations and electric fields are involved. Dielectric elastomers and piezoelectric polymers are examples of EAPs which can be subjected to these extreme scenarios. For instance, giant electrically induced deformations of 1980% have been reported in the experimental literature [8] for the most representative example of dielectric elastomers, namely, the elastomer VHB 4910. Moderate electrically induced deformations of 40% have been reported in piezoelectric polymers, such as the highly popular PolyVinylidene DiFlouride (PVDF).

Several authors [9–14] have contributed to the development of variational approaches in the context of nonlinear electro-elasticity. Very importantly in this case, the constitutive laws governing the physics of the coupled problem must satisfy physically meaningful constitutive inequalities [15]. Bustamante and Merodio [16] studied under what ranges of deformation and magnetic field the Baker-Ericksen inequality [15] would be compromised, specifically considering smart materials belonging to the class of magneto-sensitive elastomers[2]. Recently, a material stability criterion based on an incremental quasi-convexity condition of the energy functional has been introduced by Miehe et al [17].

In Reference [1], Gil and Ortigosa, following the work of Rogers [18], extend the concept of polyconvexity [15, 19–26] to the field of nonlinear electro-elasticity based on a new convex multi-variable definition of the energy functional. It should be emphasised that the new definition of multi-variable convexity ensures [1] the material stability and well posedness of the equations. The existence of minimisers would also require the study of the sequentially weak lower semicontinuity and the coercivity of the energy functional. The internal energy density, defined as a convex multi-variable function of a new electro-kinematic variable set, including the deformation

[2]There exists a clear similitude between magneto-elasticity and electro-elasticity

gradient $\boldsymbol{F}$, its adjoint $\boldsymbol{H}$, its determinant J, the Lagrangian electric displacement field $\boldsymbol{D}_0$ and an additional spatial or Eulerian vector $\boldsymbol{d}$ computed as the product between the deformation gradient tensor and the Lagrangian electric displacement field. This definition enables the most accepted constitutive inequality, namely ellipticity (rank-one convexity) [15], to be fulfilled for the entire range of deformations and electric fields. Moreover, taking advantage of a new tensor cross product operation [24, 27], tedious algebra is remarkably simplified yielding insightful representations of otherwise complex expressions (i.e. electro-mechanical tangent operators).

Crucially, the new multi-variable convexity criterion enables the incorporation of the internal energy of the vacuum as a degenerate case [1]. In addition, the consideration of convex multi-variable internal energy functionals leads to positive definiteness of the generalised electro-mechanical acoustic tensor [28–30] and hence, existence of real wave speeds in the material in the vicinity of an equilibrium configuration. This analysis is shown in Reference [31] as a by-product of the hyperbolicity of a generalised system of conservation laws, along the same lines as References [21, 32–38].

From the computational standpoint, most authors [39–43] tend to prefer Finite Element computational frameworks where only geometry and electric potential are part of the solution. However, it is well known that these types of formulations can produce non-physical results, such as volumetric locking, bending and shear locking, pressure oscillations and electro-mechanical locking, to name but a few [44–46].

The consideration of convex multi-variable energy functionals brings additional benefits, including the solution to above shortcomings. Indeed, the extended set of variables $\{\boldsymbol{F}, \boldsymbol{H}, J, \boldsymbol{D}_0, \boldsymbol{d}\}$ enables the introduction of work conjugates $\{\boldsymbol{\Sigma}_{\boldsymbol{F}}, \boldsymbol{\Sigma}_{\boldsymbol{H}}, \Sigma_J, \boldsymbol{\Sigma}_{\boldsymbol{D}_0}, \boldsymbol{\Sigma}_{\boldsymbol{d}}\}$, where the satisfaction of multi-variable convexity guarantees that the relationship between both sets is one to one and invertible. Based on this, a new family of extended Hu-Washizu type of variational principles [22, 47–54] can be introduced [1]. The development of these new mixed variational principles [1] is a robust alternative to resolve the spurious (non-physical) mechanisms associated to the more classical displacement-potential approach.

This paper is organised as follows. Section 2 briefly introduces the governing equations of the problem, with special emphasis in the extension of the concept of polyconvexity from the field of convex multi-variable nonlinear elasticity to the more general field of nonlinear electro-elasticity [1], where the basic ingredients of the new framework are presented. In addi-

tion, a series of generalised Gibbs' energy density functionals are presented, defined through the use of Legendre transformations. Section 3 presents two of the extended Hu-Washizu type of mixed variational principles presented in Reference [1], which will be the main objective of this paper. Section 4 is focussed on the Finite Element discretisation and implementation of the variational principles presented in previous Section 3. Section 5 includes a wide spectrum of challenging numerical examples in order to demonstrate the robustness and applicability of the proposed enhanced mixed formulations, ranging from simpler isotropic to more complex anisotropic convex multi-variable models. Finally, Section 6 provides some concluding remarks and a summary of the key contributions of this paper.

Three appendices have been included for the sake of completeness. Appendix A shows how to relate the various expressions of the tangent operator of the internal energy, when expressed both in terms of the displacements and electric displacement field and when expressed in terms of the extended set of electro-kinetic variables $\{\boldsymbol{F}, \boldsymbol{H}, J, \boldsymbol{D}_0, \boldsymbol{d}\}$. Appendix B establishes the relationship between the classical components of the Helmholtz's energy and those associated with the internal energy. Finally, Appendix C presents the auxiliary residuals and stiffness matrices associated with the static condensation process carried out over one of the Hu-Washizu type of mixed variational principles presented in Section 3.

2. Nonlinear continuum electromechanics

2.1. Motion and deformation

Let us consider the motion of a continuum which could represent a dielectric elastomer or a piezoelectric polymer. This continuum is defined by a domain V with boundary ∂V in its initial or material configuration[3]. After the motion, the continuum occupies a spatial configuration defined by a domain v with boundary ∂v. The motion is defined by a pseudo-time t dependent mapping field $\boldsymbol{\phi}$ which links a material particle from material configuration $\boldsymbol{X} \in V$ to spatial configuration $\boldsymbol{x} \in v$ according to $\boldsymbol{x} = \boldsymbol{\phi}(\boldsymbol{X}, t)$. Displacement boundary conditions can be defined as $\boldsymbol{x} = (\boldsymbol{\phi})_{\partial_u V}$ on the boundary $\partial_u V \subset \partial V$.

[3] A more general formulation is presented in Reference [1] including the effect of a surrounding medium (i.e. vacuum).

The deformation gradient tensor or fibre-map $\boldsymbol{F}$, is defined as the material gradient $\boldsymbol{\nabla}_0$ of the spatial configuration [15, 19, 55–62]

$$\boldsymbol{F} = \boldsymbol{\nabla}_0 \boldsymbol{x} = \frac{\partial \boldsymbol{\phi}(\boldsymbol{X}, t)}{\partial \boldsymbol{X}}. \tag{1}$$

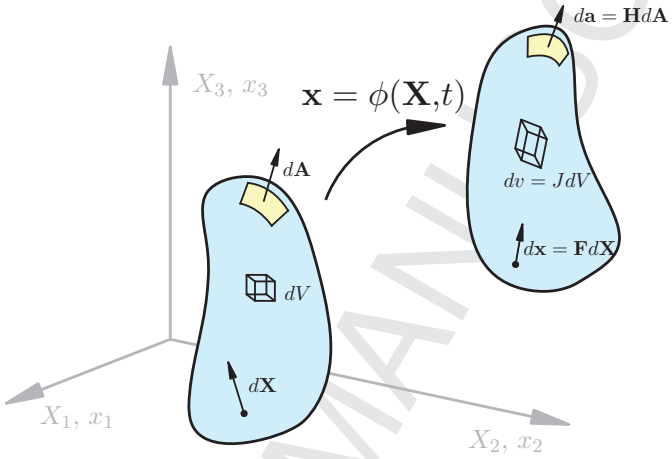

Figure 1: Deformation mapping of a continuum and definition of $\boldsymbol{F}, \boldsymbol{H}, J$.

In addition, $J = \det \boldsymbol{F}$ represents the Jacobian or volume-map of the deformation and $\boldsymbol{H} = J\boldsymbol{F}^{-T}$, the co-factor or area-map [24, 36, 55]. Figure 1 depicts the deformation process as well as how the three kinematic maps $\boldsymbol{F}$, $\boldsymbol{H}$ and J relate differential fibre, area and volume elements, respectively, between material and spatial configurations (i.e. $d\boldsymbol{x} = \boldsymbol{F}d\boldsymbol{X}$, $d\boldsymbol{a} = \boldsymbol{H}d\boldsymbol{A}$ and $dv = JdV$). With the help of the tensor cross product operation $\boldsymbol{\times}$ introduced in [27] and exploited in [24, 63, 64], it is possible to redefine conveniently the area and volume maps as

$$\boldsymbol{H} = \frac{1}{2}\boldsymbol{F} \boldsymbol{\times} \boldsymbol{F}; \qquad J = \frac{1}{3}\boldsymbol{H} : \boldsymbol{F}, \tag{2}$$

where for two-point second order tensors $\boldsymbol{A}$ and $\boldsymbol{B}$, the tensor cross operation $\boldsymbol{\times}$ is computed as $(\boldsymbol{A} \boldsymbol{\times} \boldsymbol{B})_{iI} = \mathcal{E}_{ijk}\mathcal{E}_{IJK}A_{jJ}B_{kK}$, with $\boldsymbol{\mathcal{E}}$ the third order alternating tensor. Throughout the paper, the symbol $(\cdot)$ is used to indicate

the scalar product or contraction of a single index $\boldsymbol{a}\cdot\boldsymbol{b}=a_ib_i$; the symbol (:) is used to indicate double contraction of two indices $\boldsymbol{A}:\boldsymbol{B}=A_{ij}B_{ij}$; the symbol ($\times$) is used to indicate the cross product between vectors $[\boldsymbol{a}\times\boldsymbol{b}]_i=\mathcal{E}_{ijk}a_jb_k$ and the symbol ($\otimes$) is used to indicate the outer or dyadic product $[\boldsymbol{a}\otimes\boldsymbol{b}]_{ij}=a_ib_j$.

Let us define $\delta\boldsymbol{u}$ and $\boldsymbol{u}$ as virtual and incremental variations of $\boldsymbol{x}$, which satisfy compatible displacement based boundary conditions on $\partial_u V$. Following the notation of [55] and making use of the cross product operation $\boldsymbol{\times}$ introduced above, the first and second directional derivatives of the co-factor $\boldsymbol{H}$ and the Jacobian J with respect to virtual and incremental variations of the geometry are evaluated as

$$D\boldsymbol{H}\left[\delta\boldsymbol{u}\right]=\boldsymbol{F}\boldsymbol{\times}\boldsymbol{\nabla}_0\delta\boldsymbol{u};\qquad D^2\boldsymbol{H}\left[\delta\boldsymbol{u};\boldsymbol{u}\right]=\boldsymbol{\nabla}_0\delta\boldsymbol{u}\boldsymbol{\times}\boldsymbol{\nabla}_0\boldsymbol{u};\tag{3a}$$

$$DJ\left[\delta\boldsymbol{u}\right]=\boldsymbol{H}:\boldsymbol{\nabla}_0\delta\boldsymbol{u};\qquad D^2J\left[\delta\boldsymbol{u};\boldsymbol{u}\right]=\boldsymbol{F}:\left(\boldsymbol{\nabla}_0\delta\boldsymbol{u}\boldsymbol{\times}\boldsymbol{\nabla}_0\boldsymbol{u}\right).\tag{3b}$$

2.2. Gauss and Farady laws

The dielectric elastomer represented by the continuum described in Section 2.1 is subjected in its material configuration V to an electric volume charge ρ_0^e per unit of undeformed volume and an electric surface charge ω_0^e per unit of undeformed area applied on $\partial_\omega V\subset\partial V$. For that continuum, the integral version of the Gauss law can be written in a Lagrangian format as

$$\int_{\partial_\omega V}\omega_0^e\,dA+\int_V\rho_0^e\,dV=0.\tag{4}$$

In this case, the local version of equation (4) and the associated boundary conditions can be written as[4]

$$\mathrm{DIV}\boldsymbol{D}_0=\rho_0^e\qquad\text{in } V;\tag{5a}$$

$$\boldsymbol{D}_0\cdot\boldsymbol{N}=-\omega_0^e\qquad\text{on } \partial_\omega V,\tag{5b}$$

[4]In the general case where the effect of the surrounding vacuum is considered, equation (5b) needs to be replaced with its more general version $[\![\boldsymbol{D}_0]\!]\cdot\boldsymbol{N}=\omega_0^e$ on $\partial_\omega V$, where $[\![\boldsymbol{D}_0]\!]$ represents the jump of variable $\boldsymbol{D}_0$ between the domain defined by the dielectric V and the surrounding vacuum. Moreover, for the general case where the domain V is comprised of sub-domains with interfaces $\partial V_i\cap\partial V_j, i\neq j$, the following jump condition must be satisfied, i.e $[\![\boldsymbol{D}_0]\!]\boldsymbol{N}|_{\partial V_i}=0$ on $\partial V_i\cap\partial V_j$.

where $\boldsymbol{D}_0$ is the Lagrangian electric displacement vector. Alternatively, equation (5) can be presented in a spatial description in terms of the Eulerian electric displacement field $\boldsymbol{D}$, defined as $\boldsymbol{D}_0 = \boldsymbol{H}^T\boldsymbol{D}$ [9, 65]. Analogously, the integral version of the static Faraday law can be written in a Lagrangian format for a closed curve $\mathcal{C}$ embedded in $V \cup \partial V$ as

$$\oint_{\mathcal{C}} \boldsymbol{E}_0 \cdot d\boldsymbol{X} = 0, \tag{6}$$

where $\boldsymbol{E}_0$ is the Lagrangian electric field vector. The local version of equation (6) and the associated boundary conditions can be expressed as[5]

$$\boldsymbol{E}_0 = -\boldsymbol{\nabla}_0\varphi \qquad \text{in } V; \tag{7a}$$

$$\varphi = (\varphi)_{\partial_\varphi V} \qquad \text{on } \partial_\varphi V, \tag{7b}$$

where φ is an electric potential field that can be introduced in the case of a contractible domain. In equation (7b), $\partial_\varphi V \subset \partial V$ represents the part of the boundary subjected to electric potential boundary conditions, such that $\partial_\omega V \cup \partial_\varphi V = \partial V$ and $\partial_\omega V \cap \partial_\varphi V = \emptyset$. As above equations (5), equations (7) could alternatively be presented in a spatial description in terms of the Eulerian electric field $\boldsymbol{E}$, which is related to its Lagrangian counterpart $\boldsymbol{E}_0$ through the standard fibre transformation $\boldsymbol{E}_0 = \boldsymbol{F}^T\boldsymbol{E}$ [9, 65].

2.3. Translational and rotational equilibrium

In addition to the Gauss and Faraday laws presented in Section 2.2, the kinematics of the continuum must be described through the conservation of linear momentum. In the absence of inertial effects, the global conservation of linear momentum leads to the integral translational equilibrium equations [55, 59]

$$\int_{\partial_t V} \boldsymbol{t}_0 dA + \int_V \boldsymbol{f}_0 dV = \boldsymbol{0}, \tag{8}$$

where $\boldsymbol{f}_0$ represents a body force per unit of undeformed volume applied in V and $\boldsymbol{t}_0$ a traction force per unit of undeformed area $\boldsymbol{t}_0$ applied on $\partial_t V \subset \partial V$, such that $\partial_t V \cup \partial_u V = \partial V$ and $\partial_t V \cap \partial_u V = \emptyset$. The local translational

[5] For the more general case where the domain V is comprised of sub-domains with interfaces $\partial V_i \cap \partial V_j, i \neq j$, the following jump condition must be satisfied, i.e $[\![\boldsymbol{E}_0]\!] \times \boldsymbol{N}|_{\partial V_i} = \boldsymbol{0}$ on $\partial V_i \cap \partial V_j$.

equilibrium equations and the associated boundary conditions can be written as[6]

$$\mathrm{DIV}\boldsymbol{P} + \boldsymbol{f}_0 = \boldsymbol{0} \qquad \text{in } V; \tag{9a}$$

$$\boldsymbol{P}\boldsymbol{N} = \boldsymbol{t}_0 \qquad \text{on } \partial_t V; \tag{9b}$$

$$\boldsymbol{\phi} = (\boldsymbol{\phi})_{\partial_u V} \qquad \text{on } \partial_u V, \tag{9c}$$

where $\boldsymbol{P}$ represents the first Piola-Kirchoff stress tensor. Furthermore, satisfaction of rotational equilibrium leads to the well-known tensor condition $\boldsymbol{P}\boldsymbol{F}^T = \boldsymbol{F}\boldsymbol{P}^T$.

2.4. The internal energy density: multi-variable convexity in electromechanics

For the closure of the system of equations defined by (5) and (9) describing the behaviour of the dielectric elastomer, an additional constitutive law satisfying appropriate constitutive inequalities [15] is needed. The most well accepted constitutive inequality, namely ellipticity, is automatically satisfied if the internal energy density functional e per unit of undeformed volume $e = e(\boldsymbol{\nabla}_0\boldsymbol{x}, \boldsymbol{D}_0)$ is defined as [1]

$$e\left(\boldsymbol{\nabla}_0\boldsymbol{x}, \boldsymbol{D}_0\right) = W\left(\boldsymbol{F}, \boldsymbol{H}, J, \boldsymbol{D}_0, \boldsymbol{d}\right); \quad \boldsymbol{d} = \boldsymbol{F}\boldsymbol{D}_0. \tag{10}$$

where W represents a convex muti-variable functional in terms of the extended set of arguments $\mathcal{V} = \{\boldsymbol{F}, \boldsymbol{H}, J, \boldsymbol{D}_0, \boldsymbol{d}\}$. In [1], it has been shown that the inclusion of the variable $\boldsymbol{d}$ in the set $\mathcal{V}$ enables the internal energy of the vacuum and that for an ideal dielectric elastomer model to be included as a particular degenerate case. The new extended set $\mathcal{V}$ permits the introduction of an associated set of work conjugate variables $\Sigma_{\mathcal{V}} = \{\boldsymbol{\Sigma}_{\boldsymbol{F}}, \boldsymbol{\Sigma}_{\boldsymbol{H}}, \Sigma_J, \boldsymbol{\Sigma}_{\boldsymbol{D}_0}, \boldsymbol{\Sigma}_{\boldsymbol{d}}\}$ as

$$\boldsymbol{\Sigma}_{\boldsymbol{F}} = \frac{\partial W}{\partial \boldsymbol{F}}; \quad \boldsymbol{\Sigma}_{\boldsymbol{H}} = \frac{\partial W}{\partial \boldsymbol{H}}; \quad \Sigma_J = \frac{\partial W}{\partial J}; \quad \boldsymbol{\Sigma}_{\boldsymbol{D}_0} = \frac{\partial W}{\partial \boldsymbol{D}_0}; \quad \boldsymbol{\Sigma}_{\boldsymbol{d}} = \frac{\partial W}{\partial \boldsymbol{d}}. \tag{11}$$

[6] In the general case where the effect of the surrounding vacuum is considered, equation (9b) has to be replaced with $[\![\boldsymbol{P}]\!]\boldsymbol{N} = \boldsymbol{t}_0$ on $\partial_t V$, where $[\![\boldsymbol{P}]\!]$ represents the jump between the first Piola-Kirchhoff stress tensor in the material occupying the region V and the Maxwell stress in the surrounding medium. Moreover, for the general case where the domain V represented by the electro active polymer is composed of sub-domains with interfaces $\partial V_i \cap \partial V_j, i \neq j$, the following jump condition must be satisfied, i.e $[\![\boldsymbol{P}]\!]\boldsymbol{N}|_{\partial V_i} = \boldsymbol{0}$ on $\partial V_i \cap \partial V_j$.

For notational convenience, the following sets, featuring in subsequent sections, will be introduced,

$$\begin{aligned} \mathcal{V}^m &= \{\boldsymbol{F}, \boldsymbol{H}, J\}; & \Sigma_{\mathcal{V}}^m &= \{\boldsymbol{\Sigma}_{\boldsymbol{F}}, \boldsymbol{\Sigma}_{\boldsymbol{H}}, \Sigma_J\}; \\ \mathcal{V}^e &= \{\boldsymbol{D}_0, \boldsymbol{d}\}; & \Sigma_{\mathcal{V}}^e &= \{\boldsymbol{\Sigma}_{\boldsymbol{D}_0}, \boldsymbol{\Sigma}_{\boldsymbol{d}}\}; \\ \mathcal{V} &= \{\mathcal{V}^m, \mathcal{V}^e\}; & \Sigma_{\mathcal{V}} &= \{\Sigma_{\mathcal{V}}^m, \Sigma_{\mathcal{V}}^e\}. \end{aligned} \tag{12}$$

Following a similar procedure to that of [1, 24], an expression for the first Piola-Kirchhoff stress tensor and the material electric field can be obtained in terms of the elements of both sets $\mathcal{V}$ and $\Sigma_{\mathcal{V}}$ as

$$\boldsymbol{P} = \boldsymbol{\Sigma}_{\boldsymbol{F}} + \boldsymbol{\Sigma}_{\boldsymbol{H}} \times \boldsymbol{F} + \Sigma_J \boldsymbol{H} + \boldsymbol{\Sigma}_{\boldsymbol{d}} \otimes \boldsymbol{D}_0; \quad \boldsymbol{E}_0 = \boldsymbol{\Sigma}_{\boldsymbol{D}_0} + \boldsymbol{F}^T \boldsymbol{\Sigma}_{\boldsymbol{d}}. \tag{13}$$

An expression for the Kirchhoff stress tensor [24] and the spatial electric field (needed for post-processing purposes) emerges based upon the relations $J\boldsymbol{\sigma} = \boldsymbol{\tau} = \boldsymbol{P}\boldsymbol{F}^T$ and $\boldsymbol{E} = \boldsymbol{F}^{-T}\boldsymbol{E}_0$ as

$$\begin{aligned} J\boldsymbol{\sigma} = \boldsymbol{\tau} &= \boldsymbol{\Sigma}_{\boldsymbol{F}} \boldsymbol{F}^T + \left(\boldsymbol{\Sigma}_{\boldsymbol{H}} \boldsymbol{H}^T\right) \times \boldsymbol{I} + J\Sigma_J \boldsymbol{I} + \boldsymbol{\Sigma}_{\boldsymbol{d}} \otimes \boldsymbol{d}; \\ \boldsymbol{E} &= \boldsymbol{F}^{-T} \left(\boldsymbol{\Sigma}_{\boldsymbol{D}_0} + \boldsymbol{F}^T \boldsymbol{\Sigma}_{\boldsymbol{d}}\right) = \boldsymbol{F}^{-T} \boldsymbol{\Sigma}_{\boldsymbol{D}_0} + \boldsymbol{\Sigma}_{\boldsymbol{d}}, \end{aligned} \tag{14}$$

where $\boldsymbol{I}$ denotes the second order identity tensor.

2.5. Tangent electromechanics operator for the internal energy

With a Newton-Raphson type of solution process in mind, the internal energy $e = e(\boldsymbol{\nabla}_0 \boldsymbol{x}, \boldsymbol{D}_0)$ can be further linearised leading to the tangent operator

$$D^2 e\left[\delta\boldsymbol{u}, \delta\boldsymbol{D}_0; \boldsymbol{u}, \Delta\boldsymbol{D}_0\right] = \left[\begin{array}{cc} \boldsymbol{\nabla}_0 \delta\boldsymbol{u} : & \delta\boldsymbol{D}_0 \cdot \end{array}\right] \left[\begin{array}{cc} \boldsymbol{\mathcal{C}} & \boldsymbol{\mathcal{Q}}^T \\ \boldsymbol{\mathcal{Q}} & \boldsymbol{\theta} \end{array}\right] \left[\begin{array}{c} : \boldsymbol{\nabla}_0 \boldsymbol{u} \\ \Delta\boldsymbol{D}_0 \end{array}\right], \tag{15}$$

with the fourth order tensor $\boldsymbol{\mathcal{C}}$, the third order tensor $\boldsymbol{\mathcal{Q}}$ and the second order tensor $\boldsymbol{\theta}$ defined as

$$\boldsymbol{\mathcal{C}} = \left.\frac{\partial^2 e(\boldsymbol{F}, \boldsymbol{D}_0)}{\partial \boldsymbol{F} \partial \boldsymbol{F}}\right|_{\boldsymbol{F} = \boldsymbol{\nabla}_0 \boldsymbol{x}}; \; \boldsymbol{\mathcal{Q}} = \left.\frac{\partial^2 e(\boldsymbol{F}, \boldsymbol{D}_0)}{\partial \boldsymbol{D}_0 \partial \boldsymbol{F}}\right|_{\boldsymbol{F} = \boldsymbol{\nabla}_0 \boldsymbol{x}}; \; \boldsymbol{\theta} = \left.\frac{\partial^2 e(\boldsymbol{F}, \boldsymbol{D}_0)}{\partial \boldsymbol{D}_0 \partial \boldsymbol{D}_0}\right|_{\boldsymbol{F} = \boldsymbol{\nabla}_0 \boldsymbol{x}}. \tag{16}$$

With the help of the tensor cross product [1, 24, 27], a more physically insightful representation of the tangent operator (15) is

$$\begin{aligned} D^2 e\left[\delta\boldsymbol{u}, \delta\boldsymbol{D}_0; \boldsymbol{u}, \Delta\boldsymbol{D}_0\right] = \left[\mathbb{S}_\delta\right]^T \left[\mathbb{H}_W\right] \left[\mathbb{S}_\Delta\right] + (\boldsymbol{\Sigma}_{\boldsymbol{H}} + \Sigma_J \boldsymbol{F}) : (\boldsymbol{\nabla}_0 \delta\boldsymbol{u} \times \boldsymbol{\nabla}_0 \boldsymbol{u}) \\ + \boldsymbol{\Sigma}_{\boldsymbol{d}} \cdot \left((\boldsymbol{\nabla}_0 \delta\boldsymbol{u}) \Delta\boldsymbol{D}_0 + (\boldsymbol{\nabla}_0 \boldsymbol{u}) \delta\boldsymbol{D}_0\right), \end{aligned} \tag{17}$$

where

$$\left[\mathbb{S}_\delta\right]^T = \left[(\boldsymbol{\nabla}_0\delta\boldsymbol{u}) : \quad (\boldsymbol{\nabla}_0\delta\boldsymbol{u} \times \boldsymbol{F}) : \quad (\boldsymbol{\nabla}_0\delta\boldsymbol{u} : \boldsymbol{H}) \quad \delta\boldsymbol{D}_0 \cdot \quad ((\boldsymbol{\nabla}_0\delta\boldsymbol{u})\boldsymbol{D}_0 + \boldsymbol{F}\delta\boldsymbol{D}_0)\cdot\right];$$

$$\left[\mathbb{S}_\Delta\right] = \begin{bmatrix} : (\boldsymbol{\nabla}_0\boldsymbol{u}) \\ : (\boldsymbol{F} \times \boldsymbol{\nabla}_0\boldsymbol{u}) \\ (\boldsymbol{H} : \boldsymbol{\nabla}_0\boldsymbol{u}) \\ \Delta\boldsymbol{D}_0 \\ \boldsymbol{\nabla}_0\boldsymbol{u}\boldsymbol{D}_0 + \boldsymbol{F}\Delta\boldsymbol{D}_0 \end{bmatrix}, \tag{18}$$

and with the extended Hessian operator $[\mathbb{H}_W]$ denoting the symmetric positive definite operator containing the second derivatives of $W\left(\boldsymbol{F}, \boldsymbol{H}, J, \boldsymbol{D}_0, \boldsymbol{d}\right)$ as

$$[\mathbb{H}_W] = \begin{bmatrix} W_{\boldsymbol{FF}} & W_{\boldsymbol{FH}} & W_{\boldsymbol{F}J} & W_{\boldsymbol{FD}_0} & W_{\boldsymbol{Fd}} \\ W_{\boldsymbol{HF}} & W_{\boldsymbol{HH}} & W_{\boldsymbol{H}J} & W_{\boldsymbol{HD}_0} & W_{\boldsymbol{Hd}} \\ W_{J\boldsymbol{F}} & W_{J\boldsymbol{H}} & W_{JJ} & W_{J\boldsymbol{D}_0} & W_{J\boldsymbol{d}} \\ W_{\boldsymbol{D}_0\boldsymbol{F}} & W_{\boldsymbol{D}_0\boldsymbol{H}} & W_{\boldsymbol{D}_0J} & W_{\boldsymbol{D}_0\boldsymbol{D}_0} & W_{\boldsymbol{D}_0\boldsymbol{d}} \\ W_{\boldsymbol{dF}} & W_{\boldsymbol{dH}} & W_{\boldsymbol{d}J} & W_{\boldsymbol{dD}_0} & W_{\boldsymbol{dd}} \end{bmatrix}. \tag{19}$$

As shown in Appendix A, it is possible to relate the constitutive tensors $\boldsymbol{\mathcal{C}}$, $\boldsymbol{Q}$ and $\boldsymbol{\theta}$ in equation (15) to the components of the Hessian operator $[\mathbb{H}_W]$ in (19).

As stated in [1], this additive decomposition of the tangent operator is not merely technical but, extremely useful, as the multi-physics of the problem is completely captured in the first term on the right hand side of equation (17), whilst geometrically nonlinear terms are collected on the second and third terms. In Reference [1], the authors show how the positive definiteness of the Hessian operator $[\mathbb{H}_W]$ in above (19) extends the concept of ellipticity (rank-one convexity) to the field of electromechanics. In addition, in Reference [31], the authors show how the positive definiteness of $[\mathbb{H}_W]$ guarantees the existence of physical wave speeds (Legendre-Hadamard condition [15]) and the symmetrisation of a system of conservation laws via a convex entropy function.

$\boldsymbol{F} = \frac{\partial \Upsilon}{\partial \boldsymbol{\Sigma}_{\boldsymbol{F}}}$	$\boldsymbol{H} = \frac{\partial \Upsilon}{\partial \boldsymbol{\Sigma}_{\boldsymbol{H}}}$	$J = \frac{\partial \Upsilon}{\partial \Sigma_J}$	$\boldsymbol{D}_0 = \frac{\partial \Upsilon}{\partial \boldsymbol{\Sigma}_{\boldsymbol{D}_0}}$	$\boldsymbol{d} = \frac{\partial \Upsilon}{\partial \boldsymbol{\Sigma}_{\boldsymbol{d}}}$
$\boldsymbol{F} = \frac{\partial \Psi}{\partial \boldsymbol{\Sigma}_{\boldsymbol{F}}}$	$\boldsymbol{H} = \frac{\partial \Psi}{\partial \boldsymbol{\Sigma}_{\boldsymbol{H}}}$	$J = \frac{\partial \Psi}{\partial \Sigma_J}$	$\boldsymbol{\Sigma}_{\boldsymbol{D}_0} = -\frac{\partial \Psi}{\partial \boldsymbol{D}_0}$	$\boldsymbol{\Sigma}_{\boldsymbol{d}} = -\frac{\partial \Psi}{\partial \boldsymbol{d}}$
$\boldsymbol{\Sigma}_{\boldsymbol{F}} = \frac{\partial \Phi}{\partial \boldsymbol{F}}$	$\boldsymbol{\Sigma}_{\boldsymbol{H}} = \frac{\partial \Phi}{\partial \boldsymbol{H}}$	$\Sigma_J = \frac{\partial \Phi}{\partial J}$	$\boldsymbol{D}_0 = -\frac{\partial \Phi}{\partial \boldsymbol{\Sigma}_{\boldsymbol{D}_0}}$	$\boldsymbol{d} = -\frac{\partial \Phi}{\partial \boldsymbol{\Sigma}_{\boldsymbol{d}}}$

Table 1: Expressions relating strain, stress, and electric variables for the energy functionals Υ (20a), Ψ (20b) and Φ (20c).

2.6. Alternative energy density functionals

Polyconvexity of the internal energy density $W(\mathcal{V})$ (10) with respect to its extended set of variables enables the definition of an extended Gibbs' energy density $\Upsilon(\Sigma_{\mathcal{V}})$, an extended enthalpy energy density $\Psi(\Sigma^m_{\mathcal{V}}, \mathcal{V}^e)$ and an extended Helmholtz's energy density $\Phi(\mathcal{V}^m, \Sigma^e_{\mathcal{V}})$ as

$$\Upsilon(\Sigma_{\mathcal{V}}) = \sup_{\mathcal{V}} \{T^m + T^e - W(\mathcal{V})\}; \tag{20a}$$

$$\Psi(\Sigma^m_{\mathcal{V}}, \mathcal{V}^e) = \sup_{\mathcal{V}^m} \{T^m - W(\mathcal{V})\}; \tag{20b}$$

$$\Phi(\mathcal{V}^m, \Sigma^e_{\mathcal{V}}) = -\sup_{\mathcal{V}^e} \{T^e - W(\mathcal{V})\}, \tag{20c}$$

where the sets $\mathcal{V}^m$, $\mathcal{V}^e$, $\Sigma^m_{\mathcal{V}}$ and $\Sigma^e_{\mathcal{V}}$ have been defined in (12) and with

$$T^m = \boldsymbol{\Sigma}_{\boldsymbol{F}} : \boldsymbol{F} + \boldsymbol{\Sigma}_{\boldsymbol{H}} : \boldsymbol{H} + \Sigma_J J; \qquad T^e = \boldsymbol{\Sigma}_{\boldsymbol{D_0}} \cdot \boldsymbol{D}_0 + \boldsymbol{\Sigma}_{\boldsymbol{d}} \cdot \boldsymbol{d}. \tag{21}$$

Expressions relating strain, stress and electric variables, in terms of the different energy functionals, are presented in Table 1. The definition of multi-variable convexity in (10) ensures a one to one relationship between the variables $\boldsymbol{D}_0$ and $-\boldsymbol{\nabla}_0\varphi$. In this case, it is possible to define an alternative energy functional to the internal energy $e = e(\boldsymbol{\nabla}_0\boldsymbol{x}, \boldsymbol{D}_0)$ by making use of the Legendre transform[7]. This might be a computationally convenient approach

[7] An advantage of employing a constitutive model defined by the energy functional in (10) is that it ensures the existence of the Helmholtz's energy density *ab initio*, which cannot be necessarily guaranteed otherwise.

in the case of pursuing a standard semi-discrete variational implementation via the Finite Element Method, where the scalar electric potential is preferred as an unknown over the electric displacement field vector. In this case, the Helmholtz's energy density $\Phi = \Phi(\boldsymbol{\nabla}_0 \boldsymbol{x}, -\boldsymbol{\nabla}_0 \varphi)$ can be defined as[8]

$$\Phi\left(\boldsymbol{\nabla}_0 \boldsymbol{x}, -\boldsymbol{\nabla}_0 \varphi\right) = -\sup_{\boldsymbol{D}_0} \left\{-\boldsymbol{\nabla}_0 \varphi \cdot \boldsymbol{D}_0 - e\left(\boldsymbol{\nabla}_0 \boldsymbol{x}, \boldsymbol{D}_0\right)\right\}, \tag{22}$$

leading to a definition for the stress and electric fields as

$$\boldsymbol{P} = \left.\frac{\partial \Phi(\boldsymbol{F}, \boldsymbol{E}_0)}{\partial \boldsymbol{F}}\right|_{\substack{\boldsymbol{F}=\boldsymbol{\nabla}_0 \boldsymbol{x} \\ \boldsymbol{E}_0=-\boldsymbol{\nabla}_0 \varphi}}; \qquad \boldsymbol{D}_0 = -\left.\frac{\partial \Phi(\boldsymbol{F}, \boldsymbol{E}_0)}{\partial \boldsymbol{E}_0}\right|_{\substack{\boldsymbol{F}=\boldsymbol{\nabla}_0 \boldsymbol{x} \\ \boldsymbol{E}_0=-\boldsymbol{\nabla}_0 \varphi}}. \tag{23}$$

2.6.1. Tangent operators for the Helmholtz's and extended Helmholtz's energy functionals

The tangent operator for the Helmholtz's energy density $\Phi = \Phi(\boldsymbol{\nabla}_0 \boldsymbol{x}, -\boldsymbol{\nabla}_0 \varphi)$ defined in (22) is computed as

$$D^2\Phi\left[\delta\boldsymbol{u}, \delta\varphi; \boldsymbol{u}, \Delta\varphi\right] = \left[\begin{array}{cc} \boldsymbol{\nabla}_0 \delta\boldsymbol{u} : & -\boldsymbol{\nabla}_0 \delta\varphi \cdot \end{array}\right] \left[\begin{array}{cc} \boldsymbol{\mathcal{C}}^* & -\boldsymbol{\mathcal{P}}^T \\ -\boldsymbol{\mathcal{P}} & -\boldsymbol{\varepsilon} \end{array}\right] \left[\begin{array}{c} : \boldsymbol{\nabla}_0 \boldsymbol{u} \\ -\boldsymbol{\nabla}_0 \Delta\varphi \end{array}\right], \tag{24}$$

with the fourth order elastic tensor $\boldsymbol{\mathcal{C}}^*$, the third order piezoelectric tensor $\boldsymbol{\mathcal{P}}$ and the second order dielectric tensor $\boldsymbol{\varepsilon}$ defined as

$$\boldsymbol{\mathcal{C}}^* = \left.\frac{\partial^2 \Phi(\boldsymbol{F}, \boldsymbol{E}_0)}{\partial \boldsymbol{F} \partial \boldsymbol{F}}\right|_{\substack{\boldsymbol{F}=\boldsymbol{\nabla}_0 \boldsymbol{x} \\ \boldsymbol{E}_0=-\boldsymbol{\nabla}_0 \varphi}}; \; \boldsymbol{\mathcal{P}} = -\left.\frac{\partial^2 \Phi(\boldsymbol{F}, \boldsymbol{E}_0)}{\partial \boldsymbol{F} \partial \boldsymbol{E}_0}\right|_{\substack{\boldsymbol{F}=\boldsymbol{\nabla}_0 \boldsymbol{x} \\ \boldsymbol{E}_0=-\boldsymbol{\nabla}_0 \varphi}}; \; \boldsymbol{\varepsilon} = -\left.\frac{\partial^2 \Phi(\boldsymbol{F}, \boldsymbol{E}_0)}{\partial \boldsymbol{E}_0 \partial \boldsymbol{E}_0}\right|_{\substack{\boldsymbol{F}=\boldsymbol{\nabla}_0 \boldsymbol{x} \\ \boldsymbol{E}_0=-\boldsymbol{\nabla}_0 \varphi}}. \tag{25}$$

As shown in Appendix B, it is possible to relate the constitutive tensors $\boldsymbol{\mathcal{C}}^\star$, $\boldsymbol{\mathcal{P}}$ and $\boldsymbol{\varepsilon}$ in (25) to those emerging from the tangent operator of the internal energy, namely $\boldsymbol{\mathcal{C}}$, $\boldsymbol{\mathcal{Q}}$ and $\boldsymbol{\theta}$ in (16).

Following a similar procedure to that of equation (17) and in preparation for a new mixed variational principle presented in the following Section 3, a possible tangent operator for the extended Helmholtz's energy functional $\Phi(\mathcal{V}^m, \Sigma^e_{\mathcal{V}})$ defined in equation (20c) is obtained as

$$D^2\Phi\left[\delta\boldsymbol{u}, \delta\boldsymbol{\Sigma}_{\boldsymbol{D}_0}, \delta\boldsymbol{\Sigma}_{\boldsymbol{d}}; \boldsymbol{u}, \Delta\boldsymbol{\Sigma}_{\boldsymbol{D}_0}, \Delta\boldsymbol{\Sigma}_{\boldsymbol{d}}\right] = \left[\mathbb{S}^\star_\delta\right]^T \left[\mathbb{H}_\Phi\right] \left[\mathbb{S}^\star_\Delta\right] + \left(\boldsymbol{\Sigma}_{\boldsymbol{H}} + \Sigma_J \boldsymbol{F}\right) : \left(\boldsymbol{\nabla}_0 \delta\boldsymbol{u} \times \boldsymbol{\nabla}_0 \boldsymbol{u}\right), \tag{26}$$

[8] Alternatively, an equivalent definition of the Legendre transform in equation (22) can be defined as $\Phi\left(\boldsymbol{\nabla}_0 \boldsymbol{x}, -\boldsymbol{\nabla}_0 \varphi\right) = \inf_{\boldsymbol{D}_0} \left\{\boldsymbol{\nabla}_0 \varphi \cdot \boldsymbol{D}_0 + e\left(\boldsymbol{\nabla}_0 \boldsymbol{x}, \boldsymbol{D}_0\right)\right\}$.

where

$$\left[\mathbb{S}^{\star}_{\delta}\right]^{T} = \left[(\boldsymbol{\nabla}_0\delta\boldsymbol{u}) : \ (\boldsymbol{\nabla}_0\delta\boldsymbol{u}\times\boldsymbol{F}) : \ (\boldsymbol{\nabla}_0\delta\boldsymbol{u} : \boldsymbol{H}) \ \ \delta\boldsymbol{\Sigma}_{\boldsymbol{D}_0} \cdot \ \ \delta\boldsymbol{\Sigma}_{\boldsymbol{d}} \cdot\right];$$
$$\left[\mathbb{S}^{\star}_{\Delta}\right] = \begin{bmatrix} :(\boldsymbol{\nabla}_0\boldsymbol{u}) \\ :(\boldsymbol{F}\times\boldsymbol{\nabla}_0\boldsymbol{u}) \\ (\boldsymbol{H} : \boldsymbol{\nabla}_0\boldsymbol{u}) \\ \Delta\boldsymbol{\Sigma}_{\boldsymbol{D}_0} \\ \Delta\boldsymbol{\Sigma}_{\boldsymbol{d}} \end{bmatrix}, \tag{27}$$

and with the extended Hessian operator $[\mathbb{H}_{\Phi}]$ denoting the operator containing the second derivatives of $\Phi\left(\boldsymbol{F}, \boldsymbol{H}, J, \boldsymbol{\Sigma}_{\boldsymbol{D}_0}, \boldsymbol{\Sigma}_{\boldsymbol{d}}\right)$ as

$$[\mathbb{H}_{\Phi}] = \begin{bmatrix} \Phi_{\boldsymbol{FF}} & \Phi_{\boldsymbol{FH}} & \Phi_{\boldsymbol{F}J} & \Phi_{\boldsymbol{F}\boldsymbol{\Sigma}_{\boldsymbol{D}_0}} & \Phi_{\boldsymbol{F}\boldsymbol{\Sigma}_{\boldsymbol{d}}} \\ \Phi_{\boldsymbol{HF}} & \Phi_{\boldsymbol{HH}} & \Phi_{\boldsymbol{H}J} & \Phi_{\boldsymbol{H}\boldsymbol{\Sigma}_{\boldsymbol{D}_0}} & \Phi_{\boldsymbol{H}\boldsymbol{\Sigma}_{\boldsymbol{d}}} \\ \Phi_{J\boldsymbol{F}} & \Phi_{J\boldsymbol{H}} & \Phi_{JJ} & \Phi_{J\boldsymbol{\Sigma}_{\boldsymbol{D}_0}} & \Phi_{J\boldsymbol{\Sigma}_{\boldsymbol{d}}} \\ \Phi_{\boldsymbol{\Sigma}_{\boldsymbol{D}_0}\boldsymbol{F}} & \Phi_{\boldsymbol{\Sigma}_{\boldsymbol{D}_0}\boldsymbol{F}} & \Phi_{\boldsymbol{\Sigma}_{\boldsymbol{D}_0}J} & \Phi_{\boldsymbol{\Sigma}_{\boldsymbol{D}_0}\boldsymbol{\Sigma}_{\boldsymbol{D}_0}} & \Phi_{\boldsymbol{\Sigma}_{\boldsymbol{D}_0}\boldsymbol{\Sigma}_{\boldsymbol{d}}} \\ \Phi_{\boldsymbol{\Sigma}_{\boldsymbol{d}}\boldsymbol{F}} & \Phi_{\boldsymbol{\Sigma}_{\boldsymbol{d}}\boldsymbol{F}} & \Phi_{\boldsymbol{\Sigma}_{\boldsymbol{d}}J} & \Phi_{\boldsymbol{\Sigma}_{\boldsymbol{d}}\boldsymbol{\Sigma}_{\boldsymbol{D}_0}} & \Phi_{\boldsymbol{\Sigma}_{\boldsymbol{d}}\boldsymbol{\Sigma}_{\boldsymbol{d}}} \end{bmatrix}. \tag{28}$$

Notice that the definition of multi-variable convexity in equation (10) enables to relate each of the components of the above Hessian operator $[\mathbb{H}_{\Phi}]$ (28) with the components of the Hessian operator $[\mathbb{H}_W]$ (19), as shown in Appendix B.

3. A survey of some variational principles in nonlinear electro-elasticity

The governing equations and relevant aspects concerning the constitutive modelling of electro active polymers have been presented in Section 2. The objective of this section is to present some possible variational principles in nonlinear electro-elasticity, in preparation for a subsequent Finite Element semi-discretisation.

Traditional Finite Element based implementations resort to variational principles where the geometry and the electrical potential are the only unknowns of the problem [40, 41]. A well established potential-displacement

based variational principle in terms of the Helmholtz's energy (22) is defined as

$$\Pi_{\Phi}(\boldsymbol{x}^*, \varphi^*) = \inf_{\boldsymbol{x}} \sup_{\varphi} \left\{ \int_V \Phi(\boldsymbol{\nabla}_0 \boldsymbol{x}, -\boldsymbol{\nabla}_0 \varphi) dV - \Pi_{ext}(\boldsymbol{x}, \varphi) \right\}, \tag{29}$$

where $\{\boldsymbol{x}^*, \varphi^*\}$ denotes the exact solution and where the external term $\Pi_{ext}(\boldsymbol{x}, \varphi)$ is additively decomposed as $\Pi_{ext}(\boldsymbol{x}, \varphi) = \Pi^m_{ext}(\boldsymbol{x}) + \Pi^e_{ext}(\varphi)$, with the purely mechanical $\Pi^m_{ext}(\boldsymbol{x})$ and purely electric $\Pi^e_{ext}(\varphi)$ components defined as

$$\Pi^m_{ext}(\boldsymbol{x}) = \int_V \boldsymbol{f}_0 \cdot \boldsymbol{x}\, dV + \int_{\partial_t V} \boldsymbol{t}_0 \cdot \boldsymbol{x}\, dA; \qquad \Pi^e_{ext}(\varphi) = -\int_V \rho^e_0 \varphi\, dV - \int_{\partial_\omega V} \omega^e_0 \varphi\, dA. \tag{30}$$

First and second derivatives of the Hemlholtz's energy, featuring in the stationary conditions of the variational principle Π_{Φ} (29) can be obtained implicitly in terms of the derivatives and second derivatives of the internal energy $W(\mathcal{V})$, as shown in Appendix B.2.

However, potential-displacement based formulations produce inaccurate solutions for strains, stresses, electric fields and electric displacement fields, specially when low order discretisations are used. Gradients (of displacements and electric potential) are poorly described by the solution of this type of formulations [36]. It is well known that enhanced mixed formulations [22, 47–54] can overcome these drawbacks.

A first Hu-Washizu mixed variational principle has been proposed in [1] in terms of the internal energy $W(\mathcal{V})$ of the system

$$\begin{aligned}
&\Pi_W(\boldsymbol{x}^*, \boldsymbol{F}^*, \boldsymbol{H}^*, J^*, \boldsymbol{\Sigma}^*_{\boldsymbol{F}}, \boldsymbol{\Sigma}^*_{\boldsymbol{H}}, \Sigma^*_J, \varphi^*, \boldsymbol{D}^*_0, \boldsymbol{d}^*, \boldsymbol{\Sigma}^*_{\boldsymbol{d}}) \\
&= \inf_{\boldsymbol{x}, \boldsymbol{F}, \boldsymbol{H}, J, \boldsymbol{D}_0, \boldsymbol{d}} \sup_{\boldsymbol{\Sigma}_{\boldsymbol{F}}, \boldsymbol{\Sigma}_{\boldsymbol{H}}, \Sigma_J, \varphi, \boldsymbol{\Sigma}_{\boldsymbol{d}}} \left\{ \int_V W(\mathcal{V})\, dV + \int_V \boldsymbol{D}_0 \cdot \boldsymbol{\nabla}_0 \varphi\, dV \right. \\
&+ \int_V \left[\boldsymbol{\Sigma}_{\boldsymbol{F}} : (\boldsymbol{F}_{\boldsymbol{x}} - \boldsymbol{F}) + \boldsymbol{\Sigma}_{\boldsymbol{H}} : (\boldsymbol{H}_{\boldsymbol{x}} - \boldsymbol{H}) + \Sigma_J (J_{\boldsymbol{x}} - J) \right. \\
&\left. \left. + \boldsymbol{\Sigma}_{\boldsymbol{d}} \cdot (\boldsymbol{F}_{\boldsymbol{x}} \boldsymbol{D}_0 - \boldsymbol{d}) \right] dV - \Pi_{ext}(\boldsymbol{x}, \varphi) \right\},
\end{aligned} \tag{31}$$

where $\{\boldsymbol{F}_{\boldsymbol{x}}, \boldsymbol{H}_{\boldsymbol{x}}, J_{\boldsymbol{x}}\}$ in above equation (31) denote the geometrically compatible strain measures

$$\boldsymbol{F}_{\boldsymbol{x}} = \boldsymbol{\nabla}_0 \boldsymbol{x}; \qquad \boldsymbol{H}_{\boldsymbol{x}} = \frac{1}{2} \boldsymbol{\nabla}_0 \boldsymbol{x} \times \boldsymbol{\nabla}_0 \boldsymbol{x}; \qquad J_{\boldsymbol{x}} = \det \boldsymbol{\nabla}_0 \boldsymbol{x}. \tag{32}$$

A second Hu-Washizu mixed variational principle [1] in terms of the extended Helmholtz's energy $\Phi(\mathcal{V}^m, \Sigma^e_{\mathcal{V}})$ (20c) can also be defined as

$$\begin{aligned}
&\Pi_\Phi(\boldsymbol{x}^*, \boldsymbol{F}^*, \boldsymbol{H}^*, J^*, \boldsymbol{\Sigma}^*_{\boldsymbol{F}}, \boldsymbol{\Sigma}^*_{\boldsymbol{H}}, \Sigma^*_J, \varphi^*, \boldsymbol{D}^*_0, \boldsymbol{\Sigma}^*_{\boldsymbol{D}_0}, \boldsymbol{\Sigma}_{\boldsymbol{d}}{}^*) \\
&= \inf_{\boldsymbol{x},\boldsymbol{F},\boldsymbol{H},J,\boldsymbol{D}_0} \sup_{\boldsymbol{\Sigma}_{\boldsymbol{F}},\boldsymbol{\Sigma}_{\boldsymbol{H}},\Sigma_J,\varphi,\boldsymbol{\Sigma}_{\boldsymbol{D}_0},\boldsymbol{\Sigma}_{\boldsymbol{d}}} \left\{ \int_V \Phi(\mathcal{V}^m, \Sigma^e_{\mathcal{V}}) dV \right. \\
&+ \int_V [\boldsymbol{\Sigma}_{\boldsymbol{F}} : (\boldsymbol{F}_{\boldsymbol{x}} - \boldsymbol{F}) + \boldsymbol{\Sigma}_{\boldsymbol{H}} : (\boldsymbol{H}_{\boldsymbol{x}} - \boldsymbol{H}) + \Sigma_J(J_{\boldsymbol{x}} - J) \\
&\left. + \boldsymbol{D}_0 \cdot (\boldsymbol{\Sigma}_{\boldsymbol{D}_0} + \boldsymbol{\nabla}_0 \varphi) + \boldsymbol{\Sigma}_{\boldsymbol{d}} \cdot \boldsymbol{F}_{\boldsymbol{x}} \boldsymbol{D}_0] \, dV - \Pi_{ext}(\boldsymbol{x}, \varphi) \right\} .
\end{aligned} \tag{33}$$

Notice that a systematic presentation of these (31)-(33) and other mixed variational principles has been already detailed in [1]. They all rely on the consideration of convex multi-variable constitutive models, which guarantees the existence of Legendre transformations between the various energy density functionals. For completeness, all of these relationships are presented in Appendix B.

4. Finite Element discretisation

4.1. General remarks

The implementation of the variational principles described in the previous section is based on a finite element partition (tesselation) of the domain V (representing an electro active polymer in its initial configuration) into a set of elements. Inside each element the problem variables can be interpolated in terms of a set of nodal shape functions as,

$$\boldsymbol{x} = \sum_{a=1}^{n_{\boldsymbol{x}}} \boldsymbol{x}_a N^{\boldsymbol{x}}_a; \quad \boldsymbol{F} = \sum_{a=1}^{n_{\boldsymbol{F}}} \boldsymbol{F}_a N^{\boldsymbol{F}}_a; \quad ...; \quad \boldsymbol{D}_0 = \sum_{a=1}^{n_{\boldsymbol{D}_0}} \boldsymbol{D}_{0a} N^{\boldsymbol{D}_0}_a; \quad ... \tag{34}$$

where a denotes the nodes used in the interpolation of the above variables and $n_{(\bullet)}$ denotes the number of nodes associated to the variable $(\bullet)$. In general, different interpolations are used to describe different variables. The same interpolation space is used for work conjugate pairs; that is, $N^{\boldsymbol{F}}_a = N^{\boldsymbol{\Sigma}_{\boldsymbol{F}}}_a$, $N^{\boldsymbol{D}_0}_a = N^{\boldsymbol{\Sigma}_{\boldsymbol{D}_0}}_a$ etc. All the variables and their virtual and incremental variations $\{\boldsymbol{x}, \delta\boldsymbol{u}, \boldsymbol{u}\}$, $\{\boldsymbol{F}, \delta\boldsymbol{F}, \Delta\boldsymbol{F}\}$, $\{\boldsymbol{D}_0, \delta\boldsymbol{D}_0, \Delta\boldsymbol{D}_0\}$ etc. are interpolated using the same interpolation spaces (Galerkin-type discretisation).

The variational framework associated to the variational principles Π_W and Π_Φ in (31) and (33), respectively, can be implemented using a variety of finite element spaces. Of course, not all choices will lead to effective or valid finite element formulations. In particular, the Ladyženskaja-Babuška-Brezzi [46, 66] (LBB) condition must be satisfied. Alternatively, the LBB condition can be circumvented by resorting to stabilised formulations [35, 36, 67, 68].

Mixed formulations might result in expensive computations due to the large number of additional variables involved. However, careful analysis of the continuity required for each of the variables, shows that only displacements and electric potential need to be continuous across elements. Stress, strain and electric variables can actually be discretised independently on each element of the mesh. Crucially, a static condensation procedure of the residuals and stiffness matrices associated to those variables for which continuity across elements is not required leads to a computationally comparable cost with respect to displacement-potential formulations [24].

A plausible choice [22, 24] for the interpolation functions of the different variables involved in the variational principle Π_W (31) considers a quadratic tetrahedron element for the geometry and electric potential discretisation, piecewise linear element by element interpolations for $\{\boldsymbol{F}, \boldsymbol{\Sigma_F}\}$, $\{\boldsymbol{H}, \boldsymbol{\Sigma_H}\}$, $\{\boldsymbol{d}, \boldsymbol{\Sigma_d}\}$ and $\boldsymbol{D}_0$ and piecewise constant interpolation for $\{J, \Sigma_J\}$.

Similarly, a quadratic tetrahedron element for the geometry and electric potential discretisation, piecewise linear interpolations for $\{\boldsymbol{F}, \boldsymbol{\Sigma_F}\}$, $\{\boldsymbol{H}, \boldsymbol{\Sigma_H}\}$, $\{\boldsymbol{D}_0, \boldsymbol{\Sigma}_{\boldsymbol{D}_0}\}$ and $\boldsymbol{d}$ and a piecewise constant interpolation for $\{J, \Sigma_J\}$ is used for the formulation associated to the variational principle Π_Φ (33).

In what follows, for a variational principle $\Pi_{\boldsymbol{\mathcal{U}}}$ formulated in terms of the variables $\boldsymbol{\mathcal{U}}$, for which virtual and incremental variations are denoted as $\delta\boldsymbol{\mathcal{U}}$ and $\Delta\boldsymbol{\mathcal{U}}$, respectively, a $k-$iterative Newton-Raphson process is usually established by solving a linearised system of equations for the increment $\Delta\boldsymbol{\mathcal{U}}$ as

$$D^2\Pi_{\boldsymbol{\mathcal{U}}}(\boldsymbol{\mathcal{U}}_k)[\delta\boldsymbol{\mathcal{U}}; \Delta\boldsymbol{\mathcal{U}}] = -D\Pi_{\boldsymbol{\mathcal{U}}}(\boldsymbol{\mathcal{U}}_k)[\delta\boldsymbol{\mathcal{U}}]; \qquad \boldsymbol{\mathcal{U}}_{k+1} = \boldsymbol{\mathcal{U}}_k + \Delta\boldsymbol{\mathcal{U}}. \tag{35}$$

Finite element discretisation of above system (35) results in the well known residual vector $\boldsymbol{R}_{\boldsymbol{\mathcal{U}}}$ and tangent stiffness matrix $\boldsymbol{K}_{\boldsymbol{\mathcal{U}}\boldsymbol{\mathcal{U}}}$.

4.2. Finite Element semi-discretisation of the variational principle Π_W

For notational convenience, the following set q of variables is introduced

$$q = \{\boldsymbol{x}, \varphi, \mathcal{Y}, \Sigma_{\mathcal{Y}}, \boldsymbol{D}_0\}, \tag{36}$$

where the sets $\mathcal{Y}$ and $\Sigma_{\mathcal{Y}}$ are

$$\mathcal{Y} = \{\boldsymbol{F}, \boldsymbol{H}, J, \boldsymbol{d}\}; \qquad \Sigma_{\mathcal{Y}} = \{\boldsymbol{\Sigma}_{\boldsymbol{F}}, \boldsymbol{\Sigma}_{\boldsymbol{H}}, \Sigma_J, \boldsymbol{\Sigma}_{\boldsymbol{d}}\}. \tag{37}$$

Virtual and incremental variations of the elements in the sets $\mathcal{Y}$ and $\Sigma_{\mathcal{Y}}$ in above equation (37) are denoted as

$$\begin{aligned} \delta\mathcal{Y} &= \{\delta\boldsymbol{F}, \delta\boldsymbol{H}, \delta J, \delta\boldsymbol{\Sigma}_{\boldsymbol{D}_0}\}; & \delta\Sigma_{\mathcal{Y}} &= \{\delta\boldsymbol{\Sigma}_{\boldsymbol{F}}, \delta\boldsymbol{\Sigma}_{\boldsymbol{H}}, \delta\Sigma_J, \delta\boldsymbol{\Sigma}_{\boldsymbol{d}}\}; \\ \Delta\mathcal{Y} &= \{\Delta\boldsymbol{F}, \Delta\boldsymbol{H}, \Delta J, \Delta\boldsymbol{\Sigma}_{\boldsymbol{d}}\}; & \Delta\Sigma_{\mathcal{Y}} &= \{\Delta\boldsymbol{\Sigma}_{\boldsymbol{F}}, \Delta\boldsymbol{\Sigma}_{\boldsymbol{H}}, \Delta\Sigma_J, \Delta\boldsymbol{\Sigma}_{\boldsymbol{d}}\}. \end{aligned} \tag{38}$$

The discrete stationary conditions of the variational principle Π_W (31) with respect to virtual changes in the geometry and in the electric potential (i.e. equilibrium and Gauss law) are

$$\begin{aligned} D\Pi_W[\delta\boldsymbol{u}] &= \sum_{a=1}^{n_{\boldsymbol{x}}} \boldsymbol{R}^a_{\boldsymbol{x}} \cdot \delta\boldsymbol{u}^a; \quad \boldsymbol{R}^a_{\boldsymbol{x}} = \int_V \boldsymbol{P}_W \boldsymbol{\nabla}_0 N^{\boldsymbol{x}}_a \, dV - \int_V \boldsymbol{f}_0 N^{\boldsymbol{x}}_a \, dV - \int_{\partial_t V} \boldsymbol{t}_0 N^{\boldsymbol{x}}_a \, dA; \\ D\Pi_W[\delta\varphi] &= \sum_{a=1}^{n_\varphi} R^a_\varphi \cdot \delta\varphi^a; \quad R^a_\varphi = \int_V \boldsymbol{D}_0 \cdot \boldsymbol{\nabla}_0 N^\varphi_a \, dV - \int_V \rho_0 N^\varphi_a \, dV - \int_{\partial_\omega V} \omega_0 N^\varphi_a \, dA, \end{aligned} \tag{39}$$

where the first Piola-Kirchhoff stress tensor $\boldsymbol{P}_W$ is evaluated as

$$\boldsymbol{P}_W = \boldsymbol{\Sigma}_{\boldsymbol{F}} + \boldsymbol{\Sigma}_{\boldsymbol{H}} \times \boldsymbol{F}_{\boldsymbol{x}} + \Sigma_J \boldsymbol{H}_{\boldsymbol{x}} + \boldsymbol{\Sigma}_{\boldsymbol{d}} \otimes \boldsymbol{D}_0. \tag{40}$$

The discrete stationary conditions of the variational principle Π_W (31) with respect to virtual changes of the elements of the set $\mathcal{Y}$ and $\boldsymbol{D}_0$ (i.e. constitutive and Faraday laws) is

$$\begin{aligned} D\Pi_W[\delta\mathcal{Y}, \delta\boldsymbol{D}_0] = &\sum_{a=1}^{n_{\boldsymbol{F}}} \boldsymbol{R}^a_{\boldsymbol{F}} : \delta\boldsymbol{F}^a + \sum_{a=1}^{n_{\boldsymbol{H}}} \boldsymbol{R}^a_{\boldsymbol{H}} : \delta\boldsymbol{H}^a + \sum_{a=1}^{n_J} R^a_J \delta J^a \\ &+ \sum_{a=1}^{n_{\boldsymbol{d}}} \boldsymbol{R}^a_{\boldsymbol{d}} \cdot \delta\boldsymbol{d}^a + \sum_{a=1}^{n_{\boldsymbol{D}_0}} \boldsymbol{R}^a_{\boldsymbol{D}_0} \cdot \delta\boldsymbol{D}^a_0, \end{aligned} \tag{41}$$

where the different residuals emerging in above equation (41) are

$$\begin{aligned}
\boldsymbol{R}^a_{\boldsymbol{F}} &= \int_V \left(\frac{\partial W}{\partial \boldsymbol{F}} - \boldsymbol{\Sigma}_{\boldsymbol{F}}\right) N^{\boldsymbol{F}}_a \, dV; & \boldsymbol{R}^a_{\boldsymbol{H}} &= \int_V \left(\frac{\partial W}{\partial \boldsymbol{H}} - \boldsymbol{\Sigma}_{\boldsymbol{H}}\right) N^{\boldsymbol{H}}_a \, dV; \\
R^a_J &= \int_V \left(\frac{\partial W}{\partial J} - \Sigma_J\right) N^J_a \, dV; & \boldsymbol{R}^a_{\boldsymbol{d}} &= \int_V \left(\frac{\partial W}{\partial \boldsymbol{d}} - \boldsymbol{\Sigma}_{\boldsymbol{d}}\right) N^{\boldsymbol{d}}_a \, dV; \\
\boldsymbol{R}^a_{\boldsymbol{D}_0} &= \int_V \left(\frac{\partial W}{\partial \boldsymbol{D}_0} + \boldsymbol{\nabla}_0 \varphi + \boldsymbol{F_x}^T \boldsymbol{\Sigma}_{\boldsymbol{d}}\right) N^{\boldsymbol{d}}_a \, dV.
\end{aligned} \tag{42}$$

The discrete stationary conditions with respect to the elements of the set $\Sigma_{\mathcal{Y}}$ (37) (i.e. compatibility) yields

$$\begin{aligned}
D\Pi_W[\delta\Sigma_{\mathcal{Y}}] = &\sum_{a=1}^{n_{\boldsymbol{\Sigma_F}}} \boldsymbol{R}^a_{\boldsymbol{\Sigma_F}} : \delta \boldsymbol{\Sigma_F}^a + \sum_{a=1}^{n_{\boldsymbol{\Sigma_H}}} \boldsymbol{R}^a_{\boldsymbol{\Sigma_H}} : \delta \boldsymbol{\Sigma_H}^a + \sum_{a=1}^{n_{\Sigma_J}} R^a_{\Sigma_J} \delta \Sigma^a_J \\
&+ \sum_{a=1}^{n_{\boldsymbol{\Sigma_d}}} \boldsymbol{R}^a_{\boldsymbol{\Sigma_d}} \cdot \delta \boldsymbol{\Sigma_d}^a,
\end{aligned} \tag{43}$$

where the residuals in above equation (43) are

$$\begin{aligned}
\boldsymbol{R}^a_{\boldsymbol{\Sigma_F}} &= \int_V (\boldsymbol{F_x} - \boldsymbol{F}) \, N^{\boldsymbol{F}}_a \, dV; & \boldsymbol{R}^a_{\boldsymbol{\Sigma_H}} &= \int_V (\boldsymbol{H_x} - \boldsymbol{H}) \, N^{\boldsymbol{H}}_a \, dV; \\
R^a_{\Sigma_J} &= \int_V (J_{\boldsymbol{x}} - J) \, N^J_a \, dV; & \boldsymbol{R}^a_{\boldsymbol{\Sigma_d}} &= \int_V (\boldsymbol{F_x} \boldsymbol{D}_0 - \boldsymbol{d}) \, N^{\boldsymbol{d}}_a \, dV.
\end{aligned} \tag{44}$$

The stiffness matrices arising from the variational principle Π_W (31) (before static condensation is carried out) (31) emerge as

$$D^2\Pi_W\left[\delta q; \Delta q\right] = \begin{bmatrix} \delta \mathbf{u} \\ \delta \boldsymbol{\phi} \\ \delta \boldsymbol{\mathcal{Y}} \\ \delta \boldsymbol{\Sigma}_{\mathcal{Y}} \\ \delta \mathbf{D}_0 \end{bmatrix}^T \begin{bmatrix} \boldsymbol{K}_{\boldsymbol{xx}} & \mathbf{0} & \mathbf{0} & \boldsymbol{K}_{\boldsymbol{x}\Sigma_{\mathcal{Y}}} & \boldsymbol{K}_{\boldsymbol{x}\boldsymbol{D}_0} \\ \mathbf{0} & \mathbf{0} & \mathbf{0} & \mathbf{0} & \boldsymbol{K}_{\varphi \boldsymbol{D}_0} \\ \mathbf{0} & \mathbf{0} & \boldsymbol{K}_{\mathcal{Y}\mathcal{Y}} & \boldsymbol{K}_{\mathcal{Y}\Sigma_{\mathcal{Y}}} & \boldsymbol{K}_{\mathcal{Y}\boldsymbol{D}_0} \\ \boldsymbol{K}_{\Sigma_{\mathcal{Y}}\boldsymbol{x}} & \mathbf{0} & \boldsymbol{K}_{\Sigma_{\mathcal{Y}}\mathcal{Y}} & \mathbf{0} & \boldsymbol{K}_{\Sigma_{\mathcal{Y}}\boldsymbol{D}_0} \\ \boldsymbol{K}_{\boldsymbol{D}_0\boldsymbol{x}} & \boldsymbol{K}_{\boldsymbol{D}_0\varphi} & \boldsymbol{K}_{\boldsymbol{D}_0\mathcal{Y}} & \boldsymbol{K}_{\boldsymbol{D}_0\Sigma_{\mathcal{Y}}} & \boldsymbol{K}_{\boldsymbol{D}_0\boldsymbol{D}_0} \end{bmatrix} \begin{bmatrix} \mathbf{u} \\ \Delta \boldsymbol{\phi} \\ \Delta \boldsymbol{\mathcal{Y}} \\ \Delta \boldsymbol{\Sigma}_{\mathcal{Y}} \\ \Delta \mathbf{D}_0 \end{bmatrix}, \tag{45}$$

Notice that since the above formulation emerges from a variational principle, namely Π_W in (31), the resulting global stiffness matrix is symmetric.

Hence, the following relations will be satisfied: $\boldsymbol{K}_{\Sigma_{\mathcal{Y}}\boldsymbol{x}} = \boldsymbol{K}^{T}_{\boldsymbol{x}\Sigma_{\mathcal{Y}}}$, $\boldsymbol{K}_{\boldsymbol{\Sigma_{D_0}}\boldsymbol{x}} = \boldsymbol{K}^{T}_{\boldsymbol{x}\boldsymbol{\Sigma_{D_0}}}$, etc. The expressions for the non-zero blocks in the stiffness matrix defined in equation (45) are presented below.

The procedure to obtain the stiffness matrix contribution $\boldsymbol{K}^{ab}_{\boldsymbol{xx}}$ has been already presented in Reference [24] in the context of nonlinear elasticity

$$\left[\boldsymbol{K}^{ab}_{\boldsymbol{xx}}\right]_{ij} = \mathcal{E}_{ijk}\left[\boldsymbol{k}^{ab}_{\boldsymbol{xx}}\right]_{k}; \qquad \boldsymbol{k}^{ab}_{\boldsymbol{xx}} = \int_{V} \left(\boldsymbol{\Sigma_H} + \Sigma_J \boldsymbol{F_x}\right)\left(\boldsymbol{\nabla}_0 N^{\boldsymbol{x}}_a \times \boldsymbol{\nabla}_0 N^{\boldsymbol{x}}_b\right) dV. \tag{46}$$

The stiffness matrix contribution $\boldsymbol{K}^{ab}_{\boldsymbol{x}\Sigma_{\mathcal{Y}}}$ arising from the linearisation of $\boldsymbol{R}^{a}_{\boldsymbol{x}}$ with respect to incremental changes of the elements in the set $\Sigma^{ab}_{\mathcal{Y}}$ is defined as

$$\boldsymbol{K}^{ab}_{\boldsymbol{x}\Sigma_{\mathcal{Y}}} = \left[\boldsymbol{K}^{ab}_{\boldsymbol{x}\boldsymbol{\Sigma_F}} \quad \boldsymbol{K}^{ab}_{\boldsymbol{x}\boldsymbol{\Sigma_H}} \quad \boldsymbol{K}^{ab}_{\boldsymbol{x}\Sigma_J} \quad \boldsymbol{K}^{ab}_{\boldsymbol{x}\boldsymbol{\Sigma_d}}\right], \tag{47}$$

where the individual stiffness matrices in (47) are defined as

$$\begin{aligned}
&\boldsymbol{K}^{ab}_{\boldsymbol{x}\boldsymbol{\Sigma_F}} = \int_{V} \left(\boldsymbol{I} \otimes \boldsymbol{\nabla}_0 N^{\boldsymbol{x}}_a\right) N^{\boldsymbol{F}}_b \, dV; \qquad \left[\boldsymbol{K}^{ab}_{\boldsymbol{x}\boldsymbol{\Sigma_H}}\right]_{ijI} = \mathcal{E}_{ijk}\left[\int_{V} \left(\boldsymbol{F_x} \boldsymbol{\times} \boldsymbol{\nabla}_0 N^{\boldsymbol{x}}_a\right) N^{\boldsymbol{H}}_b \, dV\right]_{kI};\\
&\boldsymbol{K}^{ab}_{\boldsymbol{x}\Sigma_J} = \int_{V} N^{J}_b \boldsymbol{H_x} \boldsymbol{\nabla}_0 N^{\boldsymbol{x}}_a \, dV; \qquad \boldsymbol{K}^{ab}_{\boldsymbol{x}\boldsymbol{\Sigma_d}} = \int_{V} \left(\boldsymbol{D}_0 \cdot \boldsymbol{\nabla}_0 N^{\boldsymbol{x}}_a\right) N^{\boldsymbol{d}}_b \boldsymbol{I} \, dV.
\end{aligned} \tag{48}$$

The stiffness matrix contribution $\boldsymbol{K}^{ab}_{\boldsymbol{x}\boldsymbol{D}_0}$ is obtained as

$$\boldsymbol{K}^{ab}_{\boldsymbol{x}\boldsymbol{D}_0} = \int_{V} \left(\boldsymbol{\Sigma_d} \otimes \boldsymbol{\nabla}_0 N^{\boldsymbol{x}}_a\right) N^{\boldsymbol{D}_0}_b \, dV. \tag{49}$$

The only stiffness matrix contribution emerging from the linearisation of the residual $\boldsymbol{R}^{a}_{\varphi}$, namely $\boldsymbol{K}^{ab}_{\varphi\boldsymbol{D}_0}$ is obtained as

$$\boldsymbol{K}^{ab}_{\varphi\boldsymbol{D}_0} = \int_{V} N^{\varphi}_a N^{\boldsymbol{D}_0}_b \boldsymbol{I} \, dV. \tag{50}$$

The stiffness matrix contribution of the diagonal block $\boldsymbol{K}_{\mathcal{Y}\mathcal{Y}}$ adopts the following expression

$$\boldsymbol{K}^{ab}_{\mathcal{Y}\mathcal{Y}} = \int_{V} \begin{bmatrix}
N^{\boldsymbol{F}}_a N^{\boldsymbol{F}}_b W_{\boldsymbol{FF}} & N^{\boldsymbol{F}}_a N^{\boldsymbol{H}}_b W_{\boldsymbol{FH}} & N^{\boldsymbol{F}}_a N^{J}_b W_{\boldsymbol{F}J} & N^{\boldsymbol{F}}_a N^{\boldsymbol{d}}_b W_{\boldsymbol{Fd}} \\
N^{\boldsymbol{H}}_a N^{\boldsymbol{F}}_b W_{\boldsymbol{HF}} & N^{\boldsymbol{H}}_a N^{\boldsymbol{H}}_b W_{\boldsymbol{HH}} & N^{\boldsymbol{H}}_a N^{J}_b W_{\boldsymbol{H}J} & N^{\boldsymbol{H}}_a N^{\boldsymbol{d}}_b W_{\boldsymbol{Hd}} \\
N^{J}_a N^{\boldsymbol{F}}_b W_{J\boldsymbol{F}} & N^{J}_a N^{\boldsymbol{H}}_b W_{J\boldsymbol{H}} & N^{J}_a N^{J}_b W_{JJ} & N^{J}_a N^{\boldsymbol{d}}_b W_{J\boldsymbol{d}} \\
N^{\boldsymbol{d}}_a N^{\boldsymbol{F}}_b W_{\boldsymbol{dF}} & N^{\boldsymbol{d}}_a N^{\boldsymbol{H}}_b W_{\boldsymbol{dH}} & N^{\boldsymbol{d}}_a N^{J}_b W_{\boldsymbol{d}J} & N^{\boldsymbol{d}}_a N^{\boldsymbol{d}}_b W_{\boldsymbol{dd}}
\end{bmatrix} dV, \tag{51}$$

where the Hessian operator $[\mathbb{H}_W]$ has been defined in equation (19). The stiffness matrix contribution $\boldsymbol{K}^{ab}_{\mathcal{Y}\Sigma_\mathcal{Y}}$ emerging from the linearisation of the residual $\boldsymbol{R}^a_\mathcal{Y}$ with respect to incremental changes in the elements of the set $\Sigma_\mathcal{Y}$ is

$$\boldsymbol{K}^{ab}_{\mathcal{Y}\Sigma_\mathcal{Y}} = -\int_V \begin{bmatrix} N^{\boldsymbol{F}}_a N^{\boldsymbol{F}}_b \boldsymbol{\mathcal{I}} & \mathbf{0} & \mathbf{0} & \mathbf{0} \\ \mathbf{0} & N^{\boldsymbol{H}}_a N^{\boldsymbol{H}}_b \boldsymbol{\mathcal{I}} & \mathbf{0} & \mathbf{0} \\ \mathbf{0} & \mathbf{0} & N^J_a N^J_b & \mathbf{0} \\ \mathbf{0} & \mathbf{0} & \mathbf{0} & N^{\boldsymbol{d}}_a N^{\boldsymbol{d}}_b \boldsymbol{I} \end{bmatrix} dV, \tag{52}$$

where $\boldsymbol{\mathcal{I}}$ denotes the components of the fourth order identity tensor, defined as $\mathcal{I}_{iIjJ} = \delta_{ij}\delta_{IJ}$. The stiffness matrix contribution associated to the residual $\boldsymbol{R}^a_\mathcal{Y}$, namely $\boldsymbol{K}^{ab}_{\mathcal{Y}\boldsymbol{D}_0}$ is defined as

$$\boldsymbol{K}^{ab}_{\mathcal{Y}\boldsymbol{D}_0} = \int_V \begin{bmatrix} N^{\boldsymbol{F}}_a N^{\boldsymbol{D}_0}_b W_{\boldsymbol{F}\boldsymbol{D}_0} & N^{\boldsymbol{H}}_a N^{\boldsymbol{D}_0}_b W_{\boldsymbol{H}\boldsymbol{D}_0} & N^J_a N^{\boldsymbol{D}_0}_b W_{J\boldsymbol{D}_0} & N^{\boldsymbol{d}}_a N^{\boldsymbol{D}_0}_b W_{\boldsymbol{d}\boldsymbol{D}_0} \end{bmatrix} dV. \tag{53}$$

The stiffness matrix contribution $\boldsymbol{K}^{ab}_{\Sigma_\mathcal{Y}\boldsymbol{D}_0}$ resulting from the linearisation of the residual $\boldsymbol{R}^a_{\Sigma_\mathcal{Y}}$ with respect to incremental changes in $\boldsymbol{D}_0$ is defined as

$$\boldsymbol{K}^{ab}_{\Sigma_\mathcal{Y}\boldsymbol{D}_0} = \begin{bmatrix} \mathbf{0} & \mathbf{0} & \mathbf{0} & \boldsymbol{K}^{ab}_{\boldsymbol{\Sigma_d}\boldsymbol{D}_0} \end{bmatrix}, \qquad \boldsymbol{K}^{ab}_{\boldsymbol{\Sigma_d}\boldsymbol{D}_0} = \int_V N^{\boldsymbol{d}}_a N^{\boldsymbol{D}_0}_b \boldsymbol{F_x}\, dV. \tag{54}$$

Finally, the block $\boldsymbol{K}^{ab}_{\boldsymbol{D}_0\boldsymbol{D}_0}$ is obtained from

$$\boldsymbol{K}^{ab}_{\boldsymbol{D}_0\boldsymbol{D}_0} = \int_V N^{\boldsymbol{D}_0}_a N^{\boldsymbol{D}_0}_b W_{\boldsymbol{D}_0\boldsymbol{D}_0}\, dV. \tag{55}$$

4.2.1. Static condensation

This process will be illustrated for the particular formulation associated to the variational principle Π_W (31). Similar procedure can be applied to the formulation associated to the variational principle Π_Φ (33). The algebraic system of equations obtained locally at a particular element e (see equation (45)) is written as

$$\boldsymbol{K}^e_{\text{local}} \Delta q^e = \tilde{\boldsymbol{R}}_{\text{local}}, \tag{56}$$

with

$$\tilde{\boldsymbol{R}}_{\text{local}} = \begin{bmatrix} \boldsymbol{R}^e_{\boldsymbol{x}} & \boldsymbol{R}^e_{\varphi} & \boldsymbol{R}^e_{\mathcal{Y}} & \boldsymbol{R}^e_{\Sigma_\mathcal{Y}} & \boldsymbol{R}^e_{\boldsymbol{D}_0} \end{bmatrix}^T; \qquad \Delta q^e = \begin{bmatrix} \mathbf{u}^e & \Delta\boldsymbol{\varphi}^e & \Delta\boldsymbol{\mathcal{Y}}^e & \Delta\boldsymbol{\Sigma}^e_\mathcal{Y} & \Delta\mathbf{D}^e_0 \end{bmatrix}^T, \tag{57}$$

and where the local stiffness matrix $\boldsymbol{K}^e_{\text{local}}$ is defined as,

$$\boldsymbol{K}^e_{\text{local}} = \begin{bmatrix} \boldsymbol{K}^e_{\boldsymbol{x}\boldsymbol{x}} & \mathbf{0} & \mathbf{0} & \boldsymbol{K}^e_{\boldsymbol{x}\Sigma_{\mathcal{Y}}} & \boldsymbol{K}^e_{\boldsymbol{x}\boldsymbol{D}_0} \\ \mathbf{0} & \mathbf{0} & \mathbf{0} & \mathbf{0} & \boldsymbol{K}^e_{\varphi\boldsymbol{D}_0} \\ \mathbf{0} & \mathbf{0} & \boldsymbol{K}^e_{\mathcal{Y}\mathcal{Y}} & \boldsymbol{K}^e_{\mathcal{Y}\Sigma_{\mathcal{Y}}} & \boldsymbol{K}^e_{\mathcal{Y}\boldsymbol{D}_0} \\ \boldsymbol{K}^e_{\Sigma_{\mathcal{Y}}\boldsymbol{x}} & \mathbf{0} & \boldsymbol{K}^e_{\Sigma_{\mathcal{Y}}\mathcal{Y}} & \mathbf{0} & \boldsymbol{K}^e_{\Sigma_{\mathcal{Y}}\boldsymbol{D}_0} \\ \boldsymbol{K}^e_{\boldsymbol{D}_0\boldsymbol{x}} & \boldsymbol{K}^e_{\boldsymbol{D}_0\varphi} & \boldsymbol{K}^e_{\boldsymbol{D}_0\mathcal{Y}} & \boldsymbol{K}^e_{\boldsymbol{D}_0\Sigma_{\mathcal{Y}}} & \boldsymbol{K}^e_{\boldsymbol{D}_0\boldsymbol{D}_0} \end{bmatrix}. \tag{58}$$

Notice that the superscript e in equations (56) and (58) has been used to denote the local (element) character of the variables involved. The fourth, fifth and third (in this order) equations (forth, fifth and third rows) in above (56) enables the local variables $\Delta\boldsymbol{\mathcal{Y}}^e$, $\Delta\mathbf{D}^e_0$ and $\Delta\boldsymbol{\Sigma}^e_{\mathcal{Y}}$ to be expressed as

$$\Delta\boldsymbol{\mathcal{Y}}^e = -\left[\boldsymbol{K}^e_{\Sigma_{\mathcal{Y}}\mathcal{Y}}\right]^{-1}\left(\boldsymbol{R}^e_{\Sigma_{\mathcal{Y}}} + \boldsymbol{K}^e_{\Sigma_{\mathcal{Y}}\boldsymbol{x}}\mathbf{u}^e + \boldsymbol{K}^e_{\Sigma_{\mathcal{Y}}\boldsymbol{D}_0}\Delta\mathbf{D}^e_0\right); \tag{59a}$$

$$\Delta\mathbf{D}^e_0 = -\left[\boldsymbol{K}^e_{\boldsymbol{D}_0\boldsymbol{D}_0}\right]^{-1}\left(\boldsymbol{R}^e_{\boldsymbol{D}_0} + \boldsymbol{K}^e_{\boldsymbol{D}_0\boldsymbol{x}}\mathbf{u}^e + \boldsymbol{K}^e_{\boldsymbol{D}_0\varphi}\Delta\boldsymbol{\varphi}^e + \boldsymbol{K}^e_{\boldsymbol{D}_0\mathcal{Y}}\Delta\boldsymbol{\mathcal{Y}}^e + \boldsymbol{K}^e_{\boldsymbol{D}_0\Sigma_{\mathcal{Y}}}\Delta\boldsymbol{\Sigma}^e_{\mathcal{Y}}\right); \tag{59b}$$

$$\Delta\boldsymbol{\Sigma}^e_{\mathcal{Y}} = -\left[\boldsymbol{K}^e_{\mathcal{Y}\Sigma_{\mathcal{Y}}}\right]^{-1}\left(\boldsymbol{R}^e_{\mathcal{Y}} + \boldsymbol{K}^e_{\mathcal{Y}\mathcal{Y}}\Delta\boldsymbol{\mathcal{Y}}^e + \boldsymbol{K}^e_{\mathcal{Y}\boldsymbol{D}_0}\Delta\mathbf{D}^e_0\right). \tag{59c}$$

Substitution of $\Delta\boldsymbol{\mathcal{Y}}^e$ (59a) into the expression for $\Delta\mathbf{D}^e_0$ in (59b) and subsequent substitution of these two into the expression for $\Delta\boldsymbol{\Sigma}^e_{\mathcal{Y}}$ in (59c) enables the local variable $\Delta\boldsymbol{\Sigma}^e_{\mathcal{Y}}$ to be expressed in terms of the geometry and electric potential as

$$\Delta\boldsymbol{\Sigma}^e_{\mathcal{Y}} = \bar{\boldsymbol{R}}^e_{\Sigma_{\mathcal{Y}}} + \boldsymbol{M}^e_{\Sigma_{\mathcal{Y}}\boldsymbol{x}}\mathbf{u}^e + \boldsymbol{M}^e_{\Sigma_{\mathcal{Y}}\varphi}\Delta\boldsymbol{\phi}^e, \tag{60}$$

where $\bar{\boldsymbol{R}}^e_{\Sigma_{\mathcal{Y}}}$, $\boldsymbol{M}^e_{\Sigma_{\mathcal{Y}}\boldsymbol{x}}$ and $\boldsymbol{M}^e_{\Sigma_{\mathcal{Y}}\varphi}$ will be defined in equation (C.1). Using this expression for $\Delta\boldsymbol{\Sigma}^e_{\mathcal{Y}}$, the fifth equation in (56) enables the local variable $\Delta\mathbf{D}^e_0$ to be expressed as

$$\Delta\mathbf{D}^e_0 = \bar{\boldsymbol{R}}^e_{\boldsymbol{D}_0} + \bar{\boldsymbol{M}}^e_{\boldsymbol{D}_0\boldsymbol{x}}\mathbf{u}^e + \bar{\boldsymbol{M}}^e_{\boldsymbol{D}_0\varphi}\Delta\boldsymbol{\phi}^e, \tag{61}$$

where the auxiliary residuals and matrices $\bar{\boldsymbol{R}}^e_{\boldsymbol{D}_0}$, $\bar{\boldsymbol{M}}^e_{\boldsymbol{D}_0\boldsymbol{x}}$ and $\bar{\boldsymbol{M}}^e_{\boldsymbol{D}_0\varphi}$ will be defined in equation (C.1). Finally, the third equation in (56) enables the local variable $\Delta\boldsymbol{\mathcal{Y}}^e$ to be expressed as

$$\Delta\boldsymbol{\mathcal{Y}}^e = \bar{\boldsymbol{R}}^e_{\mathcal{Y}} + \bar{\boldsymbol{M}}^e_{\mathcal{Y}\boldsymbol{x}}\mathbf{u}^e + \bar{\boldsymbol{M}}^e_{\mathcal{Y}\varphi}\Delta\boldsymbol{\phi}^e, \tag{62}$$

where the auxiliary residuals and matrices $\bar{\boldsymbol{R}}^e_{\mathcal{Y}}$, $\bar{\boldsymbol{M}}^e_{\mathcal{Y}\boldsymbol{x}}$ and $\bar{\boldsymbol{M}}^e_{\mathcal{Y}\varphi}$ will be defined in equation (C.1). All in all, the new expressions for the incremental

local variables $\Delta\boldsymbol{\Sigma}^e_{\mathcal{Y}}$, $\Delta\mathbf{D}^e_0$ and $\Delta\boldsymbol{\mathcal{Y}}^e$ in terms $\mathbf{u}^e$ and $\Delta\boldsymbol{\phi}^e$ enable the local algebraic system of equations in (56) to be formulated exclusively in terms of the unknowns $\mathbf{u}^e$ and $\Delta\boldsymbol{\phi}^e$ as

$$\begin{bmatrix} \bar{\boldsymbol{K}}^e_{\boldsymbol{x}\boldsymbol{x}} & \bar{\boldsymbol{K}}^e_{\boldsymbol{x}\varphi} \\ \bar{\boldsymbol{K}}^e_{\varphi\boldsymbol{x}} & \bar{\boldsymbol{K}}^e_{\varphi\varphi} \end{bmatrix} \begin{bmatrix} \mathbf{u}^e \\ \Delta\boldsymbol{\phi}^e \end{bmatrix} = \begin{bmatrix} \bar{\boldsymbol{R}}^e_{\boldsymbol{x}} \\ \bar{\boldsymbol{R}}^e_{\varphi} \end{bmatrix}, \tag{63}$$

where the modified residuals (63) are expressed as

$$\bar{\boldsymbol{R}}^e_{\boldsymbol{x}} = \boldsymbol{R}_{\boldsymbol{x}}{}^e + \boldsymbol{K}^e_{\boldsymbol{x}\Sigma_{\mathcal{Y}}}\bar{\boldsymbol{R}}^e_{\Sigma_{\mathcal{Y}}} + \boldsymbol{K}^e_{\boldsymbol{x}\boldsymbol{D}_0}\bar{\bar{\boldsymbol{R}}}^e_{\boldsymbol{D}_0}; \qquad \bar{\boldsymbol{R}}^e_{\varphi} = \boldsymbol{R}^e_{\varphi} + \boldsymbol{K}^e_{\varphi\boldsymbol{D}_0}. \tag{64}$$

Finally, the modified stiffness matrices in (63) are expressed as

$$\begin{aligned} \bar{\boldsymbol{K}}^e_{\boldsymbol{x}\boldsymbol{x}} &= \boldsymbol{K}^e_{\boldsymbol{x}\boldsymbol{x}} + \boldsymbol{K}^e_{\boldsymbol{x}\Sigma_{\mathcal{Y}}}\boldsymbol{M}^e_{\Sigma_{\mathcal{Y}}\boldsymbol{x}} + \boldsymbol{K}^e_{\boldsymbol{x}\boldsymbol{D}_0}\bar{\boldsymbol{M}}^e_{\boldsymbol{D}_0\boldsymbol{x}}; \\ \bar{\boldsymbol{K}}^e_{\boldsymbol{x}\varphi} &= \boldsymbol{K}^e_{\boldsymbol{x}\Sigma_{\mathcal{Y}}}\boldsymbol{M}^e_{\Sigma_{\mathcal{Y}}\varphi} + \boldsymbol{K}^e_{\boldsymbol{x}\boldsymbol{D}_0}\bar{\boldsymbol{M}}_{\boldsymbol{D}_0\varphi}; \\ \bar{\boldsymbol{K}}^e_{\varphi\varphi} &= \boldsymbol{K}^e_{\varphi\boldsymbol{D}_0}\bar{\boldsymbol{M}}^e_{\boldsymbol{D}_0\varphi}. \end{aligned} \tag{65}$$

The expressions for all the auxiliary residuals and stiffness matrices in equations (64) and (65) are presented in equation (C.1).

4.3. Finite Element semi-discretisation of the variational principle Π_Φ

For notational convenience, the following set of variables p is introduced

$$p = \{\boldsymbol{x}, \varphi, \mathcal{D}, \Sigma_{\mathcal{D}}, \boldsymbol{\Sigma}_{\boldsymbol{d}}\}, \tag{66}$$

with

$$\mathcal{D} = \{\boldsymbol{F}, \boldsymbol{H}, J, \boldsymbol{\Sigma}_{\boldsymbol{D}_0}\}; \qquad \Sigma_{\mathcal{D}} = \{\boldsymbol{\Sigma}_{\boldsymbol{F}}, \boldsymbol{\Sigma}_{\boldsymbol{H}}, \Sigma_J, \boldsymbol{D}_0\}. \tag{67}$$

Virtual and incremental variations of the set p are denoted as

$$\delta p = \{\delta\boldsymbol{u}, \delta\varphi, \delta\mathcal{D}, \delta\Sigma_{\mathcal{D}}, \delta\boldsymbol{\Sigma}_{\boldsymbol{d}}\}; \qquad \Delta p = \{\boldsymbol{u}, \Delta\varphi, \Delta\mathcal{D}, \Delta\Sigma_{\mathcal{D}}, \Delta\boldsymbol{\Sigma}_{\boldsymbol{d}}\}, \tag{68}$$

where the virtual and incremental variations of the elements in the sets $\mathcal{D}$ and $\Sigma_{\mathcal{D}}$ in above equation (68) are denoted as

$$\begin{aligned} \delta\mathcal{D} &= \{\delta\boldsymbol{F}, \delta\boldsymbol{H}, \delta J, \delta\boldsymbol{\Sigma}_{\boldsymbol{D}_0}\}; & \delta\Sigma_{\mathcal{D}} &= \{\delta\boldsymbol{\Sigma}_{\boldsymbol{F}}, \delta\boldsymbol{\Sigma}_{\boldsymbol{H}}, \delta\Sigma_J, \delta\boldsymbol{D}_0\}; \\ \Delta\mathcal{D} &= \{\Delta\boldsymbol{F}, \Delta\boldsymbol{H}, \Delta J, \Delta\boldsymbol{\Sigma}_{\boldsymbol{D}_0}\}; & \Delta\Sigma_{\mathcal{D}} &= \{\Delta\boldsymbol{\Sigma}_{\boldsymbol{F}}, \Delta\boldsymbol{\Sigma}_{\boldsymbol{H}}, \Delta\Sigma_J, \Delta\boldsymbol{D}_0\}. \end{aligned} \tag{69}$$

The discrete stationary conditions of the variational principle Π_Φ in (33) with respect to virtual changes of the geometry and with respect to virtual changes of the electric potential are

$$D\Pi_\Phi\left[\delta \boldsymbol{u}\right] = \sum_a \boldsymbol{R}^a_{\boldsymbol{x}} \cdot \delta \boldsymbol{u}^a; \qquad D\Pi_\Phi\left[\delta \varphi\right] = \sum_a R^a_\varphi \cdot \delta \varphi^a, \tag{70}$$

where the expressions for $\boldsymbol{R}^a_{\boldsymbol{x}}$ and R^a_φ in (70) are identical for those in (39). The discrete stationary conditions with respect to the elements in the set $\mathcal{D}$ (67) and $\boldsymbol{\Sigma_d}$ (i.e. constitutive laws) are

$$\begin{aligned} D\Pi_\Phi[\delta\mathcal{D}, \delta\boldsymbol{\Sigma_d}] = &\sum_{a=1}^{n_{\boldsymbol{F}}} \boldsymbol{R}^a_{\boldsymbol{F}} : \delta \boldsymbol{F}^a + \sum_{a=1}^{n_{\boldsymbol{H}}} \boldsymbol{R}^a_{\boldsymbol{H}} : \delta \boldsymbol{H}^a + \sum_{a=1}^{n_J} \boldsymbol{R}^a_J \delta J^a \\ &+ \sum_{a=1}^{n_{\boldsymbol{\Sigma}_{\boldsymbol{D}_0}}} \boldsymbol{R}^a_{\boldsymbol{\Sigma}_{\boldsymbol{D}_0}} \cdot \delta \boldsymbol{\Sigma}^a_{\boldsymbol{D}_0} + \sum_{a=1}^{n_{\boldsymbol{\Sigma_d}}} \boldsymbol{R}^a_{\boldsymbol{\Sigma_d}} \cdot \delta \boldsymbol{\Sigma}^a_{\boldsymbol{d}}, \end{aligned} \tag{71}$$

where the residuals in above equation (71) are

$$\begin{aligned} \boldsymbol{R}^a_{\boldsymbol{F}} &= \int_V \left(\frac{\partial \Phi}{\partial \boldsymbol{F}} - \boldsymbol{\Sigma_F} \right) N^{\boldsymbol{F}}_a \, dV; & \boldsymbol{R}^a_{\boldsymbol{H}} &= \int_V \left(\frac{\partial \Phi}{\partial \boldsymbol{H}} - \boldsymbol{\Sigma_H} \right) N^{\boldsymbol{H}}_a \, dV; \\ R^a_J &= \int_V \left(\frac{\partial \Phi}{\partial J} - \Sigma_J \right) N^J_a \, dV; & \boldsymbol{R}^a_{\boldsymbol{\Sigma}_{\boldsymbol{D}0}} &= \int_V \left(\frac{\partial \Phi}{\partial \boldsymbol{\Sigma}_{\boldsymbol{D}0}} + \boldsymbol{D}_0 \right) N^{\boldsymbol{D}_0}_a \, dV; \\ \boldsymbol{R}^a_{\boldsymbol{\Sigma_d}} &= \int_V \left(\frac{\partial \Phi}{\partial \boldsymbol{\Sigma_d}} - \boldsymbol{F_x} \boldsymbol{D}_0 \right) N^{\boldsymbol{d}}_a \, dV. \end{aligned} \tag{72}$$

The discrete stationary conditions with respect to the elements of the set $\Sigma_\mathcal{D}$ (67) yield (i.e. compatibility and Faraday laws)

$$\begin{aligned} D\Pi_\Phi[\delta\Sigma_\mathcal{D}] = &\sum_{a=1}^{n_{\boldsymbol{\Sigma_F}}} \boldsymbol{R}^a_{\boldsymbol{\Sigma_F}} : \delta {\boldsymbol{\Sigma_F}}^a + \sum_{a=1}^{n_{\boldsymbol{\Sigma_H}}} \boldsymbol{R}^a_{\boldsymbol{\Sigma_H}} : \delta {\boldsymbol{\Sigma_H}}^a + \sum_{a=1}^{n_{\Sigma_J}} R^a_{\Sigma_J} \delta \Sigma^a_J \\ &+ \sum_{a=1}^{n_{\boldsymbol{D}_0}} \boldsymbol{R}^a_{\boldsymbol{D}_0} \cdot \delta \boldsymbol{D}^a_0, \end{aligned} \tag{73}$$

where the residuals in above equation (73) are

$$\begin{aligned}
\boldsymbol{R}^a_{\boldsymbol{\Sigma_F}} &= \int_V (\boldsymbol{F_x} - \boldsymbol{F})\, N^{\boldsymbol{F}}_a \, dV; \qquad & \boldsymbol{R}^a_{\boldsymbol{\Sigma_H}} &= \int_V (\boldsymbol{H_x} - \boldsymbol{H})\, N^{\boldsymbol{H}}_a \, dV; \\
R^a_{\Sigma_J} &= \int_V (J_{\boldsymbol{x}} - J)\, N^J_a \, dV; \qquad & \boldsymbol{R}^a_{\boldsymbol{D}_0} &= \int_V \left(\boldsymbol{\Sigma_{D_0}} + \boldsymbol{F}^{\boldsymbol{T}}_{\boldsymbol{x}} \boldsymbol{\Sigma_d} + \boldsymbol{\nabla_0 \varphi}\right) N^{\boldsymbol{D}_0}_a \, dV.
\end{aligned} \tag{74}$$

The stiffness matrix contribution arising for the variational principle Π_Φ (33) before static condensation is carried out emerge as

$$D^2\Pi_\Phi\left[\delta p; \Delta p\right] = \begin{bmatrix} \delta \mathbf{u} \\ \delta \boldsymbol{\phi} \\ \delta \boldsymbol{\mathcal{D}} \\ \delta \boldsymbol{\Sigma}_{\mathcal{D}} \\ \delta \boldsymbol{\Sigma_d} \end{bmatrix}^T \begin{bmatrix} \boldsymbol{K_{xx}} & \mathbf{0} & \mathbf{0} & \boldsymbol{K}_{\boldsymbol{x}\Sigma_{\mathcal{D}}} & \boldsymbol{K_{x\Sigma_d}} \\ \mathbf{0} & \mathbf{0} & \boldsymbol{K}_{\varphi\mathcal{D}} & \mathbf{0} & \mathbf{0} \\ \mathbf{0} & \boldsymbol{K}_{\mathcal{D}\varphi} & \boldsymbol{K}_{\mathcal{D}\mathcal{D}} & \boldsymbol{K}_{\mathcal{D}\Sigma_{\mathcal{D}}} & \boldsymbol{K_{\mathcal{D}\Sigma_d}} \\ \boldsymbol{K}_{\Sigma_{\mathcal{D}}\boldsymbol{x}} & \mathbf{0} & \boldsymbol{K}_{\Sigma_{\mathcal{D}}\mathcal{D}} & \mathbf{0} & \boldsymbol{K_{\Sigma_{\mathcal{D}}\Sigma_d}} \\ \boldsymbol{K_{\Sigma_d x}} & \mathbf{0} & \boldsymbol{K_{\Sigma_d \mathcal{D}}} & \boldsymbol{K_{\Sigma_d \Sigma_{\mathcal{D}}}} & \boldsymbol{K_{\Sigma_d \Sigma_d}} \end{bmatrix} \begin{bmatrix} \mathbf{u} \\ \Delta\boldsymbol{\phi} \\ \Delta\boldsymbol{\mathcal{D}} \\ \Delta\boldsymbol{\Sigma}_{\mathcal{D}} \\ \Delta\boldsymbol{\Sigma_d} \end{bmatrix}, \tag{75}$$

The objective of the following derivations is to present the expressions for non-zero blocks of the stiffness matrix in above equation (75). The stiffness matrix contribution $\boldsymbol{K}^{ab}_{\boldsymbol{xx}}$ is obtained exactly as in equation (46). The stiffness matrix contribution $\boldsymbol{K}^{ab}_{\boldsymbol{x}\Sigma_{\mathcal{D}}}$, emerging from the linearisation of $\boldsymbol{R}^a_{\boldsymbol{x}}$ with respect to incremental changes in the set $\Sigma_{\mathcal{D}}$, can be further decomposed into each of the contributions of the elements of the set $\Sigma_{\mathcal{D}}$ as

$$\boldsymbol{K}^{ab}_{\boldsymbol{x}\Sigma_{\mathcal{D}}} = \begin{bmatrix} \boldsymbol{K}^{ab}_{\boldsymbol{x}\boldsymbol{\Sigma_F}} & \boldsymbol{K}^{ab}_{\boldsymbol{x}\boldsymbol{\Sigma_H}} & \boldsymbol{K}^{ab}_{\boldsymbol{x}\Sigma_J} & \boldsymbol{K}^{ab}_{\boldsymbol{x}\boldsymbol{D}_0} \end{bmatrix}, \tag{76}$$

where each of the individual contribution in (76) is obtained as

$$\begin{aligned}
\boldsymbol{K}^{ab}_{\boldsymbol{x}\boldsymbol{\Sigma_F}} &= \int_V (\boldsymbol{I} \otimes \boldsymbol{\nabla}_0 N^{\boldsymbol{x}}_a)\, N^{\boldsymbol{F}}_b \, dV; \qquad & \left[\boldsymbol{K}^{ab}_{\boldsymbol{x}\boldsymbol{\Sigma_H}}\right]_{ijI} &= \mathcal{E}_{ijk} \left[\int_V (\boldsymbol{F_x} \times \boldsymbol{\nabla}_0 N^{\boldsymbol{x}}_a)\, N^{\boldsymbol{H}}_b \, dV\right]_{kI}; \\
\boldsymbol{K}^{ab}_{\boldsymbol{x}\Sigma_J} &= \int_V N^J_b \boldsymbol{H_x} \boldsymbol{\nabla}_0 N^{\boldsymbol{x}}_a \, dV; \qquad & \boldsymbol{K}^{ab}_{\boldsymbol{x}\boldsymbol{D}_0} &= \int_V (\boldsymbol{\Sigma_d} \otimes \boldsymbol{\nabla}_0 N^{\boldsymbol{x}}_a)\, N^{\boldsymbol{D}_0}_b \, dV.
\end{aligned} \tag{77}$$

The stiffness matrix contribution $\boldsymbol{K}^{ab}_{\boldsymbol{x}\boldsymbol{\Sigma_d}}$ yields

$$\boldsymbol{K}^{ab}_{\boldsymbol{x}\boldsymbol{\Sigma_d}} = \int_V (\boldsymbol{D}_0 \cdot \boldsymbol{\nabla}_0 N^{\boldsymbol{x}}_a)\, N^{\boldsymbol{d}}_b \boldsymbol{I} \, dV. \tag{78}$$

The stiffness matrix contribution obtained from the linearisation of $\boldsymbol{R}^a_\varphi$ with respect to incremental changes in the elements of the set $\mathcal{D}$ is

$$\boldsymbol{K}^{ab}_{\varphi\mathcal{D}} = \begin{bmatrix}\boldsymbol{0} & \boldsymbol{0} & 0 & \boldsymbol{K}^{ab}_{\varphi\boldsymbol{D}_0}\end{bmatrix}; \qquad \boldsymbol{K}^{ab}_{\varphi\boldsymbol{D}_0} = \int_V N^\varphi_a N^{\boldsymbol{D}_0}_b \boldsymbol{I}\, dV. \tag{79}$$

The stiffness matrix contribution of the diagonal block $\boldsymbol{K}^{ab}_{\mathcal{D}\mathcal{D}}$ results in

$$\boldsymbol{K}^{ab}_{\mathcal{D}\mathcal{D}} = \int_V \begin{bmatrix} N^{\boldsymbol{F}}_a N^{\boldsymbol{F}}_b \Phi_{\boldsymbol{F}\boldsymbol{F}} & N^{\boldsymbol{F}}_a N^{\boldsymbol{H}}_b \Phi_{\boldsymbol{F}\boldsymbol{H}} & N^{\boldsymbol{F}}_a N^{J}_b \Phi_{\boldsymbol{F}J} & N^{\boldsymbol{F}}_a N^{\boldsymbol{D}_0}_b \Phi_{\boldsymbol{F}\boldsymbol{\Sigma}_{\boldsymbol{D}_0}} \\ N^{\boldsymbol{H}}_a N^{\boldsymbol{F}}_b \Phi_{\boldsymbol{H}\boldsymbol{F}} & N^{\boldsymbol{H}}_a N^{\boldsymbol{H}}_b \Phi_{\boldsymbol{H}\boldsymbol{H}} & N^{\boldsymbol{H}}_a N^{J}_b \boldsymbol{H} J & N^{\boldsymbol{H}}_a N^{\boldsymbol{D}_0}_b \Phi_{\boldsymbol{F}\boldsymbol{\Sigma}_{\boldsymbol{D}_0}} \\ N^{J}_a N^{\boldsymbol{F}}_b \Phi_{J\boldsymbol{F}} & N^{J}_a N^{\boldsymbol{H}}_b \Phi_{J\boldsymbol{H}} & N^{J}_a N^{J}_b \Phi_{JJ} & N^{J}_a N^{\boldsymbol{D}_0}_b \Phi_{J\boldsymbol{\Sigma}_{\boldsymbol{D}_0}} \\ N^{\boldsymbol{D}_0}_a N^{\boldsymbol{F}}_b \Phi_{\boldsymbol{\Sigma}_{\boldsymbol{D}_0}\boldsymbol{F}} & N^{\boldsymbol{D}_0}_a N^{\boldsymbol{H}}_b \Phi_{\boldsymbol{\Sigma}_{\boldsymbol{D}_0}\boldsymbol{H}} & N^{\boldsymbol{D}_0}_a N^{J}_b \Phi_{\boldsymbol{\Sigma}_{\boldsymbol{D}_0}J} & N^{\boldsymbol{D}_0}_a N^{\boldsymbol{D}_0}_b \Phi_{\boldsymbol{\Sigma}_{\boldsymbol{D}_0}\boldsymbol{\Sigma}_{\boldsymbol{D}_0}} \end{bmatrix} dV, \tag{80}$$

where the Hessian operator $\mathbb{H}_\Phi$ has been defined in equation (28). In the case in which an explicit representation of the extended Helmholtz's energy functional $\Phi(\boldsymbol{F}, \boldsymbol{H}, J, \boldsymbol{\Sigma}_{\boldsymbol{D}_0}, \boldsymbol{\Sigma}_{\boldsymbol{d}})$ is not available Appendix B shows the relationship between the components of the Hessian operator $\mathbb{H}_\Phi$ in terms of the components of the Hessian operator $\mathbb{H}_W$. The stiffness matrix contribution $\boldsymbol{K}^{ab}_{\mathcal{D}\Sigma_\mathcal{D}}$ arising from the linearisation of $\boldsymbol{R}^a_\mathcal{D}$ with respect to incremental changes in the elements of the set $\Sigma_\mathcal{D}$ is defined as

$$\boldsymbol{K}^{ab}_{\mathcal{D}\Sigma_\mathcal{D}} = -\int_V \begin{bmatrix} N^{\boldsymbol{F}}_a N^{\boldsymbol{F}}_b \boldsymbol{\mathcal{I}} & \boldsymbol{0} & \boldsymbol{0} & \boldsymbol{0} \\ \boldsymbol{0} & N^{\boldsymbol{H}}_a N^{\boldsymbol{H}}_b \boldsymbol{\mathcal{I}} & \boldsymbol{0} & \boldsymbol{0} \\ \boldsymbol{0} & \boldsymbol{0} & N^{J}_a N^{J}_b & \boldsymbol{0} \\ \boldsymbol{0} & \boldsymbol{0} & \boldsymbol{0} & -N^{\boldsymbol{D}_0}_a N^{\boldsymbol{D}_0}_b \boldsymbol{I} \end{bmatrix} dV. \tag{81}$$

Finally, the expression for the matrix $\boldsymbol{K}^{ab}_{\mathcal{D}\boldsymbol{\Sigma}_{\boldsymbol{d}}}$ emerges as

$$\boldsymbol{K}^{ab}_{\mathcal{D}\boldsymbol{\Sigma}_{\boldsymbol{d}}} = \int_V \begin{bmatrix} N^{\boldsymbol{F}}_a N^{\boldsymbol{d}}_b \Phi_{\boldsymbol{F}\boldsymbol{\Sigma}_{\boldsymbol{d}}} & N^{\boldsymbol{H}}_a N^{\boldsymbol{d}}_b \Phi_{\boldsymbol{H}\boldsymbol{\Sigma}_{\boldsymbol{d}}} & N^{J}_a N^{\boldsymbol{d}}_b \Phi_{J\boldsymbol{\Sigma}_{\boldsymbol{d}}} & N^{\boldsymbol{D}_0}_a N^{\boldsymbol{d}}_b \Phi_{\boldsymbol{\Sigma}_{\boldsymbol{D}_0}\boldsymbol{\Sigma}_{\boldsymbol{d}}} \end{bmatrix} dV. \tag{82}$$

The stiffness matrix contribution $\boldsymbol{K}^{ab}_{\Sigma_\mathcal{D}\boldsymbol{\Sigma}_{\boldsymbol{d}}}$ yields

$$\boldsymbol{K}^{ab}_{\Sigma_\mathcal{D}\boldsymbol{\Sigma}_{\boldsymbol{d}}} = \begin{bmatrix}\boldsymbol{0} & \boldsymbol{0} & \boldsymbol{0} & \boldsymbol{K}^{ab}_{\boldsymbol{D}_0\boldsymbol{\Sigma}_{\boldsymbol{d}}}\end{bmatrix}; \qquad \boldsymbol{K}^{ab}_{\boldsymbol{D}_0\boldsymbol{\Sigma}_{\boldsymbol{d}}} = \int_V N^{\boldsymbol{D}_0}_a N^{\boldsymbol{d}}_b \boldsymbol{F}^T_{\boldsymbol{x}}\, dV. \tag{83}$$

The last stiffness matrix involved in the variational principle Π_Φ (33), namely, $\boldsymbol{K}^{ab}_{\boldsymbol{\Sigma}_{\boldsymbol{d}}\boldsymbol{\Sigma}_{\boldsymbol{d}}}$ is obtained as

$$\boldsymbol{K}^{ab}_{\boldsymbol{\Sigma}_{\boldsymbol{d}}\boldsymbol{\Sigma}_{\boldsymbol{d}}} = \int_V N^{\boldsymbol{D}_0}_a N^{\boldsymbol{\Sigma}_{\boldsymbol{d}}}_b \Phi_{\boldsymbol{\Sigma}_{\boldsymbol{d}}\boldsymbol{\Sigma}_{\boldsymbol{d}}}\, dV. \tag{84}$$

5. Examples

The objective of this section is to present a series of numerical examples in order to prove the robustness, accuracy and applicability of the computational framework presented above. Numerical results dealing with both displacement-potential based and mixed formulations will be displayed.

Three formulations have been compared, corresponding to: i) displacement-potential based formulation, hereby denoted as **DPF** [40]; ii) an eleven field $\{p, \mathcal{D}, \Sigma_{\mathcal{D}}, \boldsymbol{\Sigma_d}\}$ (66)-(67) formulation associated to the variational principle Π_Φ (33) and described in Section (4.3), hereby denoted as **MΦF** and iii), an eleven field $\{q, \mathcal{W}, \Sigma_{\mathcal{W}}, \boldsymbol{D}_0\}$ (36)-(37) formulation associated to the variational principle Π_W (31) and described in Section (4.2), hereby denoted as **MWF**.

All of the numerical results in which mixed formulations have been used correspond to the following selection of functional spaces: continuous quadratic interpolation of the displacement field (geometry) $\boldsymbol{x}$ and the electric potential field ϕ, piecewise linear interpolation of the conjugate pairs $\{\boldsymbol{F}, \boldsymbol{\Sigma_F}\}$, $\{\boldsymbol{H}, \boldsymbol{\Sigma_H}\}$, $\{\boldsymbol{D}_0, \boldsymbol{\Sigma}_{\boldsymbol{D}_0}\}$ and $\{\boldsymbol{d}, \boldsymbol{\Sigma_d}\}$, and piecewise constant interpolation of the Jacobian J and its associated stress conjugate Σ_J. With these functional spaces, the two mixed formulations **MΦF** and **MWF** will render identical results.

5.1. Three dimensional patch test

This first numerical example includes a standard three dimensional patch test in order to asses the correctness of the computational implementation. This problem has already been presented in References [22, 24] in the context of elasticity. The constitutive model used in this case is that introduced in Reference [1], suitable to describe the behaviour of electrostrictive dielectric elastomers. The internal energy associated to this model is defined as

$$\begin{aligned} W_{el} =& \mu_1 II_{\boldsymbol{F}} + \mu_2 II_{\boldsymbol{H}} + \frac{1}{2J\varepsilon_1} II_{\boldsymbol{d}} + \mu_e \left(II_{\boldsymbol{F}}^2 + \frac{2}{\mu_e \varepsilon_e} II_{\boldsymbol{F}} II_{\boldsymbol{d}} + \frac{1}{\mu_e^2 \varepsilon_e^2} II_{\boldsymbol{d}}^2 \right) \\ &+ \frac{1}{2\varepsilon_2} II_{\boldsymbol{D}_0} - 2(\mu_1 + 2\mu_2 + 6\mu_e) \ln J + \frac{\lambda}{2}(J-1)^2, \end{aligned} \tag{85}$$

where $II_{(\bullet)}$ is the second invariant of the entity $(\bullet)$, μ_1, μ_2, μ_e and λ are elastic parameters (N/m^2) and ε_1 and ε_e, electric parameters with units (N/V^2).

The constitutive model defined in above equation (85), and also those employed in forthcoming sections, are based on a convex multi-variable combination of invariants of the set $\{\boldsymbol{F}, \boldsymbol{H}, J, \boldsymbol{D}_0, \boldsymbol{d}\}$. Although not as direct as the rest of the terms in above equation (85), the third and fourth terms (i.e. associated to the material parameters ε_1 and μ_e, respectively) can be obtained as convex combinations of the pairs $\{J, \boldsymbol{d}\}$ and $\{\boldsymbol{F}, \boldsymbol{d}\}$, respectively. Therefore, positive definiteness of the Hessian operator $[\mathbb{H}_W]$ (19) is automatically satisfied for this constitutive model [1].

Particularisation of the expressions for the elasticity tensor $\boldsymbol{\mathcal{C}}$ and the dielectric tensor $\boldsymbol{\theta}$ in equations (A.1) and (A.5) to the reference configuration, namely $\boldsymbol{F} = \boldsymbol{H} = \boldsymbol{I}$, $J = 1$ and $\boldsymbol{d} = \boldsymbol{D}_0 = \boldsymbol{0}$, enables the material parameters in (85) to be related to the classical Lamé parameters and the dielectric permittivity of the material in the reference configuration, namely μ, $\hat{\lambda}$ and ε as

$$2\mu_1 + 4\mu_2 + 12\mu_e = \mu; \qquad \lambda + 8\mu_e + 4\mu_2 = \hat{\lambda}; \qquad \frac{\varepsilon_1}{1 + c_1 + 12c_2} = \varepsilon_r \varepsilon_0 = \varepsilon, \tag{86}$$

where ε_0 is the electric permittivity of the vacuum, with $\varepsilon_0 \approx 8.854 \times 10^{-12}\, N/V^2$ and with

$$c_1 = \frac{\varepsilon_1}{\varepsilon_2}; \qquad c_2 = \frac{\varepsilon_1}{\varepsilon_e}, \tag{87}$$

The material properties in the reference configuration are chosen as $\mu = 10^5\,(Pa)$, $\hat{\lambda} = 1.094 \times 10^6\,(Pa)$ and $\varepsilon = 4.68\varepsilon 0$, which are compatible with a Poisson ratio of $\nu = 0.4582$ in the reference configuration. The material parameters, corresponding with this definition in the reference configuration, can thus be obtained and are presented in Table 2.

$\mu_1\,(Pa)$	$\mu_2\,(Pa)$	$\mu_e\,(Pa)$	$\lambda\,(Pa)$	$\varepsilon_1\,(N/V^2)$	c_1	c_2
0.225μ	$0.5\mu_1$	0.0083μ	10^6	$4.68\varepsilon_0$	0	$\frac{1}{232.84}$

Table 2: Material properties for example 5.1.

A homogeneous electric field is defined in the OX_3 direction, applied to a cubic shape domain of side L, as depicted in Figure 2. To achieve this distribution of electric field, non-zero normal (electric) Dirichlet boundary conditions are applied on the boundary faces perpendicular to the OX_3 axis

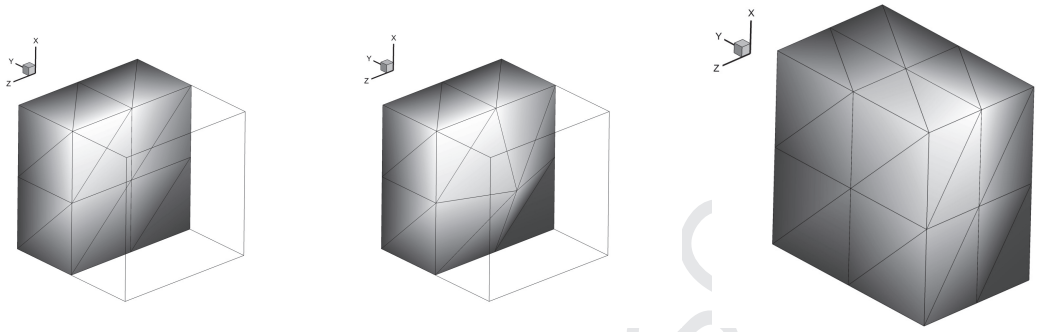

(a) (b) (c)

Figure 2: Three dimensional patch test. (a) View of half undistorted mesh in the reference configuration. (b) View of half distorted mesh in the reference configuration. (c) Example of deformed geometry after applying a voltage difference of $\Delta\varphi = 30\,MV$ in the OX_3 direction for the constitutive model defined in (85).

and zero (electric) Neumann boundary conditions are defined everywhere else. Moreover, zero (mechanical) normal Dirichlet boundary conditions are defined on three faces perpendicular to the OX_1, OX_2 and OX_3 directions and zero (mechanical) Neumann boundary conditions are applied everywhere else.

The domain is discretised using two different meshes of $(2 \times 2 \times 2) \times 6$ tetrahedral elements. First, a structured mesh is shown in Figure 2(a) and second, a distorted mesh is shown in Figure 2(b), where the interior node is displaced randomly. The objective of this example is to demonstrate that the same homogeneous solution is obtained for both meshes. As expected, hence passing the patch test, for the two mixed formulations defined, namely **MWF** and **MΦF**, the results are identical for both meshes. A homogeneous deformation gradient tensor and a Lagrangian electric field for both meshes is obtained as

$$\boldsymbol{F} = \begin{bmatrix} 1.15598 & 0 & 0 \\ 0 & 1.15598 & 0 \\ 0 & 0 & 0.749559 \end{bmatrix}; \qquad \boldsymbol{E}_0 = \begin{bmatrix} 0 \\ 0 \\ 30 \end{bmatrix} (MV/m). \tag{88}$$

For completeness, the quadratic convergence of the Newton-Raphson algorithm is displayed in Figure 3.

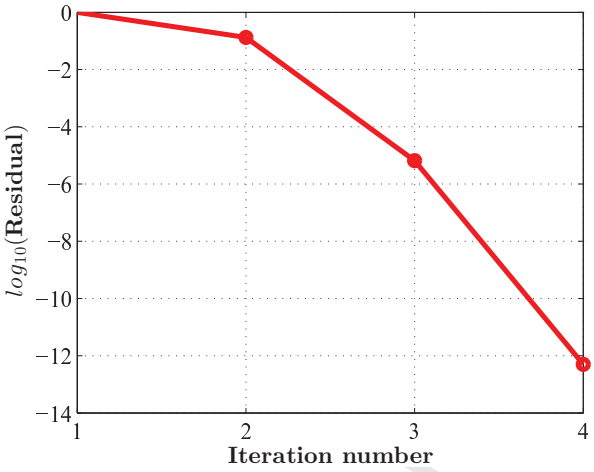

Figure 3: Three dimensional patch test: quadratic convergence of the Newton-Raphson linearisation procedure.

5.2. Convergence of the proposed formulation

The objective of this example is to demonstrate the p-order of accuracy of the different mixed formulations, as a function of the chosen finite element approximation spaces. The constitutive model considered is based on the following convex multi-variable expansion

$$W_{simple} = \mu_1 II_{\boldsymbol{F}} + \mu_2 II_{\boldsymbol{H}} - 2(\mu_1 + 2\mu_2)\ln J + \frac{\lambda}{2}(J-1)^2 + \frac{1}{2\varepsilon_1} II_{\boldsymbol{d}} + \frac{1}{2\varepsilon_2} II_{\boldsymbol{D}_0}. \tag{89}$$

The material parameters in (89) are presented in Table 3. In order to

$\mu_1\,(Pa)$	$\mu_2\,(Pa)$	$\lambda\,(Pa)$	$\varepsilon_1\,(N/V^2)$	$\varepsilon_2\,(N/V^2)$
1	$\frac{1}{2}$	1	4	4

Table 3: Material properties for example 5.2.

study the p-order of convergence of the new mixed Finite Element formulations, the analysis of an ad-hoc test problem is carried out. The problem is constructed so that smoothness of the solution is guaranteed. For that purpose, the following simple exact fields associated to the deformed or Eulerian

configuration $\boldsymbol{x}$ and the electric potential φ are considered

$$\boldsymbol{x}^{\text{exact}} = \boldsymbol{X} + \begin{bmatrix} AX_1^3 \\ BX_1^3 \\ CX_1^3 \end{bmatrix}; \qquad \varphi^{\text{exact}} = \varphi_0 X_1^3, \tag{90}$$

where the superscript in (90) is used to emphasise the exact smooth solution with $A = 0.1$, $B = 0.2$, $C = 0.3$ and $\varphi_0 = 10^4$. The deformation gradient tensor and the Lagrangian electric field are obtained via equations (1) and (7a), respectively, leading to

$$\boldsymbol{F}^{\text{exact}} = \begin{bmatrix} 1+3AX_1^2 & 0 & 0 \\ 0 & 1+3BX_2^2 & 0 \\ 0 & 0 & 1+3CX_3^2 \end{bmatrix}; \qquad \boldsymbol{E}_0^{\text{exact}} = -\begin{bmatrix} 3\varphi_0 X_1^2 \\ 0 \\ 0 \end{bmatrix}. \tag{91}$$

The remaining variables defining multi-variable convexity, namely $\{\boldsymbol{H}, J, \boldsymbol{D}_0, \boldsymbol{d}\}$ need to be obtained for the smooth displacement and electric potential fields in equation (90). Particularisation of equation (2) for the smooth fields in equations (90) enables $\boldsymbol{H}^{\text{exact}}$ and J^{exact} to be obtained as

$$\boldsymbol{H}^{\text{exact}} = \frac{1}{2}\boldsymbol{F}^{\text{exact}} \boldsymbol{\times} \boldsymbol{F}^{\text{exact}}; \qquad J^{\text{exact}} = \frac{1}{3}\boldsymbol{H}^{\text{exact}} : \boldsymbol{F}^{\text{exact}}. \tag{92}$$

Particularisation of equation (13) to the constitutive model in equation (89) leads to

$$\frac{1}{\varepsilon_2}\boldsymbol{D}_0^{\text{exact}} + \frac{1}{\varepsilon_1}\left(\boldsymbol{F}^{\text{exact}}\right)^T \boldsymbol{d}^{\text{exact}} = \boldsymbol{E}_0^{\text{exact}}. \tag{93}$$

Making use of the relationship $\boldsymbol{d}^{\text{exact}} = \boldsymbol{F}^{\text{exact}}\boldsymbol{D}_0^{\text{exact}}$ in (93) results in the final expression of the Lagrangian electric displacement field $\boldsymbol{D}_0^{\text{exact}}$ as

$$\left(\frac{1}{\varepsilon_2}\boldsymbol{I} + \frac{1}{\varepsilon_1}\boldsymbol{C}^{\text{exact}}\right)\boldsymbol{D}_0^{\text{exact}} = \boldsymbol{E}_0^{\text{exact}} \Rightarrow \boldsymbol{D}_0^{\text{exact}} = \left(\frac{1}{\varepsilon_2}\boldsymbol{I} + \frac{1}{\varepsilon_1}\boldsymbol{C}^{\text{exact}}\right)^{-1}\boldsymbol{E}_0^{\text{exact}}. \tag{94}$$

where $\boldsymbol{C}^{\text{exact}}$ is the right Cauchy-Green tensor. Once all the elements of the set $\mathcal{V}^{\text{exact}}$ have been determined, it is possible to obtain the set of exact work conjugates $\Sigma_{\mathcal{V}}^{\text{exact}}$ via equation (11). Finally, the associated volumetric force and electric charge in mechanical and electrical equilibrium with the exact first Piola Kirchhoff stress tensor $\boldsymbol{P}^{\text{exact}}$ and exact Lagrangian electric displacement field $\boldsymbol{D}_0^{\text{exact}}$ are determined from equations (9a) and (5a), respectively as

$$\boldsymbol{f}_0(\boldsymbol{x}^{\text{exact}}, \varphi^{\text{exact}}) = -\text{DIV}\boldsymbol{P}^{\text{exact}}; \qquad \rho_0(\boldsymbol{x}^{\text{exact}}, \varphi^{\text{exact}}) = \text{DIV}\boldsymbol{D}_0^{\text{exact}}, \tag{95}$$

where $\boldsymbol{D}_0^{\text{exact}}$ has been obtained in (94) and where $\boldsymbol{P}^{\text{exact}}$ can be obtained after application of equation (13).

It is then that the rate of convergence of the different variables $\{\boldsymbol{x}, \varphi, \mathcal{V}, \Sigma_{\mathcal{V}}\}$ to their analytical counterparts, namely $\{\boldsymbol{x}^{\text{exact}}, \varphi^{\text{exact}}, \mathcal{V}^{\text{exact}}, \Sigma_{\mathcal{V}}^{\text{exact}}\}$ can be studied. For that purpose, the same geometry as that presented in Section 5.2 is considered and initially discretised with $(2 \times 2 \times 2) \times 6$ tetrahedral elements and, subsequently, h-refinement is carried out generating a total of three discretisations.

The L^1 norm of the error for a particular component of the different variables involved, namely $\boldsymbol{x}$, $\boldsymbol{F}$, $\boldsymbol{H}$, J, $\boldsymbol{D}_0$, $\boldsymbol{d}$, $\boldsymbol{\Sigma}_{\boldsymbol{F}}$, $\boldsymbol{\Sigma}_{\boldsymbol{H}}$, Σ_J, $\boldsymbol{\Sigma}_{\boldsymbol{D}_0}$ and $\boldsymbol{\Sigma}_{\boldsymbol{d}}$ is investigated for two different choices of interpolation spaces, leading to the definition of two different Finite Element types. The first element, called "Element 1", corresponds to the choice of interpolation spaces described at the beginning of Section 5, namely, continuous quadratic interpolation of the displacement field (geometry) $\boldsymbol{x}$ and the electric potential field ϕ, piecewise linear interpolation of the conjugate pairs $\{\boldsymbol{F}, \boldsymbol{\Sigma}_{\boldsymbol{F}}\}$, $\{\boldsymbol{H}, \boldsymbol{\Sigma}_{\boldsymbol{H}}\}$, $\{\boldsymbol{D}_0, \boldsymbol{\Sigma}_{\boldsymbol{D}_0}\}$ and $\{\boldsymbol{d}, \boldsymbol{\Sigma}_{\boldsymbol{d}}\}$ and piecewise constant interpolation of the Jacobian J and its associated stress conjugate Σ_J. Alternatively, "Element 2" is characterised by the same choice of interpolation spaces for the electric potential (continuous quadratic interpolation) and for the pairs $\{\boldsymbol{F}, \boldsymbol{\Sigma}_{\boldsymbol{F}}\}$, $\{\boldsymbol{H}, \boldsymbol{\Sigma}_{\boldsymbol{H}}\}$, $\{\boldsymbol{D}_0, \boldsymbol{\Sigma}_{\boldsymbol{D}_0}\}$ and $\{\boldsymbol{d}, \boldsymbol{\Sigma}_{\boldsymbol{d}}\}$ (piecewise linear interpolation). The Jacobian and its work conjugate, namely J, Σ_J are interpolated using piecewise linear interpolation. Four cubic bubble functions are added at the barycentre of each face of the tetrahedron and a quartic bubble function is added at the barycentre of the tetrahedron itself, in analogy with the classical $P2^+ - P1$ Crouzeix-Raviart element [45], typically used in $u - p$ formulations for incompressible and nearly incompressible elasticity.

Figure 4 shows the order of accuracy of the different unknown variables for the mixed formulations (all yielding identical convergence pattern). Figure 4(a) displays the convergence of the variables $\{\boldsymbol{x}, \boldsymbol{F}, \boldsymbol{H}, J, \boldsymbol{D}_0, \boldsymbol{d}\}$ whereas Figure 4(c) displays the convergence of the variables $\{\boldsymbol{\Sigma}_{\boldsymbol{F}}, \boldsymbol{\Sigma}_{\boldsymbol{H}}, \Sigma_J, \boldsymbol{\Sigma}_{\boldsymbol{D}_0}, \boldsymbol{\Sigma}_{\boldsymbol{d}}\}$ for "Element 1". As expected, the constant interpolation of the Jacobian J and its work conjugate Σ_J affects the optimal convergence of the different variables, specially those purely mechanical and the pair $\{\boldsymbol{d}, \boldsymbol{\Sigma}_{\boldsymbol{d}}\}$, for which a decrease of one is observed in the order of convergence. Figure 4(b) displays the convergence of the variables $\{\boldsymbol{x}, \boldsymbol{F}, \boldsymbol{H}, J, \boldsymbol{D}_0, \boldsymbol{d}\}$ whereas Figure 4(d) displays the convergence of the variables $\{\boldsymbol{\Sigma}_{\boldsymbol{F}}, \boldsymbol{\Sigma}_{\boldsymbol{H}}, \Sigma_J, \boldsymbol{\Sigma}_{\boldsymbol{D}_0}, \boldsymbol{\Sigma}_{\boldsymbol{d}}\}$ for "Element 2". As expected, the convergence observed is $p+1$ in all the variables, since

the convergence is optimal for this element.

5.3. *Comparison of performance between displacement-potential and mixed formulations*

The objective of this example is to compare the solution obtained with the displacement-potential based formulation **DPF** against those obtained with the mixed formulations **MΦF** and **MWF** in a bending dominated scenario and near the verge of incompressibility. A standard benchmark problem typically used in the computational mechanics community to test formulations under those specific conditions is the Cook's membrane problem [22, 24].

The geometry and boundary conditions of the membrane are depicted in Figure 5. The application of an electric potential in the electrodes leads to an out of plane bending-type deformation. In fact, although in more realistic geometrical configurations (the purpose of this example is exclusively to test the mixed formulations proposed), this type of potential Dirichlet boundary conditions are used in practical applications where dielectric elastomers and piezoelectric polymers are utilised as bending actuators.

The constitutive model used is identical to that described in Section 5.1 in equations (85), (86) and (87). The material properties in the reference configuration are chosen as $\mu = 10^5\,(Pa)$, $\hat{\lambda} = 4.99 \times 10^7\,(Pa)$ and $\varepsilon = 4.68\varepsilon 0$, which are compatible with a Poisson ratio of $\nu = 0.499$ in the reference configuration. The material parameters of the model, compatible with this definition in the reference configuration (as explained in Section 5.1), are chosen according to Table 4.

$\mu_1\,(Pa)$	$\mu_2\,(Pa)$	$\mu_e\,(Pa)$	$\lambda\,(Pa)$	$\varepsilon_1\,(N/V^2)$	c_1	c_2
0.225μ	$0.5\mu_1$	0.0083μ	4.99×10^7	1.05ε	0	$\frac{1}{232.84}$

Table 4: Material properties for example 5.3. Ratios c_1 and c_2 defined as in equation (87).

Figures 6(a)-(b) show the contour plot for the hydrostatic pressure p and for the stress variable $\boldsymbol{\Sigma}_{\boldsymbol{F}23}$ obtained with the **MWF** formulation. Finally, Figures 6(c)-(d) display the contour plot for the Eulerian electric field component $\boldsymbol{E}_1$ and the Eulerian displacement field component $\boldsymbol{D}_2$ obtained with the **MWF** formulation.

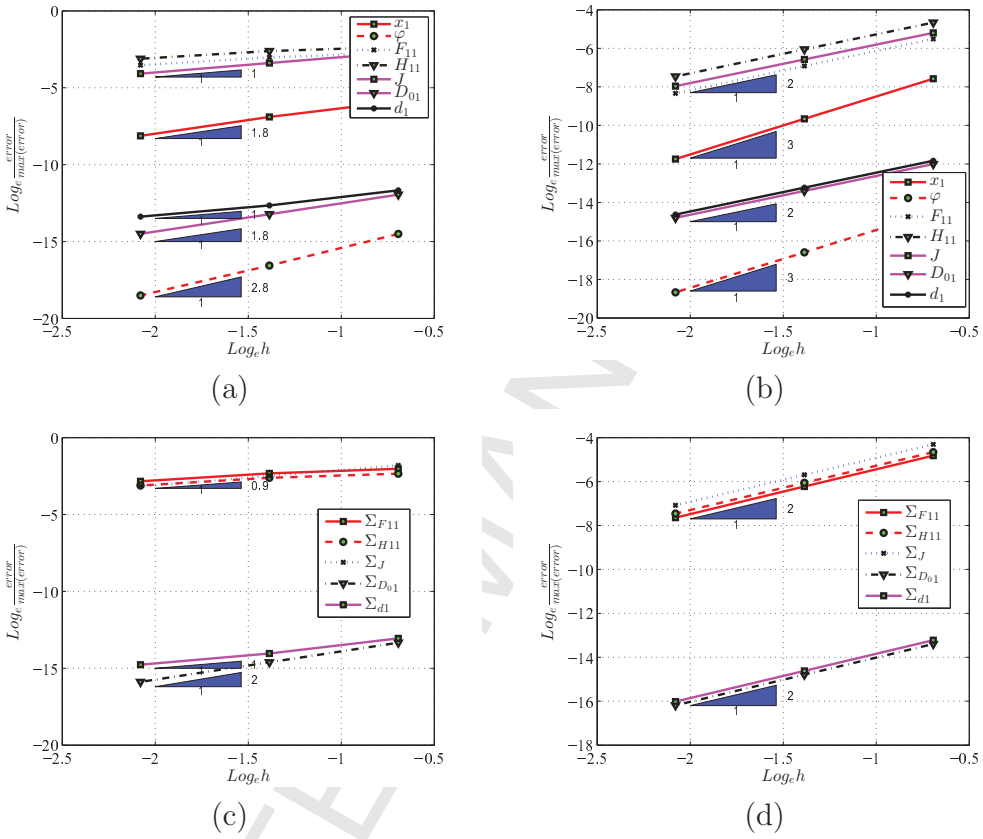

Figure 4: Convergence of the proposed formulation: order of accuracy of different strain, stress and electric magnitudes for the mixed formulations. Order of accuracy of the kinematic variables $\boldsymbol{x}$, $\boldsymbol{F}$, $\boldsymbol{H}$ and J and electric variables φ, $\boldsymbol{\Sigma}_{\boldsymbol{D}_0}$ and $\boldsymbol{\Sigma}_{\boldsymbol{d}}$ for (a) Element 1 and (b) Element 2. Order of accuracy of the kinetic variables $\boldsymbol{\Sigma}_{\boldsymbol{F}}$, $\boldsymbol{\Sigma}_{\boldsymbol{H}}$ and Σ_J and electric variables $\boldsymbol{D}_0$ and $\boldsymbol{d}$ (c) Element 1 and (d) Element 2. Constitutive model defined in (85). Results obtained with the **MΦF** formulation.

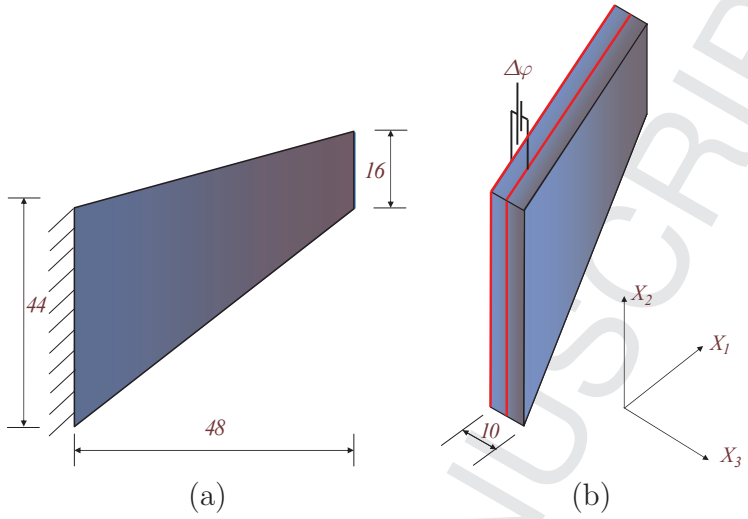

Figure 5: Comparison of performance between **DPF** and **MWF** formulations. Geometry and boundary conditions.

A detailed comparison between the results provided by the **DPF** and the mixed formulations is established in Table 6 for different meshes. For completeness, Table 5 displays the discretisation details for each of the meshes employed. Results are presented for stresses, electric displacements and displacements sampled at points A, B and C ($\mathbf{X}_A = [24 \;\; 52 \;\; -2]^T$; $\mathbf{X}_B = [24 \;\; 22 \;\; -2]^T$; $\mathbf{X}_C = [48 \;\; 60 \;\; -2]^T$). As can be noticed, the **DPF** implementation underestimates the displacements obtained with respect to those for the alternative mixed formulations. As expected, regarding the stresses, the differences are very significant between both formulations. Whereas the results for the mixed formulations show a defined convergence pattern, the results of the **DPF** do not seem to converge, with clear pressure oscillations (even with incoherent changes in sign as mesh refinement is carried out).

5.4. Torsional actuator. Fiber reinforced dielectric elastomer

The objective of this example is to observe how the behaviour of a dielectric elastomer matrix can be modified when fibres are introduced in a specific direction characterised by the unit normal vector $\boldsymbol{N}$. The geometry and boundary conditions for this example are depicted in Figure 7(a), where the dimensions a, b and c are set to $a = 1$, $b = 2$ and $c = 10$. The actu-

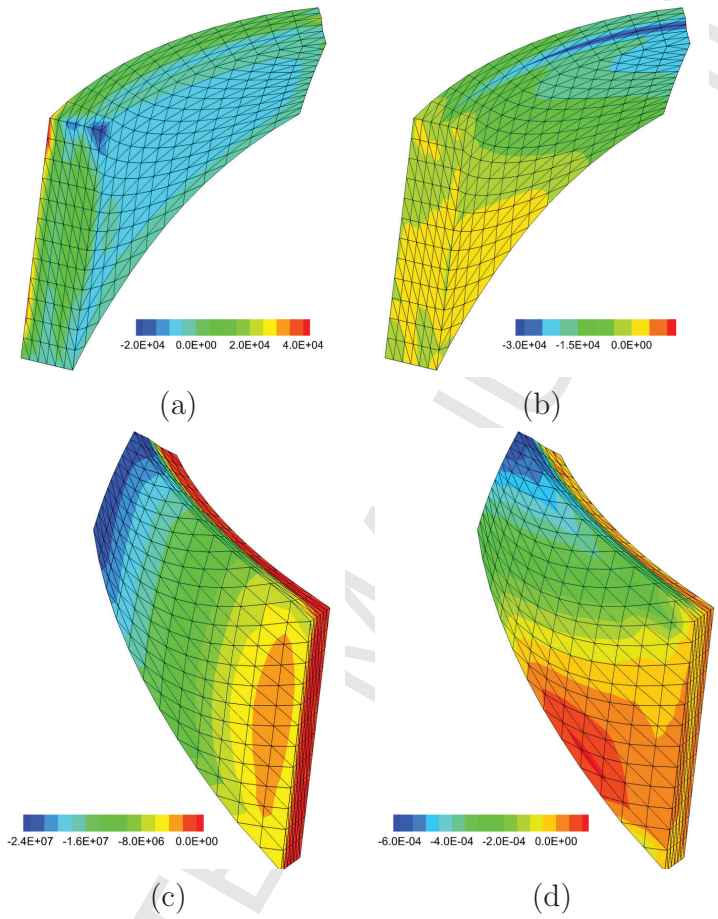

Figure 6: Contour plot of (a) the hydrostatic pressure (N/m^2), (b) stress conjugate variable $\boldsymbol{\Sigma}_{\boldsymbol{F}23}$ (N/m^2), (c) the electric field component $\boldsymbol{E}_1$ and (d) the electric displacement complement $\boldsymbol{D}_2$ for the **MWF** formulation. Polyconvex constitutive model in equation (85), with material parameters defined in Table 4. Electric potential difference $\Delta\varphi$ applied between electrodes of $140.49\,MV$. Results shown for a discretisation of $(12 \times 12 \times 4) \times 6$ tetrahedral elements ($8,125 \times 3$ and $8,125$ degrees of freedom associated to the spatial coordinates $\boldsymbol{x}$ and the electric potential, respectively).

Mesh	Elems.	Dofs. $\boldsymbol{x}$	Dofs. φ	Dofs. $\mathcal{U}$	Dofs. J, Σ_J
1	1,470	$2,475 \times 3$	2,475	$1,470 \times 4 \times 9$	$1,470 \times 1$
2	3,600	$5,730 \times 3$	5,730	$3,600 \times 4 \times 9$	$3,600 \times 1$
3	5,880	$9,251 \times 3$	9,251	$5,880 \times 4 \times 9$	$5,880 \times 1$

Table 5: Comparison of performance between **DPF** and **MWF** formulations. Mesh discretisation details. Column 2: number of tetrahedral elements (Elems.). Column 3: number of degrees of freedom (Dofs.) associated to the spatial coordinates $\boldsymbol{x}$. Columnn 4: number of degrees of freedom (Dofs.) associated to the electric potential. Column 5: number of degrees of freedom (Dofs.) associated to the fields $\mathcal{U} \equiv \{\boldsymbol{F}, \boldsymbol{H}, \boldsymbol{D}_0, \boldsymbol{\Sigma}_{\boldsymbol{F}}, \boldsymbol{\Sigma}_{\boldsymbol{H}}, \boldsymbol{\Sigma}_{\boldsymbol{D}_0}, \boldsymbol{\Sigma}_{\boldsymbol{d}}\}$. Column 6: number of degrees of freedom (Dofs.) associated to the strain/stress fields J, Σ_J.

ator is completely fixed at the position $X_3 = 0$ ($0 \leq X_3 \leq 10$) and a pair of electrodes is located in $X_1 = -0.5$ and $X_1 = 0$, where $-0.5 \leq X_1 \leq 1$. Moreover, the dielectric elastomer matrix is reinforced with fibres oriented as in Figure 7(b). For clarity, the vector $\boldsymbol{N}$ in the direction of the fibers has been parametrised spherically in terms of the angles θ and ψ (refer to Figure 7(b)). In order to produce intricate deformation patterns, different arrangements of the fibers are used in the areas defined by the constraint $X_2 > 0$ and $X_2 < 0$, where $-1 \leq X_2 \leq 1$.

In order to account for the fibres in the constitutive model, an additive decomposition of the internal energy in terms of a purely isotropic component (associated to the dielectric elastomer matrix) and an anisotropic component (associated to the fibers) is followed as

$$W_{fibre} = W_{el} + W_{ani}(\boldsymbol{F}, \boldsymbol{H}, J, \boldsymbol{N}), \tag{96}$$

where the convex multi-variable isotropic component W_{el} has been defined in equation (85) and with $W_{ani}(\boldsymbol{F}, \boldsymbol{H}, J, \boldsymbol{N})$ defined as,

$$W_{ani}(\boldsymbol{F}, \boldsymbol{H}, J, \boldsymbol{N}) = \mu_3 II_{\boldsymbol{FN}} + \mu_3 II_{\boldsymbol{HN}} - 2\mu_3 \ln J. \tag{97}$$

Notice that the above additive decomposition of the internal energy W_{fibre} in (96) into its isotropic and anisotropic contributions, namely W_{el} and W_{ani}

	DPF formulation			**MWF** formulation		
	Coarse	Medium	Fine	Coarse	Medium	Fine
σ_{xx}^{A}	1192.87	333.04	118.32	520.28	494.75	412.81
σ_{xx}^{B}	1542.95	1033.10	739.31	415.80	325.46	233.81
σ_{yy}^{A}	1064.70	112.11	-123.94	132.35	157.46	155.31
σ_{yy}^{B}	1569.10	1046.26	734.48	260.29	159.92	87.60
σ_{zz}^{A}	1506.68	821.84	693.71	1199.33	1021.09	874.46
σ_{zz}^{B}	2169.36	1836.70	1570.01	1009.44	778.38	674.34
${D_0}_z{}^{A}(\times 10^{-4})$	5.447	5.440	5.438	5.432	5.436	5.439
${D_0}_z{}^{B}(\times 10^{-4})$	5.439	5.435	5.434	5.424	5.433	5.438
u_x^C	0.455	0.456	0.456	0.455	0.456	0.456
u_y^C	0.495	0.498	0.499	0.502	0.503	0.503
u_z^C	3.708	3.802	3.843	3.897	3.933	3.948

Table 6: Comparison of performance between **DPF** and **MWF** formulations. Stress components (kPa), electric displacement components ($10^{-4}N/mV$) and displacements (m) at points A, B and C. Results obtained using the **DPF** formulation (columns 2 to 4) and mixed formulations (columns 5 to 7). Prescribed potential difference $\Delta\varphi = 62.5\,MV/m$. Coarse, medium and fine discretisations of $(8 \times 8 \times 6) \times 6$, $(12 \times 12 \times 6) \times 6$ and $(16 \times 16 \times 6) \times 6$ tetrahedral elements, respectively.

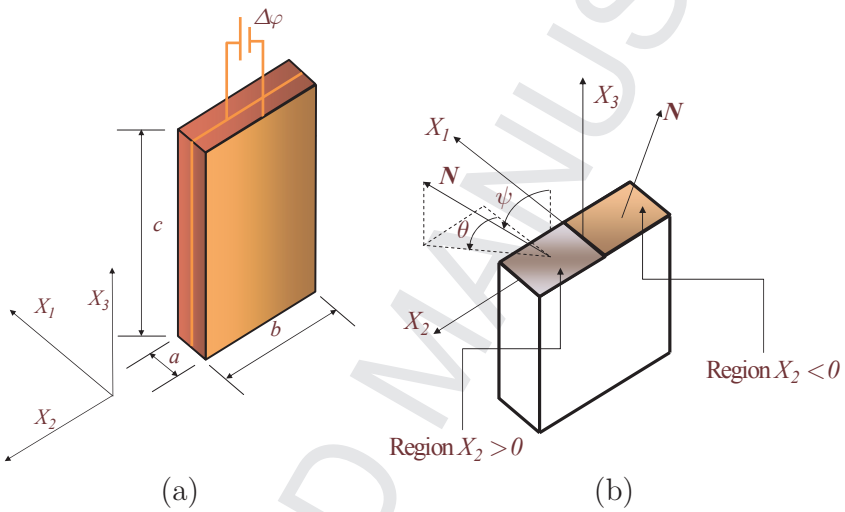

Figure 7: Torsional actuator. Fiber reinforced dielectric elastomer. (a) Geometry and boundary conditions. (b) Arrangement of the fibers within the isotropic matrix. Illustration of spherical parametrisation of the vector $\boldsymbol{N}$ in the region characterised by $X_2 > 0$.

guarantees that the stress and the electric displacement field vanish in the reference configuration. Moreover, provided that μ_3 is positive, the anisotropic component W_{ani} in (97) is convex multi-variable itself. Hence, the resulting energy functional is convex multi-variable. The following choice of material parameters is used

$\mu_1\,(Pa)$	$\mu_2\,(Pa)$	$\mu_3\,(Pa)$	$\mu_e\,(Pa)$	$\lambda\,(Pa)$	$\varepsilon_1\,(N/V^2)$	c_1	c_2
$\frac{1}{20}\mu$	$\frac{1}{40}\mu$	$\frac{1}{2.63}\mu$	$\frac{1}{300}\mu$	10^5	1.15ε	0	1.25×10^{-2}

Table 7: Material properties for example 5.4. Shear modulus in the reference configuration defined as $\mu = 10^5\,(Pa)$. The ratios c_1 and c_2 in Table 4 are defined as in equation (87).

Figure 8 shows, for the same value of the applied electric potential, the deformed shape and the contour plots for the stress conjugate $\boldsymbol{\Sigma}_{\boldsymbol{F}11}$ and the Eulerian electric field component $\boldsymbol{E}_1$ corresponding to different orientations of the angles θ and ψ parametrising the unit vector $\boldsymbol{N}$ (see Figure 7(b)). Finally, Figure 9 shows the contour plot of the hydrostatic pressure p for different stages of the deformation corresponding to different values of the prescribed voltage in the electrodes for the particular arrangement of fibers described in Figure 8(b).

5.5. Twisting of piezoelectric energy harvester

This example includes the twisting of a piezoelectric material whose geometry is characterised by a length $L = 6m$ and a squared cross sectional area of side $a = 1m$. The energy harvester is clamped at its left end and subjected to a torsion on its right end. The electric potential is fixed to zero at the plane defined by the constraint $X_1 = 0$. This example is included to demonstrate the robustness of the mixed formulations in extreme deformation scenarios. The torsion at the right end is generated through Dirichlet boundary conditions as follows

$$(\boldsymbol{I} - \boldsymbol{E}_Y \otimes \boldsymbol{E}_Y)\,\boldsymbol{x} = \theta \boldsymbol{E}_Y \times \boldsymbol{X}, \tag{98}$$

where $\boldsymbol{E}_Y$ is the unit vector normal to the cross section in the reference configuration, $\boldsymbol{X}$ are the initial coordinates, θ is the angle of rotation and $\boldsymbol{x}$ are the final coordinates. As can be observed, the section is not restricted to in-plane torsion and zero Neumann boundary conditions are imposed normal

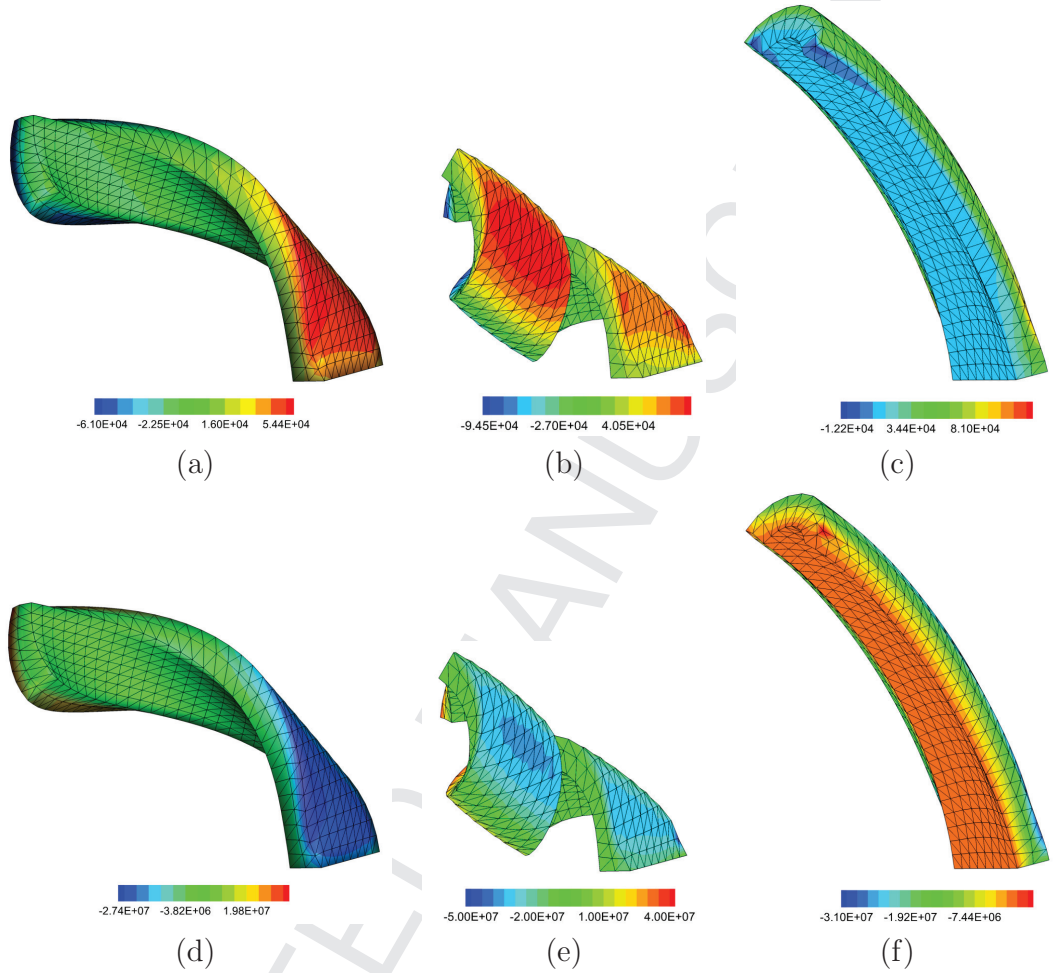

Figure 8: Torsional actuator. Fiber reinforced dielectric elastomer. Contour plot of hydrostatic pressure p and Eulerian electric field $\boldsymbol{E}_1$ for the following spherical parametrisation of the vector $\boldsymbol{N}$ in the direction of the fibers: (a) p and (d) $\boldsymbol{E}_1$ for $\theta = \pi/2$ and $\psi = \pi/4$ in $X_2 > 0$ and $\theta = -\pi/2$ and $\psi = \pi/4$ in $X_2 < 0$, (b) p and (e) $\boldsymbol{E}_1$ for $\theta = \psi = \pi/4$ in $X_2 > 0$ and $\theta = 5\pi/4$ and $\psi = \pi/4$ in $X_2 < 0$ and (c) p and (f) $\boldsymbol{E}_1$ for $\theta = \psi = 0$. Results obtained with the **MWF** formulation for $\Delta\varphi = 11.53\, MV/m$. Constitutive model defined in (96) and (97) with material parameters given in Table 7. Results shown for a discretisation of $(2 \times 8 \times 30) \times 6$ tetrahedral elements ($5,185 \times 3$ and $5,185$ degrees of freedom associated to the spatial coordinates $\boldsymbol{x}$ and electric potential, respectively).

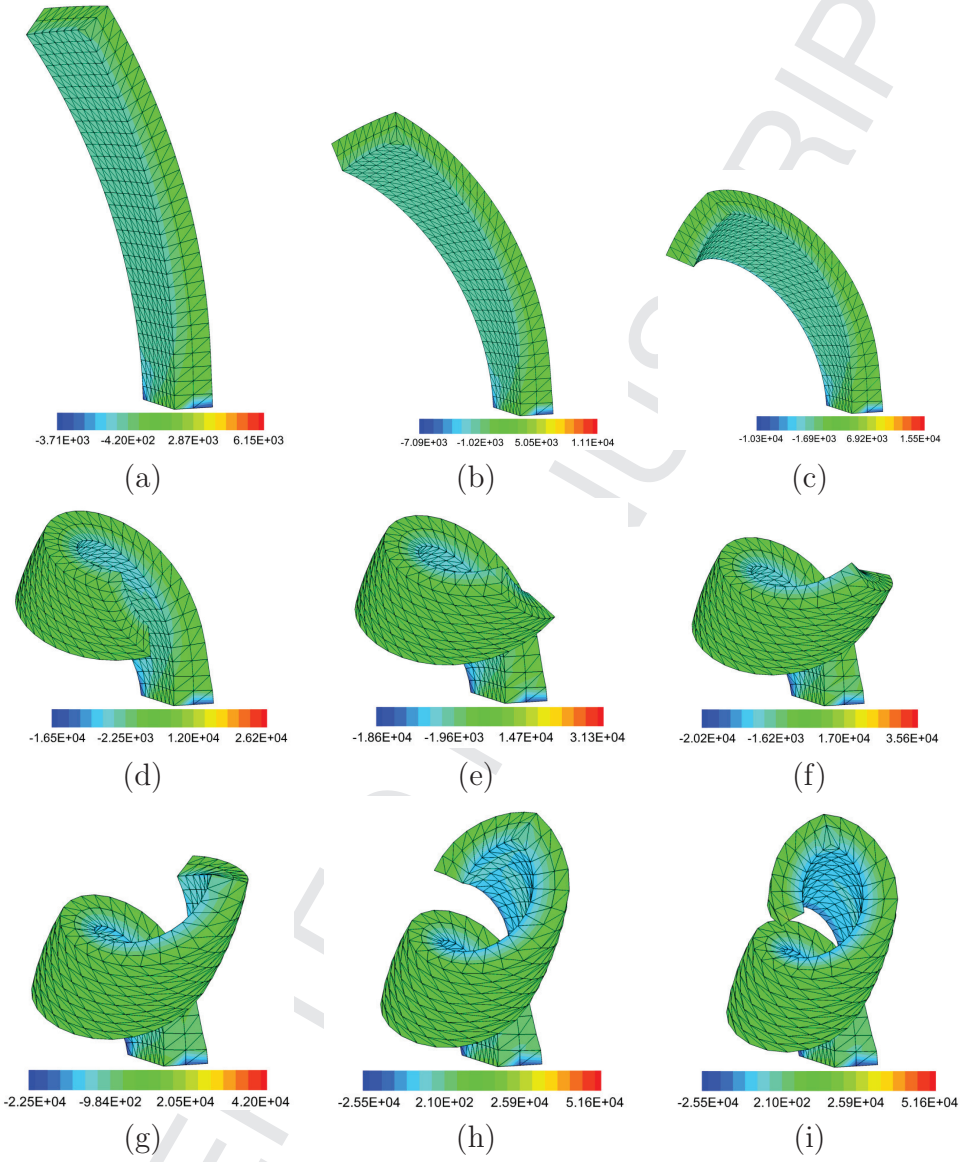

Figure 9: Torsional actuator. Fiber reinforced dielectric elastomer. Contour plot of the hydrostatic pressure p for (a) $\Delta\varphi = 5.49\,MV$, (b) $\Delta\varphi = 7.27\,MV$, (c) $\Delta\varphi = 8.43\,MV$, (d) $\Delta\varphi = 10.01\,MV$, (e) $\Delta\varphi = 10.43\,MV$, (f) $\Delta\varphi = 10.71\,MV$, (g) $\Delta\varphi = 11.07\,MV$, (h) $\Delta\varphi = 11.48\,MV$ and (i) $\Delta\varphi = 11.67\,MV$. Fibers arrangement: $\theta = \psi = \pi/4$ in $X_2 > 0$ and $\theta = 5\pi/4$ and $\psi = \pi/4$ in $X_2 < 0$. Results obtained with the mixed formulations. Constitutive model defined in (96) and (97) with material parameters given in Table 7. Results shown for a discretisation of $(2 \times 8 \times 30) \times 6$ tetrahedral elements ($5,185 \times 3$ and $5,185$ degrees of freedom associated to the spatial coordinates $\boldsymbol{x}$ and electric potential, respectively).

to the cross sectional area. The same example in the context of pure elasticity has been presented by the authors in Reference [24].

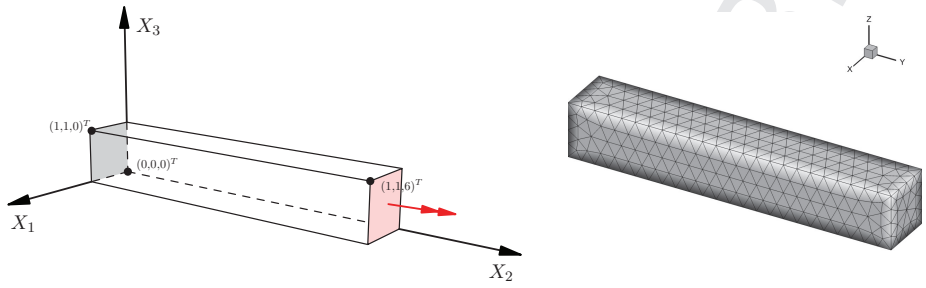

(a) (b)

Figure 10: Twisting of piezoelectric energy harvester. (a) Boundary conditions: clamped left end and twisting rotation applied at the right end. $\varphi = 0$ in plane $X_1 = 0$. Axes OX_1, OX_2 and OX_3 coincide with ox, oy and oz in (b), respectively. (b) Example of finite element discretisation: $(4 \times 4 \times 24) \times 6$ tetrahedral elements ($3,969 \times 3$ and $3,969$ degrees of freedom associated to the spatial coordinates $\boldsymbol{x}$ and electric potential, respectively).

The geometry and boundary conditions for the problem are depicted in Figure 10(a). In this example, a simple convex multi-variable constitutive model able to generate the direct piezoelectric effect is proposed. In particular, a transversely isotropic material characterised by a preferred direction $\boldsymbol{N}$ parallel to the axis OX_2 is considered. Notice that the aim of this example is not to fully characterise this specific material symmetry class. A simple convex multi-variable constitutive law for transverse isotropy incorporating piezoelectricity is proposed as,

$$W_p = \mu_1 II_{\boldsymbol{F}} + \mu_2 II_{\boldsymbol{H}} + \frac{1}{2J\varepsilon_1} II_{\boldsymbol{d}} + \frac{1}{2\varepsilon_2} II_{\boldsymbol{D}_0} + \mu_3 II_{\boldsymbol{v}} + g(J, \boldsymbol{D}_0, \boldsymbol{N}), \tag{99}$$

where the vector $\boldsymbol{v}$ in above equation (99) is defined as,

$$\boldsymbol{v} = \frac{\boldsymbol{d}}{\sqrt{\mu_3 \varepsilon_3}} + \boldsymbol{F}\boldsymbol{N}, \tag{100}$$

where μ_3 has units of stress, namely (Pa) and ε_3 of electric permittivity, namely (N/V^2) . The convex function g in above equation (99) has been

introduced to guarantee that both the stress and the electric field in the reference configuration vanish. A possible choice of g which satisfies that condition is,

$$g(J, \boldsymbol{D}_0, \boldsymbol{N}) = -\left(2\mu_1 + 4\mu_2 + 2\mu_3\right) \ln J + \frac{\lambda}{2}\left(J-1\right)^2 - 2\sqrt{\frac{\mu_3}{\varepsilon_3}}\boldsymbol{D}_0 \cdot \boldsymbol{N}. \quad (101)$$

Notice that the proposed constitutive law defined in equations (99) and (101) is convex multi-variable. The material parameters in above equation (99) has been chosen according to Table 8.

$\mu_1\,(GPa)$	$\mu_2\,(GPa)$	$\mu_3\,(GPa)$	$\lambda\,(GPa)$	$\varepsilon_1\,(N/V^2)$	$\varepsilon_2\,(N/V^2)$	$\varepsilon_3\,(N/V^2)$
1	$\frac{1}{2}$	$\frac{1}{2}$	495	$4.68\varepsilon_0$	$10^6\varepsilon_1$	$10^3\varepsilon_1$

Table 8: Material properties for example 5.5.

Notice that now the material parameters in Table 8 are more consistent with those of piezoelectric polymers. Figures 11(a)-(d) display the contour plot of the stress component $\boldsymbol{\sigma}_{12}$, the stress conjugate $\boldsymbol{\Sigma}_{\boldsymbol{F}32}$, and the components of the Eulerian electric displacement field $\boldsymbol{D}_1$ and $\boldsymbol{D}_3$, respectively.

6. Concluding remarks

This paper has presented a new computational framework tailor–made for the numerical simulation of electro active polymers subjected to extreme deformations and/or electric fields. In a previous work, Gil and Ortigosa [1] extended the concept of polyconvexity to the field of nonlinear electro-elasticity. The new concept of multi-variable convexity enables a new family of Hu-Washizu mixed variational principles to be defined within the context of nonlinear electro-elasticity. The internal energy density is defined as a convex multi-variable function of the deformation gradient $\boldsymbol{F}$, its adjoint $\boldsymbol{H}$, its determinant J, the Lagrangian electric displacement field $\boldsymbol{D}_0$ and an additional spatial or Eulerian vector $\boldsymbol{d}$ computed as the product between the deformation gradient tensor and the Lagrangian electric displacement field. This paper has focussed on the Finite Element discretisation of two types of mixed variational principles, introduced for the first time in [1].

These types of Finite Element enhanced methodologies are necessary in scenarios in which the simpler displacement-potential based formulation

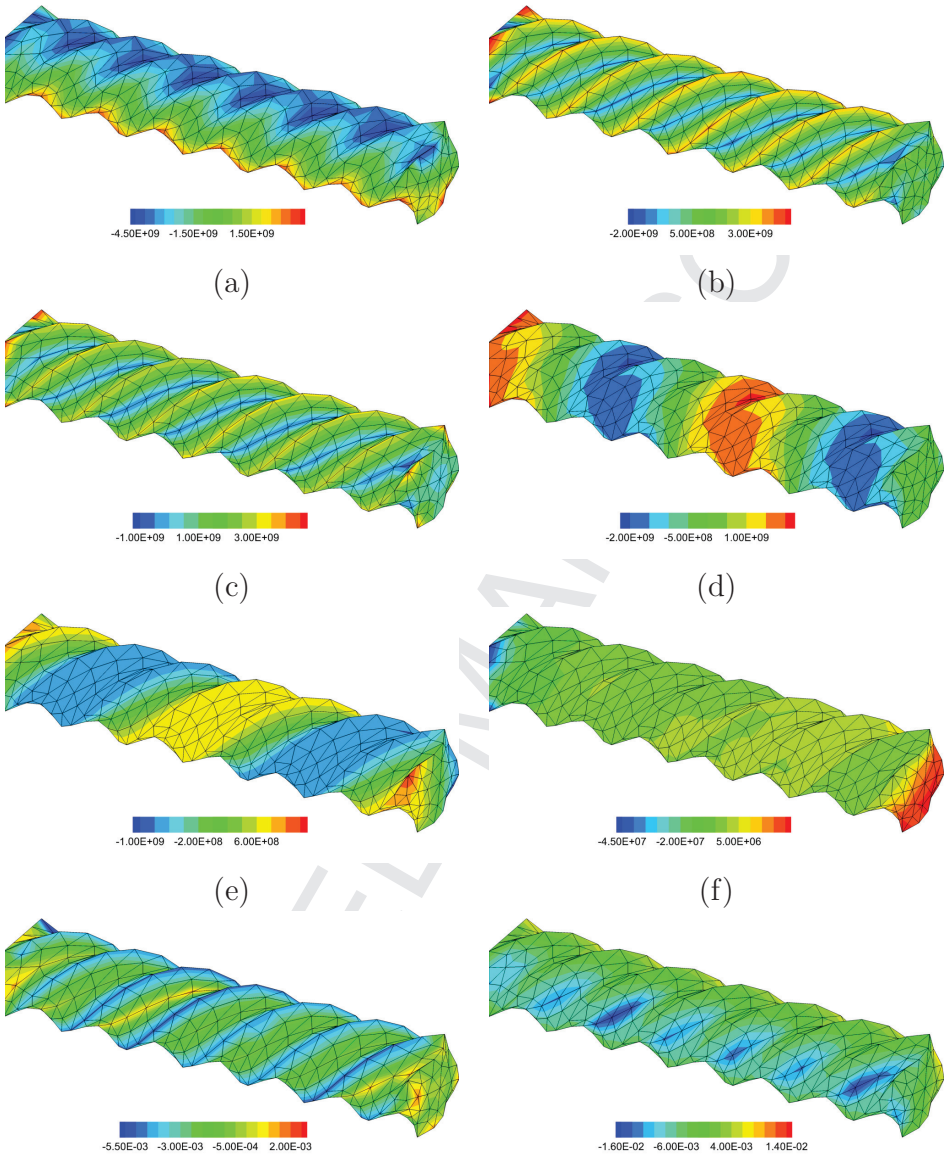

Figure 11: Twisting of piezoelectric energy harvester. Contour plots corresponding to (a) $\boldsymbol{\sigma}_{12}$, (b) $\boldsymbol{\sigma}_{22}$, (c) p, (d) $\boldsymbol{\Sigma}_{\boldsymbol{F}11}$, (e) $\boldsymbol{\Sigma}_{\boldsymbol{H}21}$, (f) φ, (g) $\boldsymbol{D}_2$ and (h) $\boldsymbol{D}_3$. Results obtained with the new mixed formulations. Constitutive model defined in (99) and (101) with material parameters given Table 8. Results shown for a discretisation of $(4 \times 4 \times 24) \times 6$ tetrahedral elements ($3,969 \times 3$ and $3,969$ degrees of freedom associated to the spatial coordinates $\boldsymbol{x}$ and electric potential, respectively).

yields non-physical results, such as volumetric locking, bending and shear locking, pressure oscillations and electro-mechanical locking, to name but a few. The applicability, accuracy and robustness of the new formulation are demonstrated via a series of challenging numerical examples, including both isotropic and anisotropic polyconvex constitutive models.

For the two mixed formulations included in this paper, the use of interpolation spaces in which the sets $\{\boldsymbol{F}, \boldsymbol{H}, J, \boldsymbol{D}_0, \boldsymbol{d}\}$ and its dual counterpart $\{\boldsymbol{\Sigma}_{\boldsymbol{F}}, \boldsymbol{\Sigma}_{\boldsymbol{H}}, \Sigma_J, \boldsymbol{\Sigma}_{\boldsymbol{D}_0}, \boldsymbol{\Sigma}_{\boldsymbol{d}}\}$ are described as piecewise discontinuous across elements enables these fields to be resolved locally, following a standard static condensation procedure, thus leading to a computational cost comparable to that of the displacement-potential based approach, yet with far more accuracy.

The new framework presented opens very interesting possibilities to similar multi-physics problems within the field of smart materials, which are the current focus of the authors.

Acknowledgements
The first author would like to acknowledge the financial support received through "The Leverhulme Prize" awarded by The Leverhulme Trust, United Kingdom. Both authors acknowledge the financial support provided by the Sêr Cymru National Research Network for Advanced Engineering and Materials.

Appendix A. Relationship between the constitutive tensors of the internal energy in terms of its reduced and extended representations

As stated in Section 2.5, it might be convenient to resort to a representation of the internal energy in terms of the set $\mathcal{V} = \{\boldsymbol{F}, \boldsymbol{H}, J, \boldsymbol{D}_0, \boldsymbol{d}\}$. However, for material characterisation purposes, it is necessary to obtain the relationship between the components of the Hessian operator $[\mathbb{H}_W]$ and those of the constitutive tensors $\boldsymbol{\mathcal{C}}$, $\boldsymbol{\mathcal{Q}}$ and $\boldsymbol{\theta}$ (16) resulting from the equivalent reduced representation of the internal energy $e(\boldsymbol{\nabla}_0\boldsymbol{x}, \boldsymbol{D}_0)$. Following Reference [1], the constitutive tensor $\boldsymbol{\mathcal{C}}$ (16) can be obtained in terms of the components of the Hessian operator $[\mathbb{H}_W]$ as

$$\begin{aligned}\boldsymbol{\mathcal{C}} = {} & W_{\boldsymbol{FF}} + \boldsymbol{F} \bigtimes (W_{\boldsymbol{HH}} \bigtimes \boldsymbol{F}) + W_{JJ}\boldsymbol{H} \otimes \boldsymbol{H} + \boldsymbol{\mathcal{C}}_1 \\ & + 2(W_{\boldsymbol{FH}} \bigtimes \boldsymbol{F})^{\text{sym}} + 2(W_{\boldsymbol{F}J} \otimes \boldsymbol{H})^{\text{sym}} + 2(W_{\boldsymbol{Fd}} \otimes \boldsymbol{D}_0)^{\text{sym}} \\ & + 2((\boldsymbol{F} \bigtimes W_{\boldsymbol{H}J}) \otimes \boldsymbol{H})^{\text{sym}} + 2((\boldsymbol{F} \bigtimes W_{\boldsymbol{Hd}}) \otimes \boldsymbol{D}_0)^{\text{sym}} \\ & + 2(\boldsymbol{H} \otimes (W_{J\boldsymbol{d}} \otimes \boldsymbol{D}_0))^{\text{sym}} + \boldsymbol{\mathcal{A}},\end{aligned} \tag{A.1}$$

where

$$\mathcal{A}_{iIjJ} = \mathcal{E}_{ijp}\mathcal{E}_{IJP}\left(\boldsymbol{\Sigma}_{\boldsymbol{H}} + \Sigma_J\boldsymbol{\Sigma}_{\boldsymbol{H}}\right)_{pP}; \quad \mathcal{C}_{1,iIjJ} = (W_{\boldsymbol{dd}})_{ij}\, D_{0I}D_{0J}. \tag{A.2}$$

Moreover, for any fourth order tensor $\boldsymbol{\mathcal{T}}$ included in equation (A.1), the symmetrised tensor $\boldsymbol{\mathcal{T}}^{\text{sym}}$ is defined as $\mathcal{T}^{\text{sym}}_{iIjJ} = \frac{1}{2}\left(\mathcal{T}_{iIjJ} + \mathcal{T}_{iJjI}\right)$. The third order constitutive tensor $\boldsymbol{\mathcal{Q}}^T$ (16) is obtained as

$$\begin{aligned}\boldsymbol{\mathcal{Q}}^T = {} & W_{\boldsymbol{FD}_0} + \boldsymbol{F} \bigtimes W_{\boldsymbol{HD}_0} + \boldsymbol{H} \otimes W_{J\boldsymbol{D}_0} + \boldsymbol{\mathcal{Q}}^T_1 \\ & + \boldsymbol{\mathcal{Q}}^T_2 + \boldsymbol{\mathcal{Q}}^T_3 + \boldsymbol{\mathcal{Q}}^T_4 + \boldsymbol{\mathcal{Q}}^T_5 + \boldsymbol{\Sigma}_{\boldsymbol{d}} \otimes \boldsymbol{I}.\end{aligned} \tag{A.3}$$

where tensors $\boldsymbol{\mathcal{Q}}^T_i$ in above equation (A.3) are

$$\left(\boldsymbol{\mathcal{Q}}^T_1\right)_{iIJ} = (W_{\boldsymbol{dD}_0})_{iJ}\, D_{0I}; \tag{A.4a}$$

$$\left(\boldsymbol{\mathcal{Q}}^T_2\right)_{iIJ} = \left(W_{\boldsymbol{Fd}iIj}\right) F_{jJ}; \tag{A.4b}$$

$$\left(\boldsymbol{\mathcal{Q}}^T_3\right)_{iIJ} = (\boldsymbol{F} \bigtimes W_{\boldsymbol{Hd}})_{iIj}F_{jJ}; \tag{A.4c}$$

$$\left(\boldsymbol{\mathcal{Q}}^T_4\right)_{iIJ} = (\boldsymbol{H} \otimes W_{J\boldsymbol{d}})_{iIj}F_{jJ}; \tag{A.4d}$$

$$\left(\boldsymbol{\mathcal{Q}}^T_5\right)_{iIJ} = (W_{\boldsymbol{dd}})_{ij}\, F_{jJ}D_{0I}. \tag{A.4e}$$

Finally, the second order constitutive tensor $\boldsymbol{\theta}$ (16) can be obtained as

$$\boldsymbol{\theta} = W_{\boldsymbol{D}_0\boldsymbol{D}_0} + (W_{\boldsymbol{D}_0\boldsymbol{d}}\boldsymbol{F} + \boldsymbol{F}^T W_{\boldsymbol{d}\boldsymbol{D}_0}) + \boldsymbol{F}^T W_{\boldsymbol{dd}}\boldsymbol{F}. \tag{A.5}$$

Appendix B. Relationships between the Hessian operator of the Helmholtz's energy functional and that for the internal energy

When an explicit representation of the Helmholtz's and extended Helmholtz's energy functionals introduced in Section 2.6.1, namely $\Phi(\boldsymbol{\nabla}_0\boldsymbol{x}, -\boldsymbol{\nabla}_0\varphi)$ (22) and $\Phi(\boldsymbol{F}, \boldsymbol{H}, J, \boldsymbol{\Sigma}_{\boldsymbol{D}_0}, \boldsymbol{\Sigma}_{\boldsymbol{d}})$ (20c) is not available, their associated Hessian operators need to be obtained in terms of the components of the Hessian operators associated to the internal energy function $e(\boldsymbol{\nabla}_0\boldsymbol{x}, \boldsymbol{D}_0)$ and its extended representation $W(\boldsymbol{F}, \boldsymbol{H}, J, \boldsymbol{D}_0, \boldsymbol{d})$ respectively, by exploiting the partial Legendre transforms presented in equations (22) and (20c), respectively.

Starting with a generic partial Legendre transform between two generic energy functionals, this section shows how to relate the Hessian operators of $\Phi(\boldsymbol{\nabla}_0\boldsymbol{x}, -\boldsymbol{\nabla}_0\varphi)$ and $\Phi(\boldsymbol{F}, \boldsymbol{H}, J, \boldsymbol{\Sigma}_{\boldsymbol{D}_0}, \boldsymbol{\Sigma}_{\boldsymbol{d}})$ to those for $e(\boldsymbol{\nabla}_0\boldsymbol{x}, \boldsymbol{D}_0)$ and its extended representation $W(\boldsymbol{F}, \boldsymbol{H}, J, \boldsymbol{D}_0, \boldsymbol{d})$.

Appendix B.1. Generic transformation between Hessian operators

Let $\mathcal{F}(\mathcal{A}, \mathcal{B})$ be an energy functional convex in the sets of variables $\{\mathcal{A}, \mathcal{B}\}$. Convexity of the energy functional enables a new energy functional $\mathcal{L}(\mathcal{A}, \Sigma_{\mathcal{B}})$ depending upon the set of variables $\mathcal{A}$ and a set of variables $\Sigma_{\mathcal{B}}$ (work conjugate to those contained in the set $\mathcal{B}$) to be defined via the following partial Legendre transformation,

$$\mathcal{L}(\mathcal{A}, \Sigma_{\mathcal{B}}) = -\max_{\mathcal{B}} \left\{\Sigma_{\mathcal{B}} : \mathcal{B} - \mathcal{F}(\mathcal{A}, \mathcal{B})\right\}. \tag{B.1}$$

Let the first derivatives of the energy functional $\mathcal{L}(\mathcal{A}, \Sigma_{\mathcal{B}})$ and the sets of variables $\Sigma_{\mathcal{A}}$ and $\Sigma_{\mathcal{B}}$ be related as

$$\frac{\partial \mathcal{F}}{\partial \mathcal{A}} = \Sigma_{\mathcal{A}}; \qquad \frac{\partial \mathcal{F}}{\partial \mathcal{B}} = \Sigma_{\mathcal{B}}. \tag{B.2}$$

Combination of equations (B.1) and (B.2) enables the first derivatives of the energy functional $\mathcal{L}(\mathcal{A}, \Sigma_{\mathcal{B}})$ to be obtained as,

$$\frac{\partial \mathcal{L}}{\partial \mathcal{A}} = \Sigma_{\mathcal{A}}; \qquad \frac{\partial \mathcal{L}}{\partial \Sigma_{\mathcal{B}}} = -\mathcal{B}. \tag{B.3}$$

Let the Hessian operators of both energy functionals $\mathcal{F}(\mathcal{A}, \mathcal{B})$ and $\mathcal{F}(\mathcal{A}, \mathcal{B})$ be represented as,

$$[\mathbb{H}_{\mathcal{L}}] = \begin{bmatrix} \mathcal{L}_{\mathcal{A}\mathcal{A}} & \mathcal{L}_{\mathcal{A}\Sigma_{\mathcal{B}}} \\ \mathcal{L}_{\Sigma_{\mathcal{B}}\mathcal{A}} & \mathcal{L}_{\Sigma_{\mathcal{B}}\Sigma_{\mathcal{B}}} \end{bmatrix}; \qquad [\mathbb{H}_{\mathcal{F}}] = \begin{bmatrix} \mathcal{F}_{\mathcal{A}\mathcal{A}} & \mathcal{F}_{\mathcal{A}\mathcal{B}} \\ \mathcal{F}_{\mathcal{B}\mathcal{A}} & \mathcal{F}_{\mathcal{B}\mathcal{B}} \end{bmatrix}, \tag{B.4}$$

with $\mathcal{L}_{\mathcal{CD}} = \frac{\partial^2 \mathcal{L}}{\partial \mathcal{C} \partial \mathcal{D}}$. The components of the Hessian operator $[\mathbb{H}_{\mathcal{F}}]$ can obtained in terms of the components of the Hessian operator $[\mathbb{H}_{\mathcal{L}}]$ in a standard manner as

$$\mathcal{L}_{\Sigma_{\mathcal{B}}\Sigma_{\mathcal{B}}} = -\left[\mathcal{F}_{\mathcal{BB}}\right]^{-1}; \tag{B.5a}$$

$$\mathcal{L}_{\mathcal{A}\Sigma_{\mathcal{B}}} = -\mathcal{F}_{\mathcal{AB}}\mathcal{L}_{\Sigma_{\mathcal{B}}\Sigma_{\mathcal{B}}}; \tag{B.5b}$$

$$\mathcal{L}_{\mathcal{AA}} = \mathcal{F}_{\mathcal{AA}} - \mathcal{F}_{\mathcal{AB}}\mathcal{L}_{\Sigma_{\mathcal{B}}\mathcal{A}};, \tag{B.5c}$$

where $\mathcal{L}_{\mathcal{A}\Sigma_{\mathcal{B}}} = \left[\mathcal{L}_{\Sigma_{\mathcal{B}}\mathcal{A}}\right]^T$.

Appendix B.2. Relation between the Hessian operator of the Helmholtz's energy $\Phi(\boldsymbol{\nabla}_0\boldsymbol{x}, \boldsymbol{\nabla}_0\varphi)$ and the Hessian operator of the internal energy $e(\boldsymbol{\nabla}_0\boldsymbol{x}, \boldsymbol{D}_0)$

Let the set of variables $\mathcal{A}$, $\mathcal{B}$, $\Sigma_{\mathcal{A}}$ and $\Sigma_{\mathcal{B}}$ (B.1) be defined as,

$$\begin{aligned} \mathcal{A} &= \boldsymbol{\nabla}_0\boldsymbol{x}; & \mathcal{B} &= \boldsymbol{D}_0; \\ \Sigma_{\mathcal{A}} &= \boldsymbol{P}; & \Sigma_{\mathcal{B}} &= -\boldsymbol{\nabla}_0\varphi. \end{aligned} \tag{B.6}$$

For this particular case, the energy functions $\mathcal{L}(\mathcal{A}, \Sigma_{\mathcal{B}})$ and $\mathcal{F}(\mathcal{A}, \mathcal{B})$ coincide with the Helmholtz's energy functional $\Phi(\boldsymbol{\nabla}_0\boldsymbol{x}, -\boldsymbol{\nabla}_0\varphi)$ and the internal energy $e(\boldsymbol{\nabla}_0\boldsymbol{x}, \boldsymbol{D}_0)$, respectively, namely

$$\mathcal{L}(\mathcal{A}, \Sigma_{\mathcal{B}}) = \Phi(\boldsymbol{\nabla}_0\boldsymbol{x}, -\boldsymbol{\nabla}_0\varphi); \qquad \mathcal{F}(\mathcal{A}, \mathcal{B}) = e(\boldsymbol{\nabla}_0\boldsymbol{x}, \boldsymbol{D}_0). \tag{B.7}$$

For these two energy functionals, the equivalent expression to that in (B.5a), relating electrical components of the Hessian operators of $\Phi(\boldsymbol{\nabla}_0\boldsymbol{x}, -\boldsymbol{\nabla}_0\varphi)$ and $e(\boldsymbol{\nabla}_0\boldsymbol{x}, \boldsymbol{D}_0)$, namely $\boldsymbol{\varepsilon}$ (25) and $\boldsymbol{\theta}$ (16), respectively is

$$\boldsymbol{\varepsilon} = \boldsymbol{\theta}^{-1}. \tag{B.8}$$

The equivalent expression to equation (B.5b), relating the coupled contributions of both Hessian operators, namely $\boldsymbol{\mathcal{P}}$ (25) and $\boldsymbol{\mathcal{Q}}$ (16), yields

$$-\boldsymbol{\mathcal{P}}^T = \boldsymbol{\mathcal{Q}}^T \bullet \boldsymbol{\varepsilon}, \tag{B.9}$$

where the operation $\bullet$ in above (B.9) indicates the contraction of the last and first components of the tensors on the left and right hand sides of the operation symbol $\bullet$, respectively. Finally, the mechanical component of the

Hessian operator of the Helmholtz energy, namely $\boldsymbol{\mathcal{C}}^\star$ (16) emerges after applying equation (B.5a), yielding

$$\boldsymbol{\mathcal{C}}^\star = \boldsymbol{\mathcal{C}} + \boldsymbol{\mathcal{Q}} \bullet \boldsymbol{\mathcal{P}}, \tag{B.10}$$

with $\boldsymbol{\mathcal{C}}$ defined in (16).

Appendix B.3. Relation between the Hessian operator $[\mathbb{H}_\Phi]$ *and the Hessian operator* $[\mathbb{H}_W]$

Let the set of variables $\mathcal{A}$, $\mathcal{B}$, $\Sigma_\mathcal{A}$ and $\Sigma_\mathcal{B}$ (B.1) be defined as,

$$\begin{aligned} \mathcal{A} &= \{\boldsymbol{F}, \boldsymbol{H}, J\}; & \mathcal{B} &= \{\boldsymbol{D}_0, \boldsymbol{d}\}; \\ \Sigma_\mathcal{A} &= \{\boldsymbol{\Sigma}_{\boldsymbol{F}}, \boldsymbol{\Sigma}_{\boldsymbol{H}}, \Sigma_J\}; & \Sigma_\mathcal{B} &= \{\Sigma_{\boldsymbol{D}_0}, \Sigma_{\boldsymbol{d}}\}. \end{aligned} \tag{B.11}$$

For this particular case, the energy functions $\mathcal{L}(\mathcal{A}, \Sigma_\mathcal{B})$ and $\mathcal{F}(\mathcal{A}, \mathcal{B})$ coincide with the extended Helmholtz's energy $\Phi(\boldsymbol{F}, \boldsymbol{H}, J, \boldsymbol{\Sigma}_{\boldsymbol{D}_0}, \boldsymbol{\Sigma}_{\boldsymbol{d}})$ and the internal energy $W(\boldsymbol{F}, \boldsymbol{H}, J, \boldsymbol{D}_0, \boldsymbol{d})$, respectively, namely

$$\mathcal{L}(\mathcal{A}, \Sigma_\mathcal{B}) = \Phi(\boldsymbol{F}, \boldsymbol{H}, J, \boldsymbol{\Sigma}_{\boldsymbol{D}_0}, \boldsymbol{\Sigma}_{\boldsymbol{d}}); \qquad \mathcal{F}(\mathcal{A}, \mathcal{B}) = W(\boldsymbol{F}, \boldsymbol{H}, J, \boldsymbol{D}_0, \boldsymbol{d}). \tag{B.12}$$

For these two energy functionals, the equivalent expression to that in (B.5a), relating some of the components of the Hessian operators $[\mathbb{H}_\Phi]$ and $[\mathbb{H}_W]$ reads as

$$\begin{bmatrix} \Phi_{\boldsymbol{\Sigma}_{\boldsymbol{D}_0}\boldsymbol{\Sigma}_{\boldsymbol{D}_0}} & \Phi_{\boldsymbol{\Sigma}_{\boldsymbol{D}_0}\boldsymbol{\Sigma}_{\boldsymbol{d}}} \\ \Phi_{\boldsymbol{\Sigma}_{\boldsymbol{d}}\boldsymbol{\Sigma}_{\boldsymbol{D}_0}} & \Phi_{\boldsymbol{\Sigma}_{\boldsymbol{d}}\boldsymbol{\Sigma}_{\boldsymbol{d}}} \end{bmatrix} = - \begin{bmatrix} W_{\boldsymbol{D}_0\boldsymbol{D}_0} & W_{\boldsymbol{D}_0\boldsymbol{d}} \\ W_{\boldsymbol{d}\boldsymbol{D}_0} & W_{\boldsymbol{d}\boldsymbol{d}} \end{bmatrix}^{-1}. \tag{B.13}$$

Analogously, the equivalent expression to equation (B.5b) yields

$$\begin{bmatrix} \Phi_{\boldsymbol{F}\boldsymbol{\Sigma}_{\boldsymbol{D}_0}} \\ \Phi_{\boldsymbol{H}\boldsymbol{\Sigma}_{\boldsymbol{D}_0}} \\ \Phi_{J\boldsymbol{\Sigma}_{\boldsymbol{D}_0}} \end{bmatrix} = - \begin{bmatrix} W_{\boldsymbol{F}\boldsymbol{D}_0} \\ W_{\boldsymbol{H}\boldsymbol{D}_0} \\ W_{J\boldsymbol{D}_0} \end{bmatrix} \left[\Phi_{\boldsymbol{\Sigma}_{\boldsymbol{D}_0}\boldsymbol{\Sigma}_{\boldsymbol{D}_0}}\right]; \qquad \begin{bmatrix} \Phi_{\boldsymbol{F}\boldsymbol{\Sigma}_{\boldsymbol{d}}} \\ \Phi_{\boldsymbol{H}\boldsymbol{\Sigma}_{\boldsymbol{d}}} \\ \Phi_{J\boldsymbol{\Sigma}_{\boldsymbol{d}}} \end{bmatrix} = - \begin{bmatrix} W_{\boldsymbol{F}\boldsymbol{V}} \\ W_{\boldsymbol{H}\boldsymbol{V}} \\ W_{J\boldsymbol{d}} \end{bmatrix} \left[\Phi_{\boldsymbol{\Sigma}_{\boldsymbol{d}}\boldsymbol{\Sigma}_{\boldsymbol{d}}}\right]. \tag{B.14}$$

Finally, the remaining components of the Hessian operator $[\mathbb{H}_\Phi]$ emerge

after applying equation (B.5a), yielding

$$\Phi_{\boldsymbol{FF}} = W_{\boldsymbol{FF}} - \begin{bmatrix} W_{\boldsymbol{FD}_0} & W_{\boldsymbol{Fd}} \end{bmatrix} \begin{bmatrix} \Phi_{\boldsymbol{\Sigma}_{\boldsymbol{D}_0}\boldsymbol{F}} \\ \Phi_{\boldsymbol{\Sigma}_{\boldsymbol{d}}\boldsymbol{F}} \end{bmatrix}; \tag{B.15a}$$

$$\Phi_{\boldsymbol{FH}} = W_{\boldsymbol{FH}} - \begin{bmatrix} W_{\boldsymbol{FD}_0} & W_{\boldsymbol{Fd}} \end{bmatrix} \begin{bmatrix} \Phi_{\boldsymbol{\Sigma}_{\boldsymbol{D}_0}\boldsymbol{H}} \\ \Phi_{\boldsymbol{\Sigma}_{\boldsymbol{d}}\boldsymbol{H}} \end{bmatrix}; \tag{B.15b}$$

$$\Phi_{\boldsymbol{F}J} = W_{\boldsymbol{F}J} - \begin{bmatrix} W_{\boldsymbol{FD}_0} & W_{\boldsymbol{Fd}} \end{bmatrix} \begin{bmatrix} \Phi_{\boldsymbol{\Sigma}_{\boldsymbol{D}_0}J} \\ \Phi_{\boldsymbol{\Sigma}_{\boldsymbol{d}}J} \end{bmatrix}; \tag{B.15c}$$

$$\Phi_{\boldsymbol{HH}} = W_{\boldsymbol{HH}} - \begin{bmatrix} W_{\boldsymbol{HD}_0} & W_{\boldsymbol{Hd}} \end{bmatrix} \begin{bmatrix} \Phi_{\boldsymbol{\Sigma}_{\boldsymbol{D}_0}\boldsymbol{H}} \\ \Phi_{\boldsymbol{\Sigma}_{\boldsymbol{d}}\boldsymbol{H}} \end{bmatrix}; \tag{B.15d}$$

$$\Phi_{\boldsymbol{H}J} = W_{\boldsymbol{H}J} - \begin{bmatrix} W_{\boldsymbol{HD}_0} & W_{\boldsymbol{Hd}} \end{bmatrix} \begin{bmatrix} \Phi_{\boldsymbol{\Sigma}_{\boldsymbol{D}_0}J} \\ \Phi_{\boldsymbol{\Sigma}_{\boldsymbol{d}}J} \end{bmatrix}; \tag{B.15e}$$

$$\Phi_{JJ} = W_{JJ} - \begin{bmatrix} W_{J\boldsymbol{D}_0} & W_{J\boldsymbol{d}} \end{bmatrix} \begin{bmatrix} \Phi_{\boldsymbol{\Sigma}_{\boldsymbol{D}_0}J} \\ \Phi_{\boldsymbol{\Sigma}_{\boldsymbol{d}}J} \end{bmatrix}. \tag{B.15f}$$

Appendix C. Auxiliary residuals and stiffness matrices associated to static condensation procedure

The auxiliary residuals and stiffness matrices arising in the static condensation procedure for the variational principle Π_W (31) (see equations (60), (61), (62), (64) and (65)) are

$$\bar{\boldsymbol{R}}^e_{\Sigma_\mathcal{Y}} = -[\boldsymbol{M}^e_3]^{-1}\left(\boldsymbol{R}^e_\mathcal{Y} + \boldsymbol{K}^e_{\mathcal{Y}\mathcal{Y}}\bar{\boldsymbol{R}}^e_\mathcal{Y} - \boldsymbol{M}^e_2\boldsymbol{M}^e_1\left(\boldsymbol{R}^e_{\boldsymbol{D}_0} + \boldsymbol{K}^e_{\boldsymbol{D}_0\mathcal{Y}}\bar{\boldsymbol{R}}^e_\mathcal{Y}\right)\right); \tag{C.1a}$$

$$\bar{\bar{\boldsymbol{R}}}^e_{\boldsymbol{D}_0} = -\boldsymbol{M}^e_1\left(\boldsymbol{R}^e_{\boldsymbol{D}_0} + \boldsymbol{K}^e_{\boldsymbol{D}_0\mathcal{Y}}\bar{\boldsymbol{R}}^e_\mathcal{Y} + \boldsymbol{K}^e_{\boldsymbol{D}_0\Sigma_\mathcal{Y}}\bar{\boldsymbol{R}}^e_{\Sigma_\mathcal{Y}}\right); \tag{C.1b}$$

$$\bar{\boldsymbol{R}}^e_\mathcal{Y} = -[\boldsymbol{K}^e_{\Sigma_\mathcal{Y}\mathcal{Y}}]^{-1}\boldsymbol{R}^e_{\Sigma_\mathcal{Y}}; \tag{C.1c}$$

$$\boldsymbol{M}^e_1 = [\boldsymbol{K}^e_{\boldsymbol{D}_0\boldsymbol{D}_0} - \boldsymbol{K}^e_{\boldsymbol{D}_0\mathcal{Y}}\left([\boldsymbol{K}^e_{\Sigma_\mathcal{Y}\mathcal{Y}}]^{-1}\boldsymbol{K}^e_{\Sigma_\mathcal{Y}\boldsymbol{D}_0}\right)]^{-1}; \tag{C.1d}$$

$$\boldsymbol{M}^e_2 = [\boldsymbol{K}^e_{\mathcal{Y}\boldsymbol{D}_0} - \boldsymbol{K}^e_{\mathcal{Y}\mathcal{Y}}\left([\boldsymbol{K}^e_{\Sigma_\mathcal{Y}\mathcal{Y}}]^{-1}\boldsymbol{K}^e_{\Sigma_\mathcal{Y}\boldsymbol{D}_0}\right)]^{-1}; \tag{C.1e}$$

$$\boldsymbol{M}^e_3 = [\boldsymbol{K}^e_{\mathcal{Y}\Sigma_\mathcal{Y}} - \boldsymbol{M}^e_2\boldsymbol{M}^e_1\boldsymbol{K}^e_{\boldsymbol{D}_0\Sigma_\mathcal{Y}}]^{-1}; \tag{C.1f}$$

$$\boldsymbol{M}^e_{\mathcal{Y}\boldsymbol{x}} = -[\boldsymbol{K}^e_{\Sigma_\mathcal{Y}\mathcal{Y}}]^{-1}\boldsymbol{K}^e_{\Sigma_\mathcal{Y}\boldsymbol{x}}; \tag{C.1g}$$

$$\boldsymbol{M}^e_{\Sigma_\mathcal{Y}\boldsymbol{x}} = -\boldsymbol{M}^e_3\left(\boldsymbol{K}^e_{\mathcal{Y}\mathcal{Y}}\boldsymbol{M}^e_{\mathcal{Y}\boldsymbol{x}} - \boldsymbol{M}^e_2\boldsymbol{M}^e_1\left(\boldsymbol{K}^e_{\boldsymbol{D}_0\boldsymbol{x}} + \boldsymbol{K}^e_{\boldsymbol{D}_0\mathcal{Y}}\boldsymbol{M}^e_{\mathcal{Y}\boldsymbol{x}}\right)\right); \tag{C.1h}$$

$$\boldsymbol{M}^e_{\Sigma_\mathcal{Y}\varphi} = \boldsymbol{M}^e_3\boldsymbol{M}^e_2\boldsymbol{M}^e_1\boldsymbol{K}^e_{\boldsymbol{D}_0\varphi}; \tag{C.1i}$$

$$\bar{\boldsymbol{M}}^e_{\boldsymbol{D}_0\boldsymbol{x}} = -\boldsymbol{M}^e_1\left(\boldsymbol{K}^e_{\boldsymbol{D}_0\Sigma_\mathcal{Y}}\boldsymbol{M}^e_{\Sigma_\mathcal{Y}\boldsymbol{x}} + \boldsymbol{K}^e_{\boldsymbol{D}_0\boldsymbol{x}} + \boldsymbol{K}^e_{\boldsymbol{D}_0\mathcal{Y}}\boldsymbol{M}^e_{\mathcal{Y}\boldsymbol{x}}\right); \tag{C.1j}$$

$$\bar{\boldsymbol{M}}^e_{\boldsymbol{D}_0\varphi} = -\boldsymbol{M}^e_1\left(\boldsymbol{K}^e_{\boldsymbol{D}_0\Sigma_\mathcal{Y}}\boldsymbol{M}^e_{\Sigma_\mathcal{Y}\varphi} + \boldsymbol{K}^e_{\boldsymbol{D}_0\varphi}\right); \tag{C.1k}$$

$$\bar{\boldsymbol{M}}^e_{\mathcal{Y}\boldsymbol{x}} = \boldsymbol{M}^e_{\mathcal{Y}\boldsymbol{x}} - [\boldsymbol{K}^e_{\Sigma_\mathcal{Y}\mathcal{Y}}]^{-1}\boldsymbol{K}^e_{\Sigma_\mathcal{Y}\boldsymbol{D}_0}\bar{\boldsymbol{M}}^e_{\boldsymbol{D}_0\boldsymbol{x}}; \tag{C.1l}$$

$$\bar{\boldsymbol{M}}^e_{\mathcal{Y}\varphi} = -[\boldsymbol{K}^e_{\Sigma_\mathcal{Y}\mathcal{Y}}]^{-1}\boldsymbol{K}^e_{\Sigma_\mathcal{Y}\boldsymbol{D}_0}\bar{\boldsymbol{M}}^e_{\boldsymbol{D}_0\varphi}. \tag{C.1m}$$

References

[1] A. J. Gil, R. Ortigosa, A new framework for large strain electromechanics based on convex multi-variable strain energies: variational formulation and material characterisation, Computer Methods in Applied Mechanics and Engineering (In print).

[2] A. O'Halloran, F. O'Malley, P. McHugh, A review on dielectric elastomer actuators, technology, applications, and challenges, Journal of Applied Physics 104 (2008).

[3] R. E. Pelrine, R. D. Kornbluh, J. P. Joseph, Electrostriction of polymer dielectrics with compliant electrodes as a means of actuation, Sensors and Actuators A: Physical 64 (1998) 77–85. Tenth {IEEE} International Workshop on Micro Electro Mechanical Systems.

[4] R. Pelrine, R. Kornbluh, Q. Pei, J. Joseph, High-speed electrically actuated elastomers with strain greater than 100 %, Science 287 (2000) 836–839.

[5] G. Kofod, P. Sommer-Larsen, R. Kornbluh, R. Pelrine, Actuation response of polyacrylate dielectric elastomers, Journal of Intelligent Material Systems and Structures 14 (2003) 787–793.

[6] R. Pelrine, R. D. Kornbluh, Q. Pei, S. Stanford, S. Oh, J. Eckerle, R. J. Full, M. A. Rosenthal, K. Meijer, Dielectric elastomer artificial muscle actuators: toward biomimetic motion, 2002.

[7] X. Zhao, Z. Suo, Electrostriction in elastic dielectrics undergoing large deformation, Journal of Applied Physics 104 (2008) 123530.

[8] T. Li, C. Keplinger, R. Baumgartner, S. Bauer, W. Yang, Z. Suo, Giant voltage-induced deformation in dielectric elastomers near the verge of snap-through instability, Journal of the Mechanics and Physics of Solids 61 (2013) 611–628.

[9] A. Dorfmann, R. W. Ogden, Nonlinear electroelasticity, Acta Mechanica 174 (2005) 167–183.

[10] R. Bustamante, A. Dorfmann, R. Ogden, Nonlinear electroelastostatics: a variational framework, Zeitschrift für angewandte Mathematik und Physik 60 (2009) 154–177.

[11] R. Bustamante, A. Dorfmann, R. Ogden, On electric body forces and Maxwell stresses in nonlinearly electroelastic solids, International Journal of Engineering Science 47 (2009) 1131–1141. Mechanics, Mathematics and Materials a Special Issue in memory of A.J.M. Spencer {FRS} In Memory of Professor A.J.M. Spencer {FRS}.

[12] R. Bustamante, Transversely isotropic non-linear electro-active elastomers, Acta Mechanica 206 (2009) 237–259.

[13] R. Bustamante, J. Merodio, Constitutive structure in coupled non-linear electro-elasticity: Invariant descriptions and constitutive restrictions, International Journal of Non-Linear Mechanics 46 (2011) 1315–1323.

[14] Z. Suo, X. Zhao, W. H. Greene, A nonlinear field theory of deformable dielectrics, Journal of the Mechanics and Physics of Solids 56 (2008) 467–486.

[15] J. E. Marsden, T. J. R. Hughes, Mathematical foundations of elasticity, 1994.

[16] R. Bustamante, J. Merodio, On simple constitutive restrictions for transversely isotropic nonlinearly elastic materials and isotropic magneto-sensitive elastomers, Journal of Engineering Mathematics 68 (2010) 15–26.

[17] C. Miehe, D. Vallicotti, D. Zäh, Computational structural and material stability analysis in finite electro-elasto-statics of electro-active materials, International Journal for Numerical Methods in Engineering 102 (2015) 1605–1637. Nme.4855.

[18] R. Rogers, Nonlocal variational problems in nonlinear electromagneto-elastostatics, SIAM Journal on Mathematical Analysis 19 (1988) 1329–1347.

[19] J. M. Ball, Convexity conditions and existence theorems in nonlinear elasticity, Archive for Rational Mechanics and Analysis 63 (1976) 337–403.

[20] J. Schröder, P. Neff, D. Balzani, A variational approach for materially stable anisotropic hyperelasticity, International Journal of Solids and Structures 42 (2005) 4352–4371.

[21] M. Aguirre, A. J. Gil, J. Bonet, A. A. Carreño, A vertex centred finite volume Jameson-Schmidt-Turkel (JST) algorithm for a mixed conservation formulation in solid dynamics, Journal of Computational Physics 259 (2014) 672–699.

[22] J. Schröder, P. Wriggers, D. Balzani, A new mixed finite element based on different approximations of the minors of deformation tensors, Computer Methods in Applied Mechanics and Engineering 200 (2011) 3583–3600.

[23] J. Schröder, Anisotropic polyconvex energies, in: J. Schröder, P. Neff (Eds.), Poly-, quasi- and rank-one convexity in Applied Mechanics, volume 516 of CISM Courses and Lectures, volume 516 of CISM Courses and Lectures, Springer-Verlag, 2010, pp. 53–105.

[24] J. Bonet, A. J. Gil, R. Ortigosa, A computational framework for polyconvex large strain elasticity, Computer Methods in Applied Mechanics and Engineering 283 (2015) 1061–1094.

[25] M. Itskov, A. Ehret, D. Mavrilas, A polyconvex anisotropic strain-energy function for soft collagenous tissues, Biomechanics and Modeling in Mechanobiology 5 (2006) 17–26.

[26] A. E. Ehret, M. Itskov, A polyconvex hyperelastic model for fiber-reinforced materials in application to soft tissues, Journal of Materials Science 42 (2007) 8853–8863.

[27] R. de Boer, Vektor- und Tensorrechnung für Ingenieure, Springer-Verlag, 1982.

[28] A. Dorfmann, R. W. Ogden, Electroelastic waves in a finitely deformed electroactive material, IMA Journal of Applied Mathematics 75 (2010) 603–636.

[29] M. H. Siboni, P. P. Castañeda, Fiber-constrained, dielectric-elastomer composites: Finite-strain response and stability analysis, Journal of the Mechanics and Physics of Solids 68 (2014) 211–238.

[30] M. H. Siboni, R. Avazmohammadi, P. P. Castañeda, Electromechanical instabilities in fiber-constrained, dielectric-elastomer composites subjected to all-around dead-loading, Mathematics and Mechanics of Solids (2014).

[31] A. J. Gil, R. Ortigosa, A new framework for large strain electromechanics based on convex multi-variable strain energies: hyperbolicity and conservation laws, Computer Methods in Applied Mechanics and Engineering (Under review).

[32] C. H. Lee, A. J. Gil, J. Bonet, Development of a cell centred upwind finite volume algorithm for a new conservation law formulation in structural dynamics, Computers and Structures 118 (2012) 13–38.

[33] K. Izian, C. H. Lee, A. J. Gil, J. Bonet, A Two-Step Taylor-Galerkin method for explicit solid dynamics, Engineering Computations 31 (2013) 366–387.

[34] C. H. Lee, A. J. Gil, J. Bonet, Development of a stabilised Petrov-Galerkin formulation for conservation laws in Lagrangian fast solid dynamics, Computer Methods in Applied Mechanics and Engineering 268 (2014) 40–64.

[35] A. J. Gil, C. H. Lee, J. Bonet, M. Aguirre, A stabilised Petrov-Galerkin formulation for linear tetrahedral elements in compressible, nearly incompressible and truly incompressible fast dynamics, Computer Methods in Applied Mechanics and Engineering 276 (2014) 659–690.

[36] J. Bonet, A. J. Gil, C. H. Lee, M. Aguirre, R. Ortigosa, A first order hyperbolic framework for large strain computational solid dynamics - Part I: Total Lagrangian isothermal elasticity, Computer Methods in Applied Mechanics and Engineering 283 (2015) 689–732.

[37] A. J. Gil, C. H. Lee, J. Bonet, R. Ortigosa, A first order hyperbolic framework for large strain computational solid dynamics - Part II: Total Lagrangian compressible, nearly incompressible and truly incompressible elasticity (2015) 10.1016/j.cma.2015.11.010.

[38] M. Aguirre, A. J. Gil, J. Bonet, C. H. Lee, An upwind vertex centred finite volume solver for Lagrangian solid dynamics, Journal of Computational Physics 300 (2015) 387–422.

[39] S. Skatulla, C. Sansour, A. Arockiarajan, A multiplicative approach for nonlinear electro-elasticity, Computer Methods in Applied Mechanics and Engineering 245-246 (2012) 243–255.

[40] D. K. Vu, P. Steinmann, G. Possart, Numerical modelling of non-linear electroelasticity, International Journal for Numerical Methods in Engineering 70 (2007) 685–704.

[41] J. Zhou, W. Hong, X. Zhao, Z. Zhang, Z. Suo, Propagation of instability in dielectric elastomers, International Journal of Solids and Structures 45 (2008) 3739–3750. Special Issue Honoring K.C. Hwang Fracture, Plasticity, Micro- and Nanomechanics Special Issue Honoring K.C. Hwang.

[42] D. Vu, P. Steinmann, On 3-D coupled BEM-FEM simulation of nonlinear electro-elastostatics, Computer Methods in Applied Mechanics and Engineering 201-204 (2012) 82–90.

[43] D. Vu, P. Steinmann, A 2-D coupled BEM-FEM simulation of electro-elastostatics at large strain, Computer Methods in Applied Mechanics and Engineering 199 (2010) 1124–1133.

[44] T. J. R. Hughes, The finite element method: Linear static and dynamic finite element analysis, Dover Publications, 2000.

[45] K. J. Bathe, Finite Element Procedures, Prentice Hall, 1996.

[46] F. Brezzi, M. Fortin, Mixed and Hybrid Finite Element Methods, Springer-Verlag New York, Inc., New York, NY, USA, 1991.

[47] J. Bonet, P. Bhargava, A uniform deformation gradient hexahedron element with artificial hourglass control, International Journal for Numerical Methods in Engineering 38 (1995) 2809–2828.

[48] J. C. Simo, F. Armero, K. S. Pister, Variational and projection methods for the volume constraint in finite deformation elasto-plasticity, Computational Methods for Applied Mechanical Engineering 51 (1985) 177–208.

[49] R. Stenberg, A family of mixed finite elements for elasticity problems, Numerische Mathematik 48 (1988) 513–538.

[50] F. Auricchio, L. B. de Veiga, C. Lovadina, A. Reali, A stability study of some mixed finite elements for large deformation elasticity problems, Computational Methods for Applied Mechanical Engineering 194 (2005) 1075–1092.

[51] R. L. Taylor, A mixed-enhanced formulation for tetrahedral finite elements, International Journal for Numerical Methods in Engineering 47 (2000) 205–227.

[52] C. R. Dohrmann, M. W. Heinstein, J. Jung, S. W. Key, W. R. Witkowski, Node-based uniform strain elements for three-node triangular and four-node tetrahedral meshes, International Journal for Numerical Methods in Engineering 47 (2000) 1549–1568.

[53] Q. Tiehu, Symmetrizing nonlinear elastodynamic system, Journal of Elasticity 50 (1998) 245–252.

[54] F. Vogel, R. Bustamante, P. Steinmann, On some mixed variational principles in electro-elastostatics, International Journal of Non-Linear Mechanics 47 (2012) 341–354. Nonlinear Continuum Theories.

[55] J. Bonet, R. D. Wood, Nonlinear Continuum Mechanics for Finite Element Analysis, Cambridge University Press, second edition, 2008.

[56] R. Hill, On uniqueness and stability in the theory of finite elastic strain, Journal of the Mechanics and Physics of Solids 5 (1957) 229–241.

[57] B. D. Coleman, W. Noll, On the thermostatics of continuous media, Archive for Rational Mechanics and Analysis 4 (1959) 97–128.

[58] P. G. Ciarlet, Mathematical Elasticity. Volume 1: Three Dimensional Elasticity, 1988.

[59] O. Gonzalez, A. M. Stuart, A first course in Continuum Mechanics, Cambridge University Press, 2008.

[60] J. M. Ball, Geometry, Mechanics and Dynamics, Springer, pp. 3–59.

[61] J. M. Ball, F. Murat, $W^{1,p}$-quasiconvexity and variational problems for multiple integrals, Journal of Functional Analysis 58 (1984) 225–253.

[62] J. M. Ball, Energy-minimising configurations in nonlinear elasticity, Archive for Rational Mechanics and Analysis 63 (1976) 337–403.

[63] J. Bonet, A. J. Gil, R. Ortigosa, On a tensor cross product based formulation of large strain solid mechanics, International Journal of Solids and Structures (Under review).

[64] R. Ortigosa, A. J. Gil, J. Bonet, C. Hesch, A computational framework for polyconvex large strain elasticity for geometrically exact beam theory, Computational Mechanics doi: 10.1007/s00466-015-1231-5 (2015).

[65] A. Dorfmann, R. Ogden, Nonlinear electroelastic deformations, Journal of Elasticity 82 (2006) 99–127.

[66] I. Babuška, The finite element method with Lagrangian multipliers, Numerische Mathematik 20 (1973) 179–192.

[67] J. Donea, A. Huerta, Finite Element Methods for Flow Problems, John Wiley and Sons, 2003.

[68] A. N. Brooks, T. J. R. Hughes, Streamline upwind/Petrov-Galerkin formulations for convection dominated flows with particular emphasis on the incompressible Navier-Stokes equations, Computer Methods in Applied Mechanics and Engineering 32 (1982) 199–259.